UNCERTAINTY ANALYSIS OF CO_2 LEAKAGE FROM GEOLOGIC CO_2 SEQUESTRATION RESERVOIRS

by

Ting Xiao

A dissertation submitted to the faculty of
The University of Utah
in partial fulfillment of the requirements for the degree of

Doctor of Philosophy

Department of Civil and Environmental Engineering

The University of Utah

August 2017

The University of Utah Graduate School

STATEMENT OF DISSERTATION APPROVAL

The dissertation of **Ting Xiao**

has been approved by the following supervisory committee members:

Brian McPherson	, Chair	**04/03/2017** Date Approved
Steven Burian	, Member	**04/03/2017** Date Approved
Andy Hong	, Member	**04/04/2017** Date Approved
Edward Trujillo	, Member	**04/03/2017** Date Approved
Diana Bacon	, Member	**04/25/2017** Date Approved
Tianfu Xu	, Member	**04/13/2017** Date Approved

and by **Michael Barber**, Chair/Dean of

the Department/College/School of **Civil and Environmental Engineering**

and by David B. Kieda, Dean of The Graduate School.

ABSTRACT

Geologic CO_2 sequestration (GCS) is believed to play a critical role for mitigating CO_2 emissions. Many geologic carbon storage site options include not only excellent storage reservoirs bounded by effective seal layers, but also Underground Sources of Drinking Water (USDWs). An effective risk assessment of potential CO_2 leakage from the reservoirs provides maximum protection for USDWs. A primary purpose of this dissertation is to quantify possible risks of CO_2 leakage to USDWs, specifically risks associated with chemical impacts.

Wellbore provides possible leakage pathways for CO_2, and its integrity is a key risk factor for geological CO_2 storage. This dissertation firstly presents an analysis on the impacts of CO_2 leakage through wellbore cement and surrounding caprock with a gap (annulus) in between. Mechanisms of chemical reactions associated with cement-CO_2-brine interactions are predicted, and wellbore integrity under CO_2-rich conditions is analyzed with a case study example – the Farnsworth CO_2 enhanced oil recovery (EOR) unit (FWU) in the northern Anadarko Basin in Texas.

The second part of this dissertation focuses on quantification of possible risks of CO_2 leakage through fractured wellbores to overlying USDWs. To understand how CO_2 is likely to influence geochemical processes in aquifer sediments, a response surface methodology (RSM) with geochemical simulations is used to quantify associated risks. The case study example for this analysis is the Ogallala aquifer overlying the FWU.

Increased CO_2 concentrations in shallow groundwater aquifers could result in release and mobilization of toxic trace metals. This dissertation also presents an integrated framework of combined batch experiments and reactive transport simulations to quantify trace metal mobilization responses to CO_2 leakage into USDWs. The mechanisms of trace metal mobilization are elucidated, and the key parameters are quantified. The case study includes elevated CO_2 conditions at the Chimayo site in northern New Mexico, a natural analog with CO_2 upwelling.

TABLE OF CONTENTS

ACKNOWLEDGEMENTS

Firstly, I would like to express my most sincere appreciation to my advisor, Dr. Brian McPherson, for his support, encouragements, and trust. Brian is not only an advisor for me, but also a friend. He has plenty of good ideas, which are significant for my research. During my five-year study, I have spent a pleasant time working with him, and I also learned a lot from him.

I would like to thank Drs. Zhenxue Dai and Hari Viswanathan of Los Alamos National Laboratory for their help with my dissertation. They provided great ideas and useful skills for me. I appreciate their time and effort for my research.

I want to thank my supervisory committee, Drs. Steve Burian, Andy Hong, Edward Trujillo, Diana Bacon, and Tianfu Xu, who gave me valuable comments and suggestions on all of my manuscript drafts and dissertation. Also thanks to Dr. Amanda Bordelon at the University of Utah for her precious ideas on cement chemical reactions.

Our research group, CSERs of University of Utah, always gave me good ideas and help when I needed suggestions and assistance. I would like to thank you all – Rich Esser, Wei Jia, Trevor Irons, Feng Pan, Nate Moodie, Dan Stout, Richard Franz, Seongjun Lee, and Megan Walsh.

I would like to thank all collaborators of the Southwest Regional Partnership on Carbon Sequestration (SWP), and colleagues of the New Mexico Institute of Mining and Technology.

I would like to express my deepest and most special appreciation to my husband, Lei Xu, for his unreserved love, support, and encouragements. He also shared all my good and bad moments and gave me hopes for the future.

Finally, I would like to express my acknowledgement to my parents for all of their support and understanding of my decisions.

CHAPTER 1

INTRODUCTION

Global warming and climate change are known to be caused by emissions of greenhouse gases (CO_2, CH_4, N_2O, etc.) into the atmosphere, at least in part. Carbon dioxide (CO_2) is the primary greenhouse gas emitted through human activities (EPA, 2017). From 1990 to 2015, total gross U.S. CO_2 emission increased by 5.6 %, with about 5,410 million metric tons (MMT) of CO_2 emitted in 2015 (EPA, 2017). Fossil fuel combustion from centralized sources contributes up to 93% of the total CO_2 emission (EPA, 2017).

To avoid further global warming, reducing CO_2 emission, especially from stationary sources such as power plants, is desirable. Carbon capture, utilization, and storage (CCUS) technologies are believed to play a critical role for mitigating such CO_2 emissions (Litynski et al., 2013; NETL, 2015). Geologic CO_2 sequestration (GCS), as one of the sequestration options, has gained much attention because of its feasibility and capacity (Bachu, 2000). Enhanced Oil Recovery (EOR) with CO_2 (CO_2-EOR), as one of the GCS targets, offers the potential economic benefit of increased oil production, which may offset some costs of CO_2 capture and storage, and has become a promising method for CCUS (IPCC, 2005).

1.1 Potential Risks of CO_2 Leakage

CO_2 leakage through caprock or wellbores from CO_2 storage reservoirs (sealing integrity) is considered as a key risk factor by many studies, and wells are identified as a greater risk than geological features such as faults and fractures (Bachu and Watson, 2009; Viswanathan et al., 2008; Wigand et al., 2009). Wells in oil fields are usually completed with Portland cement as sealing material with portlandite ($Ca(OH)_2$) and calcium-silicate-hydrate (CSH) as the main components (Scherer et al., 2005). When attacked by CO_2, portlandite and CSH would degrade sequentially and form calcite and hydrated silica gel, which may impact the cement structural integrity (Carey et al., 2007; Kutchko et al., 2007).

Most GCS sites are overlain by groundwater aquifers. Another major concern of CCUS application is the risk of CO_2 leakage from deep sequestration reservoirs through highly-permeable zones into overlying Underground Sources of Drinking Water (USDW). CO_2 itself is not hazardous to water quality, but increased CO_2 concentrations in shallow groundwater aquifers could reduce pH and enhance geochemical reactions between groundwater and aquifer sediments, resulting in release and mobilization of toxic trace metals (Little and Jackson, 2010; Zheng et al., 2009).

Multiple environmental variables such as wellbore properties, aquifer geology, mineralogy, and groundwater chemistry play an important role in the responses of wellbores and groundwater to CO_2 leakage (Bacon et al., 2014; Carroll et al., 2016; Frye et al., 2012). These geological variables suggest site-specific uncertainty/risk assessment is essential for safe and effective application of carbon sequestration (Little and Jackson, 2010; Wilkin and Diguilio, 2010).

1.2 Research Approaches

Specific research interests of impacts of CO_2 leakage include CO_2 leakage rate assessment, CO_2-wellbore cement interactions, impacts of CO_2 leakage into overlying USDWs, and early detection criteria. To date, most research on such assessments rely on lab-scale experiments (Bachu and Bennion, 2009; Frye et al., 2012; Little and Jackson, 2010), field-scale tests (Carey et al., 2007; Yang et al., 2013; Zheng et al., 2012), and numerical modeling (Bacon et al., 2016; Carey and Lichtner, 2007; Viswanathan et al., 2012). However, these approaches have their own disadvantages. For example, lab-scale experiments are usually conducted under ambient pressure and temperature, and with well-mixed water-sediment systems, the water-rock-CO_2 interactions are not fully representative of geochemically heterogeneous sediment system with flow (Trautz et al., 2013; Yang et al., 2014); field-scale tests are often with a longer experimental cycle, and the test water tends to mix with local groundwater which might affect the results (Mickler et al., 2013); simulations results are not necessarily representative of a realistic case because simplified models are usually used (Yang et al., 2014).

To overcome the defects of these study approaches listed above, modeling approaches combined with laboratory/field observations and site-specific uncertainty assessments are of interest for safe and effective application of carbon sequestration in recent research (Wilkin and Diguilio, 2010). Carey et al. (2007) collected one cement core sample recovered from a well exposed to CO_2-rich brine at the SACROC CO_2-EOR site, which provides an opportunity to investigate the performance of CO_2-cement interaction with a real case calibration. Carroll et al. (2014) discussed the probability of detecting a CO_2 leakage plume into groundwater aquifer with multi-phase flow and reactive transport

simulations combined with reduced order models. They also introduced “impact thresholds” for a no-impact contaminant level based on site-specific data, which is easier for assessing the site-specific groundwater quality change. Yang et al. (2014) developed an inverse multicomponent geochemical modeling approach to interpret responses of water chemistry to the introduction of CO_2 into a set of laboratory batch reactors containing carbonate-poor and carbonate-rich potable aquifer sediments.

In this dissertation, modeling approaches calibrated with laboratory and field observation data and uncertainty assessments are applied to quantify uncertainty and forecast the responses of wellbore cement and overlying USDWs to CO_2 leakage from the reservoir. Results of this study are intended to improve ability to quantify risks associated with potential leakage of CO_2 from reservoirs.

1.3 Overview

Geologic carbon storage site options usually include not only storage reservoirs bounded by effective seal layers, but also Underground Sources of Drinking Water (USDWs). An effective risk assessment of potential CO_2 leakage from the reservoirs provides maximum protection for USDWs. A primary purpose of this dissertation is to quantify possible risks of CO_2 leakage to USDWs, specifically risks associated with chemical impacts. This dissertation contains five chapters, including an introduction, three published journal articles, and a general conclusion.

Chapter 1 (this chapter) introduces the concepts of CCUS, GCS, CO_2-EOR, and potential risks of CO_2 leakage from a storage reservoir. The significance of uncertainty analysis by combining simulation and experimental/field observation data is also

emphasized in this chapter.

In Chapter 2, impacts on wellbore integrity under CO_2-rich conditions within an operational time scale are analyzed, and mechanisms of chemical reactions associated with cement-CO_2-brine interactions are also discussed. Key parameters for cement-CO_2 interactions are verified with a cement core sample exposed to CO_2 for 30 years. The uncertainty of wellbore integrity is also analyzed for the Farnsworth CO_2 enhanced oil recovery (EOR) unit (FWU) in the northern Anadarko Basin in Texas.

Chapter 3 applies an effective risk assessment to quantify possible risks to USDWs, specifically risks associated with chemical impacts on USDWs by reduced order models (ROM). The case study example for this analysis is the Ogallala aquifer overlying the FWU, and water chemistry factors for early detection criteria are also identified.

In Chapter 4, an integrated framework of combined batch experiments and reactive transport simulations is developed to quantify water-rock-CO_2 interactions and arsenic (As) mobilization responses to CO_2 and/or saline water leakage into USDWs. This study is intended to improve ability to quantify risks associated with potential leakage of reservoir fluids into shallow aquifers, in particular the possible environmental impacts of As mobilization at carbon sequestration sites.

Chapter 5 summarizes the general conclusions and recommendations for all three chapters presented in this dissertation.

1.4 References

Bachu, S., 2000. Sequestration of CO2 in geological media: Criteria and approach for site selection in response to climate change. Energy Convers. Manage. 41 (9), 953-970.

Bachu, S., Bennion, D. B., 2009. Experimental assessment of brine and/or CO2 leakage through well cements at reservoir conditions. Int. J. Greenh. Gas Control 3, 494-501.

Bacon, D. H., Dai, Z., Zheng, L., 2014. Geochemical impacts of carbon dioxide, brine, trace metal and organic leakage into an unconfined, oxidizing limestone aquifer. Energy Procedia 63, 4684-4707.

Bacon, D. H., Qafoku, N. P., Dai, Z., Keating, E. H., Brown, C. F., 2016 Modeling the impact of carbon dioxide leakage into an unconfined, oxidizing carbonate aquifer. Int. J. Greenhouse Gas Control 44, 290-299.

Carey J. W., Lichtner, P. C., 2007. Calcium silicate hydrate (C-S-H) solid solution model applied to cement degradation using the continuum reactive transport model FLOTRAN. In: Mobasher, B. and Skalny, J. (Eds), Transport Properties and Concrete Qeality: Materials Science of Concrete, Special Volume. American Ceramic Society, John Wiley & Sons, Inc., Hoboken, NJ, USA. pp. 73-106

Carey, J. W., Wigand, M., Chipera, S. J., WoldeGabriel, G., Pawar, R., Lichtner, P. C., Wehner, S. C., Raines, M. A., Guthrie Jr., G. D., 2007. Analysis and performance of oil well cement with 30 years of CO2 exposure from the SACROC Unit, West Texas, USA. Int. J. Greenh. Gas Control 1, 75-85.

Carroll, S. A., Keating, E., Mansoor, K., Dai, Z., Sun, Y., Trainor-Guitton, W., Brown, C., Bacon, D., 2014. Key factors for determining groundwater impacts due to leakage from geologic carbon sequestration reservoirs. Int. J. Greenh. Gas Control 29, 153-168.

Carroll, S., Carey, J. W., Dzombak, D., Huerta, N. J., Li, L., Richard, T., Um, W., Walsh, S. D. C., Zhang, L., 2016. Review: Role of chemistry, mechanics, and transport on well integrity in CO2 storage environments. Int. J. Greenh. Gas Control 49, 149-160.

EPA, 2017. Draft Inventory of U.S. Greenhouse Gas Emissions and Sinks: 1990-2015. https://www.epa.gov/ghgemissions/draft-inventory-us-greenhouse-gas-emissions-and-sinks-1990-2015 (accessed 03/23/2017).

Frye, E., Bao, C., Li, L., Blumsack, S., 2012. Environmental controls of cadmium desorption during CO2 leakage. Environ. Sci. Technol. 46, 4388-4395.

Kutchko, B. G., Strazisar, B. R., Dzombak, D. A., Lowry, G. V., Thaulow, N., 2007. Degradation of well cement by CO2 under geologic sequestration conditions; Environ. Sci. Technol. 41, 4787-4792.

Little, M. G., Jackson, R. B., 2010. Potential impacts of leakage from deep CO2 geosequestration on overlying freshwater aquifers. Environ. Sci. Technol. 44(23), 9225-9232.

Litynski, J., Rodosta, T., Vikara, D., Srivastava, R., 2013. U.S. DOE's R&D program to develop infrastructure for carbon storage: overview of the regional carbon sequestration partnerships and other R&D field projects. Energy Procedia 37, 6527-6543.

Mickler, P. J., Yang, C., Scanlon, B. R., Reedy, R., Lu, J., 2013. Potential impacts of CO2 leakage on groundwater chemistry from laboratory batch experiments and field push-pull tests. Environ. Sci. Technol. 47, 10694-10702.

NETL, 2015. Carbon storage atlas, 5th ed. National energy technology laboratory, Morgantown, WV, USA. Available at http://www.netl.doe.gov/research/coal/carbon-storage/atlasv (accessed 03/23/2017).

Scherer, G. W., Celia, M. A., Prévost, J. H., Bachu, S., Bruant, R. G., Duguid, A., Fuller, R., Gasda, S. E., Radonjic, M., Vichit-Vadakan, W., 2005. Leakage of CO2 through abandoned wells: Role of corrosion of cement. In: Thomas, D. C., Benson, S. M. (Eds), Carbon Dioxide Capture for Storage in Deep Geologic Formations, vol. 2. Elsevier Ltd, Amsterdam, Netherland. pp. 827-848.

Trautz, R. C., Pugh, J. D., Varadharajan, C., Zheng, L., Bianchi, M., Nico, P. S., Spycher, N. F., Newell, D. L., Esposito, R. A., Wu, Y., Dafflon, b., Hubbard, S. S., Birkholzer, J. T., 2013. Effect of dissolved CO2 on a shallow groundwater system: A controlled release field experiment. Environ. Sci. Technol. 47 (1), 298-305.

Viswanathan, H., Dai, Z., Lopano, C., Keating, E., Hakala, J. A., Scheckel, K. G., Zheng, L., Guthrie, G. D., Pawar, R.. 2012. Developing a robust geochemical and reactive transport model to evaluate possible sources of arsenic at the CO2 sequestration natural analog site in Chimayo, New Mexico. Int. J. Greenhouse Gas Control 10, 199-214.

Viswanathan, H. S., Pawar, R. J., Stauffer, P. H., Kaszuba, J. P., Carey, J. W., Olsen, S. C., Keating, G. N., Kavetski, D., Guthrie, G. D., 2008. Development of a hybrid process and system model for the assessment of wellbore leakage at a geologic CO2 sequestration site. Environ. Sci. Technol. 42, 7280-7286.

Wigand, M., Kaszuba, J. P., Carey, J. W., Hollis, W. K., 2009. Geochemical effects of CO2 sequestration on fractured wellbore cement at the cement/caprock interface. Chem. Geol. 265, 122-133.

Wilkin, R.T., Digiulio, D.C., 2010. Geochemical impacts to groundwater from geologic carbon sequestration: controls on pH and inorganic carbon concentrations from reaction path and kinetic modeling. Environ. Sci. Technol. 44, 4821-4827.

Yang, C., Dai, Z., Romanak, K. D., Hovorka, S. D., Treviño, R. H., 2014. Inverse modeling of water-rock-CO2 batch experiments: Potential impacts on groundwater resources at carbon sequestration sites. Environ. Sci. Technol. 48, 2798-2806.

Yang, C., Mickler, P., Reedy, R., Scanlon, B. R., Romanak, K. D., Nicot, J. P., Hovorka, S. D., Larson, T., 2013. Single-well push-pull test for assessing potential impacts of CO2 leakage on groundwater quality in a shallow gulf coast aquifer in Cranfield, Mississippi. Int. J. Greenhouse Gas Control 18, 375-387.

Zheng, L., Apps, J. A., Zhang, Y., Xu, T., Birkholzer, J. T., 2009. On mobilization of lead

and arsenic in groundwater in response to CO2 leakage from deep geological storage. Chem. Ceol. 268, 281-297.

Zheng, L., Apps, J. A., Spycher, N., Birkholzer, J. T., Kharaka, Y. K., Thordsen, J., Beers, S. R., Herkelrath, W. N., Kakouros, E., Trautz, R.C., 2012. Geochemical modeling of changes in shallow groundwater chemistry observed during the MSU-ZERT CO2 injection experiment. Int. J. Greenhouse Gas Control 7, 202-217.

CHAPTER 2

QUANTIFICATION OF CO_2-CEMENT-ROCK INTERACTIONS AT THE WELL-CAPROCK-RESERVOIR INTERFACE AND IMPLICATIONS FOR GEOLOGICAL CO_2 STORAGE

Reprinted from International Journal of Greenhouse Gas Control 63, Ting Xiao, Brian McPherson, Amanda Bordelon, Hari Viswanathan, Zhenxue Dai, Hailong Tian, Rich Esser, Wei Jia, William Carey, Quantification of CO_2-cement-rock interactions at the well-caprock-reservoir interface and implications for geological CO_2 storage, 126-140, 2017, with permission from Elsevier. https://doi.org/10.1016/j.ijggc.2017.05.009.

Carbon dioxide (CO_2) leakage through wellbores and surrounding caprock from CO_2 storage reservoirs is considered as a key risk factor for geological CO_2 storage. Carbon dioxide can react with wellbore cement, and with the degradation of the cement, it might lose its structural integrity and provide extra leaking pathways for CO_2. It is important to investigate the performance of CO_2-cement interactions and analyze the potential risks for CO_2 leakage through wellbore cement.

In this chapter, we analyze the impacts of CO_2 leakage through wellbore cement and surrounding caprock with a gap (annulus) in between. Key parameters for cement-CO_2 interactions are verified with the cement core sample from the SACROC Unit exposed to CO_2 for 30 years, and such parameters are used in our reactive transport simulations for forecasting the wellbore structural integrity. The Farnsworth Unit (FWU), an oilfield in the northern Anadarko Basin in Texas undergoing active CO_2 enhanced oil recovery (EOR), is selected as a case study.

International Journal of Greenhouse Gas Control 63 (2017) 126–140

Contents lists available at ScienceDirect

International Journal of Greenhouse Gas Control

journal homepage: www.elsevier.com/locate/ijggc

Quantification of CO_2-cement-rock interactions at the well-caprock-reservoir interface and implications for geological CO_2 storage

Ting Xiao[a,b], Brian McPherson[a,b,*], Amanda Bordelon[a], Hari Viswanathan[c], Zhenxue Dai[c,d], Hailong Tian[d], Rich Esser[a,b], Wei Jia[a,b], William Carey[c]

[a] Department of Civil and Environmental Engineering, University of Utah, Salt Lake City, UT, 84112, USA
[b] Energy and Geoscience Institute, University of Utah, Salt Lake City, UT, 84108, USA
[c] Earth and Environmental Sciences Division, Los Alamos National Laboratory, Los Alamos, NM, 87545, USA
[d] Key Laboratory of Groundwater Resources and Environment, Ministry of Education, Jilin University, Changchun, Jilin, China

ARTICLE INFO

Keywords:
Wellbore integrity
CO_2 leakage
Cement-caprock interface
Reactive transport simulation

ABSTRACT

Wellbore integrity is a key risk factor for geological CO_2 storage. A primary purpose of this study is to analyze the impacts of CO_2 leakage through wellbore cement and surrounding caprock with a gap (annulus) in between. Key parameters for cement-CO_2 interactions were verified with a cement core sample from the SACROC Unit exposed to CO_2 for 30 years. These parameters and other data served as the basis of reactive transport model simulations. The case study example for this analysis is the Farnsworth CO_2 enhanced oil recovery (EOR) unit (FWU) in the northern Anadarko Basin in Texas. Specific objectives of this study are: (1) to analyze impacts on wellbore integrity under CO_2-rich conditions within an operational time scale; and (2) to predict mechanisms of chemical reactions associated with cement-CO_2-brine interactions.

Simulation results suggest that cement tortuosity and diffusion coefficient are the two most important parameters that dictate cement carbonation penetration distance. Portlandite ($Ca(OH)_2$) reacts with CO_2 and forms calcite, reducing porosity, in turn directly impacting CO_2 leakage rates by infilling pathways. Simulated calcium-silicate-hydrate (CSH) degradation is limited, suggesting that a wellbore will maintain its integrity and structure under the considered conditions. Simulations also suggest that sulfate concentration < 2500 mg/L in the leaking brine would not cause monosulfate degradation. Without an existing fracture, CO_2 will likely not enter the caprock, and the cement would not degrade accordingly. For the FWU specifically, the wellbore cement would likely keep its structure and integrity after 100 years. However, if a fracture exists at the cement-caprock interface, calcite dissolution in the limestone caprock fracture could occur and increase the fracture volume, a concern for caprock integrity.

1. Introduction

Carbon capture, utilization, and storage (CCUS) technologies are believed to play a critical role for mitigating CO_2 emissions from stationary sources (Litynski et al., 2013; NETL, 2015). Particularly, CO_2-enhanced oil recovery (CO_2-EOR) with CO_2 injected into oil reservoirs is a well-established and relatively mature technology that offers potential economic benefits of increasing oil production and reducing the cost of CO_2 storage (NETL, 2012; Dai et al., 2014, 2016). CO_2 leakage through caprock or wellbores from CO_2 storage reservoirs (sealing integrity) is considered as a key risk factor by many studies, and wells are identified as a greater risk than geological features such as faults and fractures (Bachu and Watson, 2009; Viswanathan et al., 2008; Wigand et al., 2009).

Wells in oil fields are usually completed with Portland cement as sealing material (Scherer et al., 2005). After hydration, portlandite ($Ca(OH)_2$) and calcium-silicate-hydrate (CSH) become the main components that react with CO_2 to form calcite and hydrated silica gel (Bertos et al., 2004; Kutchko et al., 2007). Reactions of cement carbonation (degradation) are summarized in Eqs. (1)–(4) (Kutchko et al., 2007). This process is a complex function of the cement properties (density, alkalinity and others), fluid dynamics, reaction kinetics, and stress state of the wellbore environment (Carey et al., 2010; Carroll et al., 2016; Li, 2011). In particular, portlandite and CSH are dissolved sequentially, and with the calcite ($CaCO_3$) precipitation, porosity and permeability decrease to provide a less permeable front to the acid attack. After portlandite has been depleted, CSH starts to react with CO_2 and form hydrated silica gel, which may impact the cement structural integrity

* Corresponding author at: Department of Civil and Environmental Engineering, University of Utah, Salt Lake City, UT, 84112, USA.
E-mail address: b.j.mcpherson@utah.edu (B. McPherson).

http://dx.doi.org/10.1016/j.ijggc.2017.05.009
Received 24 February 2017; Received in revised form 4 May 2017; Accepted 12 May 2017

(Carey et al., 2007; Kutchko et al., 2007).

$$CO_{2(aq)} + H_2O \rightarrow HCO_3^- + H^+ \quad (1)$$

$$Ca(OH)_{2(s)} \rightarrow Ca^{2+} + 2OH^- \quad (2)$$

$$Ca^{2+} + HCO_3^- + OH^- \rightarrow CaCO_{3(s)} + H_2O \quad (3)$$

$$H^+ + CSH_{(s)} \rightarrow Ca^{2+} + H_2O + SiO_2{\cdot}H_2O_{(s)} \quad (4)$$

Wellbore cement integrity and cement-CO_2 interactions under CO_2-rich environment were studied via experiments (Bachu and Bennion, 2009; Carey et al., 2010; Huerta et al., 2016; Kutchko et al., 2007, 2008; Li et al., 2015; Rimmelé et al., 2008; Wigand et al., 2009), simulations (Cao et al., 2015; Carey and Lichtner, 2007; Huet et al., 2010; Viswanathan et al., 2008; Wertz et al., 2013), and field analyses (Carey et al., 2007). Specific research interests of these studies include possible degradation mechanisms and reaction pathways, CO_2 penetration rate and wellbore integrity, and geological variables that impact CO_2-cement interactions. In particular, the cement core sample recovered from a well exposed to CO_2-rich brine at the SACROC CO_2-EOR site (Carey et al., 2007) provides an opportunity to investigate the performance of CO_2-cement interaction with a real case. The uncertainties of the reservoir and cement properties (such as interface between CO_2 and cement, the size of opening to let CO_2 access, brine composition, reaction kinetics, and diffusion/advection) require sensitivity/uncertainty analysis with site-specific conditions and further quantifications of the roles of these factors. Carey et al. (2007) applied a one-dimensional model and considered tortuosity and porosity of the cement with mineral reaction rates as key variables controlling the reactions. However, the process of fluid migration upwards was neglected in their study. We suggest that it is appropriate to predict how far CO_2 could migrate (the sample was taken from 4 to 6 m above the reservoir). The Carey model also neglected the impact of brine composition (brine is flowing in the reservoir with various compositions at different locations) and the possible concentration of CO_2 in the brine. Thus, we suggest that a 2-D (at least) model is necessary to discuss the impacts of upward migration of CO_2 and the brine composition to cement degradation.

To understand the mechanisms of cement degradation under CO_2 sequestration conditions in CO_2-EOR reservoirs, geochemical models of wellbore cement-caprock-reservoir interface were developed. Specific objectives of this study include: (1) to understand how CO_2 is likely to influence wellbore cement degradation and wellbore integrity; (2) to analyze the effects of possible uncertainty parameters that control reaction characteristics; and (3) to verify/calibrate the numerical simulation model with results from the SACROC field study and to confirm that numerical modeling is an effective tool for forecasting wellbore cement-CO_2-brine interactions in other cases. Finally, the Farnsworth Unit (FWU), an oilfield in the northern Anadarko Basin in Texas undergoing active CO_2 enhanced oil recovery (EOR) is selected as a case study. However, because we do not have cement samples from the FWU, we assigned cement material parameters based on the SACROC sample because both of the two sites use Portland cement for well casing. All simulations were performed with TOUGHREACT V2 (Xu et al., 2011) and an equation of state for multiphase CO_2 and brine, ECO2N (Pruess, 2005).

2. Methods

2.1. The SACROC Unit

The SACROC Unit is located in the Permian Basin, western Texas (Vest, 1970). The Wolfcamp Shale Formation of the lower Permian forms the low permeability caprock above the Pennsylvanian limestone Cisco and Canyon formations of the reservoir at about 2400 m depth, with an average 240 m in thickness (Han et al., 2010; Jia et al., 2016; Jia et al., 2017). The reservoir temperature is about 54 °C, and the pressure is about 18 MPa (Carey et al., 2007). The operational well focused on by Carey et al. (2007) was drilled in 1950 with Portland cement, and was exposed to CO_2 since 1975 during a 17-year CO_2 injection. The core sample of the wellbore cement and caprock was collected after 30 years of CO_2 exposure.

Table 1
1-D model grid specifications.

Rock domain	Number of elements	Thickness (mm)	Grid name
Cement	4	10	A11 1 – A11 4
Cement	10	1	A11 5 – A1114
Fracture	2	2	A1115 – A1116
Fracture	1	4	A1117
Fracture	1	8	A1118
Fracture	1	20	A1119
Fracture	1	50	A1120
Fracture	1	120	A1121

2.2. SACROC simulation verification

To reproduce and extend the simulation results of Carey et al. (2007), a one-dimensional model was created. The initial and boundary conditions were mostly based on the design and specifications discussed in Carey et al. (2007) and Carey and Lichtner (2007). The model included 0.05 m CO_2-free cement (porosity = 30%, permeability = 10^{-17} m^2) adjacent to a 0.2 m CO_2 saturated shale-fragment zone (porosity = 70%, permeability = 10^{-13} m^2) with 21 grid cells (Table 1, Fig. 1). Simulation thermodynamic conditions included 18 MPa pressure and 50 °C temperature, to mimic in-situ conditions. Note that 25 °C temperature was assigned by Carey et al. (2007) and Carey and Lichtner (2007), and we deviated from this specification. Cement tortuosity was set at 0.0004 (Carey et al., 2007), and the diffusion coefficient for aqueous species was set at 10^{-9} m^2/s (Gherardi et al., 2007). Molecular diffusion was considered as the only mechanism for mass transport in this case.

The van Genuchten-Mualem model and Corey's model were selected for aqueous and gas relative permeability calculations, respectively; the van Genuchten function was selected for capillary pressure calculations (Pruess et al., 2012). Specific settings for this model are summarized in Table 2.

The initial cement and fractured caprock mineralogy is summarized in Table 3. The Ca/Si ratio for CSH used in this study was 1.7 (Allen et al., 2007), which was slightly different than the Ca/Si = 1.77 used in Carey and Lichtner (2007). Mineral reaction rates were determined by reaction kinetics and mineral surface area in this study. Rather than neglecting the surface area of minerals (Carey et al., 2007), both kinetic rate law and surface area were considered. Assuming spherical grains of the minerals, specific surface area (SSA) of each mineral was calculated by (Labus and Bujok, 2011):

$$\mathrm{SSA} = \frac{\mathrm{A}\cdot\mathrm{v}}{V\cdot MW} \quad (5)$$

where A is spherical area, v is molar volume, V is sphere volume, and MW is molecular weight. Molar volume and molecular weight of each mineral were obtained from EQ3/6 database (Wolery, 1992). In this study, the mineral surface areas were changed to analyze their impacts on geochemical reactions. In the verification case, minerals were assumed as spheres with 1 mm diameter. The brine in the shale was set to equilibrium with saturated CO_2, according to the initial fluid composition assessed by Carey and Lichtner (2007). The initial cement fluid chemistry was also calculated for equilibrium conditions of cement minerals. The initial fluid compositions are summarized in Table 4.

Porosity and permeability may change due to the mineral precipita-

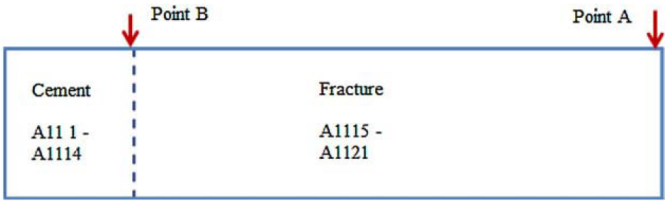

Fig. 1. The 1-D conceptual model set-up.

Table 2
Relative permeability and capillary pressure function settings (Gherardi et al., 2007).

Relative permeability				
Rock domain	λ	S_{lr}	S_{ls}	S_{gr}
Cement	0.457	0.3	1.0	0.05
Fracture	0.457	0.3	1.0	0.05

Capillary pressure					
Rock domain	λ	S_{lr}	S_{ls}	$1/P_0$	P_{max}
Cement	0.457	0.0	0.999	1.6×10^{-7}	10^8
Fracture	0.457	0.0	0.999	5.1×10^{-5}	10^7

tion/dissolution. In the simulations of this study, permeability change was approximated via porosity change as (Xu et al., 2012):

$$k = k_i\left(\frac{\phi}{\phi_i}\right)^3 \tag{6}$$

where k_i and ϕ_i are the initial permeability and porosity, and k and ϕ are the modified permeability and porosity, respectively.

2.3. Impacts of key variables

It is likely that CO_2 diffusion from a fracture is the most significant transport process when it degrades the wellbore cement (Carey et al., 2007; Wertz et al., 2013). In this study, CO_2 flow was considered to be controlled by diffusion. Diffusivity, mineral particle size (surface area), permeability of cement and fractured caprock, fractured caprock porosity, boundary conditions and brine chemistry were considered as the subject factors for a sensitivity analysis of CO_2-cement reaction characteristics. The model applied for the sensitivity analysis was the 1-D model described in the previous section (Table 1), with specific initial conditions listed in Table 5. Specifically, different mineral sizes considered in this study were set within the range of cement particle sizes (Sobolev and Gutiérrez, 2005). The base case followed the settings of the simulation of Carey et al. (2007). Reasons for these specific settings of diffusivity and brine chemistry are discussed in the following sections.

2.3.1. Diffusivity for aqueous species

In general, molecular diffusion plays a significant role when advective flow across the cement is insignificant. In the case of wellbore cements exposed to CO_2, advection is insignificant unless fractures are present, and thus diffusion was explicitly included in all simulations. Diffusive flux of chemical mass is proportional to the concentration gradient and diffusion coefficient (Fick's law):

$$f = -d\nabla C \tag{7}$$

where f is the diffusive flux, d is effective diffusivity, and C is the concentration of the subject ion. In the subsurface, diffusion occurs within a porous medium, and the tortuosity of the flow path increases the diffusion distance, thus tortuosity (τ) and porosity (ϕ) of the porous

Table 3
Summary of simulated initial mineral abundance and reaction rate constants.

Mineral	Volume fraction (% of solid)	Kinetic rate law								Source[a]
		Neutral		Acid			Base			
		k25 (mol/(m^2 s))	Ea (kJ/mol)	k25	Ea	n (H^+)	k25	Ea	n (H^+)	
Shale										
Illite	66.0	1.660×10^{-13}	35.0	1.047×10^{-11}	23.6	0.34	3.020×10^{-17}	58.9	−0.40	1
Quartz	22.0	1.259×10^{-14}	87.5							1
Albite	4.4	2.754×10^{-13}	69.8	6.920×10^{-11}	65.0	0.457	2.510×10^{-16}	71.0	−0.472	1
Kaolinite	3.3	6.918×10^{-14}	22.2	4.898×10^{-12}	65.9	0.777	8.912×10^{-18}	17.9	−0.472	1
Calcite	2.2	1.600×10^{-6}	23.5	0.501	14.4	1.0				1
Dolomite	2.2	2.951×10^{-8}	52.2	6.456×10^{-4}	36.1	0.5				1
Cement										
CSH	54.1	1.000×10^{-12}	38.0							2
Portlandite	22.0	1.000×10^{-6}	1.122							3
Monosulfate	19.3	1.14×10^{-12}	40.0							3
Kaotite	4.7	1.600×10^{-18}	0.0	5.940×10^{-8}	0.0	0.275				4
Secondary										
SiO_2 (am)	0.0	3.66×10^{-13}	73.06							1
Gypsum	0.0	1.620×10^{-3}	0.0							1
Gibbsite	0.0	3.160×10^{-12}	61.2	2.240×10^{-8}	47.5	0.992	2.240×10^{-17}	80.1	−0.784	1
Friedel's Salt	0.0	1.000×10^{-12}	0.0							5
Ettringite	0.0	1.14×10^{-12}	40.0							2
Brucite	0.0	5.750×10^{-9}	42.0	1.860×10^{-5}	59.0	0.5				1
Dawsonite	0.0	1.000×10^{-7}	62.8							1
Magnesite	0.0	4.570×10^{-10}	23.5	4.170×10^{-7}	14.4	1.0				1

[a] Source: 1 Palandri and Kharaka (2004); 2 Baur et al. (2004); 3 Regnault et al. (2009); 4 Wertz et al. (2013); 5 Carey and Lichtner (2007).

Table 4
Initial fluid compositions assigned in the simulations (unit: mol/kg).

Name	Concentration in shale	Concentration in cement	Name	Concentration in shale	Concentration in cement
pH (unitless)	5.69	11.66	Ca^{2+}	1.4×10^{-3}	5.8×10^{-3}
Mg^{2+}	7.3×10^{-5}	1.0×10^{-7}	Na^{+}	1.3	1.0×10^{-12}
K^{+}	1.1×10^{-1}	1.0×10^{-12}	Fe^{2+}	1.0×10^{-10}	5.3×10^{-12}
SiO_2 (aq)	1.0×10^{-3}	1.0×10^{-5}	HCO_3^{-}	1.7	2.7×10^{-5}
NO_3^{-}	1.0×10^{-10}	1.0×10^{-10}	SO_4^{2-}	5.9×10^{-3}	3.3×10^{-5}
Cl^{-}	1.7	1.0×10^{-12}	AlO_2^{-}	2.3×10^{-10}	1.5×10^{-3}

Table 5
Simulated cases for the reaction characteristics analysis.

	Mineral size (mm)	Shale porosity	Cement tortuosity	Cement diffusion coefficient (aqueous) (m^2/s)	Cement permeability	Shale permeability	CO_2 source saturation	Shale length (cm)
Base	1	0.7	0.0004	10^{-9}	10^{-17}	10^{-13}	0	20
Tort1	1	0.7	0.04	10^{-9}	10^{-17}	10^{-13}	0	20
Tort2	1	0.7	0.004	10^{-9}	10^{-17}	10^{-13}	0	20
Tort3	1	0.7	0.00004	10^{-9}	10^{-17}	10^{-13}	0	20
Tort4	1	0.7	Default	10^{-9}	10^{-17}	10^{-13}	0	20
Diff1	1	0.7	0.0004	10^{-10}	10^{-17}	10^{-13}	0	20
Diff2	1	0.7	0.0004	10^{-11}	10^{-17}	10^{-13}	0	20
SSA1	0.1	0.7	0.0004	10^{-9}	10^{-17}	10^{-13}	0	20
SSA2	0.01	0.7	0.0004	10^{-9}	10^{-17}	10^{-13}	0	20
Bound1	1	0.7	0.0004	10^{-9}	10^{-17}	10^{-13}	0	∞
Bound2	1	0.7	0.0004	10^{-9}	10^{-17}	10^{-13}	0	1
Poro1	1	0.3	0.0004	10^{-9}	10^{-17}	10^{-13}	0	20
Poro2	1	0.09	0.0004	10^{-9}	10^{-17}	10^{-13}	0	20
Perm1	1	0.7	0.0004	10^{-9}	10^{-18}	10^{-13}	0	20
Perm2	1	0.7	0.0004	10^{-9}	10^{-17}	10^{-14}	0	20
Sg1	1	0.7	0.01	10^{-11}	10^{-17}	10^{-13}	0	20
Sg2	1	0.7	0.01	10^{-11}	10^{-17}	10^{-13}	0.3	20
Sg3	1	0.7	0.01	10^{-11}	10^{-17}	10^{-13}	0.5	20
Sg4	1	0.7	0.01	10^{-11}	10^{-17}	10^{-13}	0.9	20
Chem1-11	1	0.7	0.0004	10^{-9}	10^{-17}	10^{-13}	0	20

media must be considered (Ingebritsen et al., 2006). The multiphase diffusion equation solved by TOUGHREACT is (Pruess et al., 2012):

$$f_\beta^\kappa = -\phi\tau_0\tau_\beta\rho_\beta d_\beta^\kappa \nabla X_\beta^\kappa \tag{8}$$

where ϕ is porosity, $\tau_0\tau_\beta$ is the tortuosity that includes a porous medium dependent factor τ_0 and a coefficient that depends on phase saturation S_β, $\tau_\beta = \tau_\beta(S_\beta)$, ρ_β is density, d_β^κ is the diffusion coefficient of component κ in bulk fluid phase β, and X_β^κ is the mass fraction of component κ in phase β.

If no tortuosity factor is assigned explicitly, a porosity and saturation-dependent tortuosity are calculated internally (Pruess et al., 2012) via

$$\tau_0\tau_\beta = \phi^{1/3}S_\beta^{10/3} \tag{9}$$

In this study, initial porosity of the cement was assigned to be 0.3 (Carey and Lichtner, 2007), initial water saturation was considered 100%, and tortuosity by default under this condition was ~0.6 (Eq. (9)). Therefore, an order of magnitude of tortuosity, ranging between 10^{-5} and 6×10^{-1}, was considered in this study.

Diffusion flux also depends on the diffusion coefficient. Although the diffusion coefficient depends on ion charge and radius, typical values range between 10^{-10}–10^{-8} m^2/s for aqueous species in water (Ingebritsen et al., 2006) and 10^{-12}–10^{-8} m^2/s in fractured rocks (Zhou et al., 2007); 10^{-9} m^2/s has been assigned in previous TOUGHREACT simulation studies (Gherardi et al., 2007). Goto and Roy (1981) calculated diffusion coefficients of ions in hardened cement pastes for temperature ranging between 27 and 60 °C, and the resulting values ranged between 10^{-12} to 10^{-10} m^2/s. In this study, therefore, diffusion coefficient for aqueous species was assigned the range of 10^{-11}–10^{-9} m^2/s.

2.3.2. Diffusivity for gaseous CO_2

When injected with CO_2, supercritical CO_2 may be trapped in the reservoir underneath a sealing formation (usually called "structural trapping" or "stratigraphic trapping"), especially in the first few decades, near injection wells (IPCC, 2005). Supercritical free gas phase may easily leak via buoyant flow through a fractured caprock with a higher permeability (Tian et al., 2014). Therefore, gaseous CO_2 diffusion is the primary transport mechanism for facilitating cement-CO_2 interactions. In this study, gaseous CO_2 saturations (Sg) of 0.0, 0.3, 0.5 and 0.9 were analyzed with the 1-D model (Table 1), and a specific location Point A (Fig. 1) was considered as a CO_2 source boundary. The initial gas saturation of Point A was considered to be an uncertainty parameter, and no CO_2 was dissolved in the fractured caprock brine initially. Studies on gas diffusivity in cement (Houst and Wittmann, 1994; Sercombe et al., 2007) show the effective diffusion coefficient range 10^{-13}–10^{-6} m^2/s, depending on different parameters such as water saturation and porosity. Diffusion coefficient for gaseous species (CO_2 here) was set with 10^{-6} m^2/s accordingly, diffusion coefficient for aqueous species was set with 10^{-11} m^2/s, and tortuosity was set with 0.01 for cement. Other parameters are summarized in Table 5.

2.3.3. Reservoir brine chemistry

Mineral composition in the reservoir affects the brine composition and salinity (Møller, 1988). However, the time for mineral and brine to reach equilibrium is relatively long. With the impacts of mineral heterogeneity, regional flow, and water injection for enhanced oil recovery, brine composition and salinity can vary tremendously within a reservoir (Tang and Morrow, 1999). Brine composition also affects the solubility of CO_2 (Enick and Klara, 1990) and may further impact the process of cement carbonation when leaking brine is exposed to cement.

To assess potential impacts of reservoir brine chemistry on cement-

Table 6
Selected brine chemistry of monitoring data from the SACROC Unit (unit: mg/L).

	TDS	Na^+	Cl^-	K^+	Ca^{2+}	Mg^{2+}	SO_4^{2-}
Chem1	10822	4195	5707	0	0	0	0
Chem2	10447	3202	5735	0	538	127	217
Chem3	28984	8847	17230	0	1805	319	493
Chem4	40037	12832	23909	0	1946	446	624
Chem5	55110	18059	31125	0	2486	376	2554
Chem6	70271	21047	42710	145	4572	907	562
Chem7	85438	28718	50851	0	3112	839	1672
Chem8	100022	28898	61303	245	7331	1420	652
Chem9	114178	34754	69938	0	7101	1504	669
Chem10	130128	38407	80000	350	8620	1975	591
Chem11	145121	46022	88901	0	7832	1582	692

CO_2-brine interactions, 11 different brine chemical compositions (with salinity varied between 1.0–14.5%, shown in Table 6) were chosen from the USGS database (Blondes et al., 2016) based on over 200 specific data points for the SACROC reservoir. Iron and aluminum concentrations from this reservoir were negligible with non-detected values; pH and HCO_3^- were calculated with saturated CO_2. The same 1-D model described in Section 2.2 was simulated. To simulate the process of CO_2-saturated brine migration through the fracture to the cement (Point A to Point B on Fig. 1), the initial water chemistry of point A on Fig. 1 (the inflow boundary) was modified to be CO_2 saturated brine, and no CO_2 was dissolved in the fractured caprock initially. Molecular diffusion was considered as the primary mechanism for dissolved CO_2 transport. The results corresponding to the grid point adjacent to shale-fragment (the cement-fracture interface, point B on Fig. 1) were of specific interest. The simulation duration was 100 years to ensure the time for mineral-brine-CO_2 interactions.

2.4. Two dimensional simulation

To evaluate the impacts of upward CO_2 migration on cement degradation, a 2-D radial model was developed to simulate CO_2 leakage pathways and reactions with cement at the wellbore-reservoir-caprock interface (Fig. 2). Because cement degradation at the cement-casing interface was limited (Carey et al., 2007), casing was not included in our model. The domain is 10 m in depth and ~20 cm in radius, with 805 (24 × 35) grid cells. The formations (specific model domain sections) from the central line of this domain include 10 cm casing (not included in this model), 5 cm cement (ϕ = 0.3), 0.5 cm fracture (ϕ = 0.7), and 2.6 cm caprock (ϕ = 0.08). Initial temperature was set to 50 °C throughout the domain, and the temperature difference could be ignored within 10 m depth near the reservoir. Initial pressure was set at 18 MPa at the domain bottom with a hydrostatic gradient assigned within other layers. A constant pressure CO_2 source was assigned at the bottom of the domain, and a constant pressure boundary was set at the upper corner of the caprock formation. Other boundaries were set as no-flux conditions. Initial water chemistry and mineral assignments were identical to those described in previous sections. The simulation duration was 100 years.

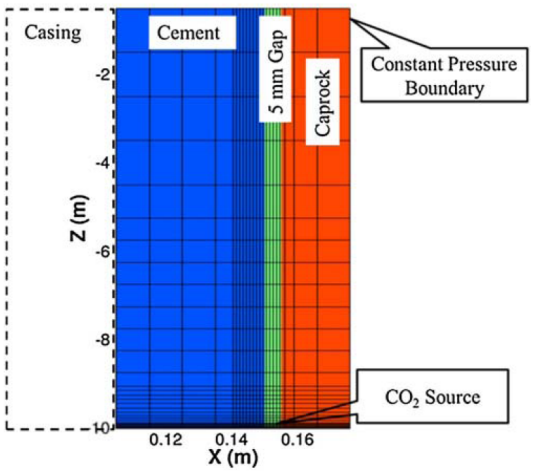

Fig. 2. The 2-D model set-up.

2.5. Reaction kinetics of cement minerals

Because CSHs with highly disordered structures do not exhibit a stable formula, their thermodynamic properties are not fully understood (Kulic and Kersten, 2001). Soler (2007) reviewed the main methodologies for calculating CSH dissolution equilibrium constant (logK), which is an important parameter for numerical simulations to understand the evolution and degradation of hydrated cement. In this study, amorphous SiO_2 (am), tobermorite ($5Ca(OH)_2{\cdot}6SiO_2{\cdot}5H_2O$), jennite ($10Ca(OH)_2{\cdot}6SiO_2{\cdot}6H_2O$), and portlandite were chosen as end-members to decide reactive constants for CSH dissolution with various Ca/Si ratios (Kulic and Kersten, 2001). This method was also applied by Soler et al. (2011) for a study on water-cementitious grout reactions in a fractured rock. The molecular weight was calculated with the stoichiometry formula and the molecular surface area was according to Lothenbach and Winnefeld (2006). The formula and equilibrium constants for CSH used in this study at 25 °C are shown in Table 7.

3. Results

3.1. SACROC simulation verification

Fig. 3 shows selected simulated mineralogy and pH profiles across the carbonation zone after 30 years. At the cement-shale interface, portlandite is consumed with the attack of CO_2. Meanwhile, pH drops significantly from ~12 to ~6 and calcite precipitates. CSH and katoite show negligible consumption, with insignificant SiO_2 and gibbsite precipitation accordingly. These simulation results suggest that wellbore Portland cement will not lose its integrity after 30 years CO_2 exposure. We infer that the penetration depth of calcite precipitation represents the depth of CO_2 intrusion (and this is < 1 cm). The simulation results of this verification case generally reproduce the results of Carey et al. (2007), but with slightly different specific results; such might be due to the difference of initial conditions and reaction kinetic parameters. Significant amounts of CSH dissolve to form secondary CSH and amorphous silica in the simulation results of Carey et al. (2007), but this outcome is not as significant in our simulation results. This might be due to different mineral reaction kinetics used in the two studies. However, it is difficult to authenticate simulated results by samples from the field because they all exhibit

Table 7
Equilibrium constants (logK) and stoichiometric coefficients for CSH.

	logK (25 °C)	Stoichiometric coefficients			
		Ca^{2+}	SiO_2	H^+	H_2O
CSH_02	1.9648	0.23	1.16	−0.46	0.69
CSH_04	6.4767	0.56	1.39	−1.12	1.68
CSH_06	13.271	1.03	1.72	−2.06	3.09
CSH_08	24.631	1.82	2.27	−3.64	5.46
CSH_10	14.583	1.00	1.00	−2.00	2.86
CSH_12	18.801	1.20	1.00	−2.40	3.31
CSH_14	23.124	1.40	1.00	−2.80	3.75
CSH_17	28.634	1.70	1.00	−3.40	5.70
CSH_20	29.133	2.00	1.00	−4.00	6.00

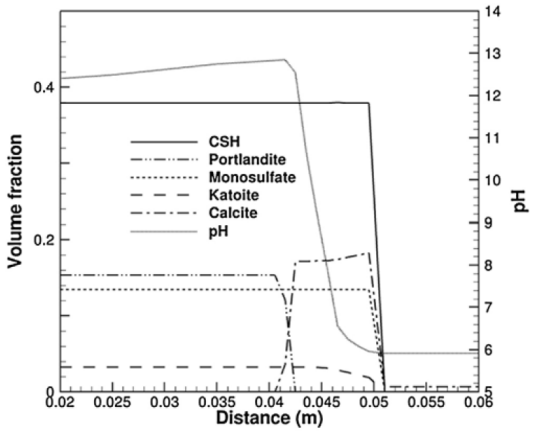

Fig. 3. Selected mineralogy and pH profile across the carbonation zone at 30 years.

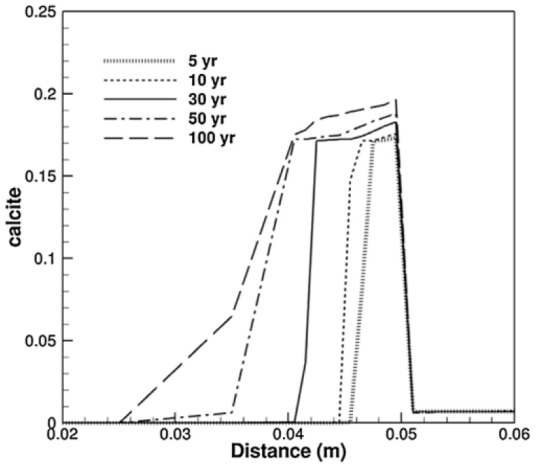

Fig. 4. Calcite precipitations across the carbonation zone at 5, 10, 30, 50 and 100 years.

amorphous status. When CSH reacts with CO_2, hydrated silica/CSH with decreased Ca/Si ratio will occur, causing porous and weakened structure and loss of integrity (Kutchko et al., 2007). The core samples from the SACROC Unit showed no such structure loss, which could indicate that the degradation of CSH was not significant. Fig. 4 shows calcite precipitation during 100 years of simulated CO_2 exposure. The CO_2 intrusion rate decreases with time because porosity and permeability decreases with calcite precipitation, which in turn reduces further chemical reactions between cement and CO_2.

3.2. Impacts of key variables on cement-CO_2 saturated brine interactions

Under diffusive-controlled mass transport conditions, many different variables may induce uncertainty, including cement diffusivity, mineral reaction rates, permeability of cement and fractured caprock, boundary conditions, porosity of the fractured caprock, and chemical composition of leaking brine. A total of 30 cases (Tables 5 and 6) were simulated to test the impacts of these variables during cement-CO_2 saturated brine interaction. Fig. 5 shows simulated calcite and porosity across the carbonation zone at 30 years with different initial conditions of key variables. Permeability of cement and fractured caprock does not affect CO_2 intrusion into wellbore cement when molecular diffusion is the dominant flow mechanism. For sake of brevity, we do not show the results for cases of different permeability.

With the rate constant coefficient (k_{25}) set as a constant value, the assigned mineral surface area will dictate the reaction rate (e.g. smaller particle size, larger surface area and faster reaction rate). Simulated results indicate (Fig. 5(a)) that with decreasing particle size of cement from 1 mm to 0.01 mm, calcite precipitation and porosity reduction is more significant at the cement-fractured caprock interface (calcite volume fraction increases from 17% to 23%). However, the depth of CO_2 intrusion is not affected by different cement particle sizes because CO_2 barely penetrates the surface when diffusion dominates. For larger volumes of CO_2 saturated shale at the domain boundary, deeper cement carbonation takes place (Fig. 5(b)). However, comparing the base case (20 cm in length of shale fragment) and the boundary with constant CO_2-saturated brine source (infinite volume), the difference of the CO_2 intrusion depth is negligible. This result suggests that the base case could simulate a steady source of CO_2 saturated brine and reduce the computational time. The effect of varying fractured caprock porosity (Fig. 5(c)) is similar to that of the setting of boundary condition (Fig. 5(b)). With decreasing shale porosity, the volume of CO_2 saturated brine decreases, which further impacts the carbonation zone depth.

Varying diffusivity (tortuosity and diffusion coefficient) produced the most significant impact on the depth of carbonation zone (Fig. 5(d) and (e)). With tortuosity range of 10^{-5}–~10^{-1} and diffusion coefficient range of 10^{-9}–10^{-11} m^2/s, the carbonation depth varies from less than 2 mm to total penetration of the cement (5 cm). Therefore, diffusivity variables should be chosen carefully. Studies of cement diffusion behaviors suggest that diffusivity could be affected by pore geometry, curing age, temperature, water/cement ratio and other parameters (Goto and Roy, 1981; Promentilla et al., 2009; Provis et al., 2012). Results of these previous experimental studies indicate that diffusion coefficient ranges between 10^{-12} and 10^{-10} m^2/s (Goto and Roy, 1981) at reservoir temperature, tortuosity ranging from 10^{-3} to 1 (Promentilla et al., 2009; Provis et al., 2012), and the effective diffusion coefficient is approximately 10^{-12} m^2/s (Caré, 2003). Our simulated tortuosity 0.0004 is significantly less than the experimental results mentioned above. Based on the diffusivity parameters suggested in the literature, it seems more reasonable to set cement tortuosity to 10^{-2} and diffusion coefficient 10^{-11} m^2/s to fit the carbonation zone depth (~5 mm) of the core sample (Fig. 5(f)). Wertz et al. (2013) also used similar diffusivity parameters in their simulation study of cement-CO_2 interaction. However, diffusivity data at field conditions in the reservoirs are usually very difficult to obtain, and thus treating this variable as an uncertainty parameter might be the best option for forecasting the behavior of CO_2 leakage through wellbore cement.

The impact of leaking gaseous CO_2 on cement is shown in Fig. 5(f). With gaseous CO_2 saturation (Sg) 0–0.9 at the source, no impact on the simulated depth of carbonated cement zone is observed; and indeed these Sg results suggest that gaseous CO_2 does not penetrate the front layer of cement. This indicates that diffusion of the aqueous species (dissolved CO_2) is probably the only transport mechanism that facilitates cement degradation, and diffusivity of the aqueous phase controls this process. Mineral precipitation results also indicate that Sg impacts the geochemical reactions at the cement-fracture interface. When Sg = 0.3, calcite obtains 23% volume fraction at the cement-fracture interface, compared to 19% of other cases, suggesting higher amount of CO_2 trapped in mineral phase (as calcite). However, with larger Sg values (0.5 and 0.9), the precipitation of calcite does not show much difference with the case Sg = 0. It is because the model assumes that the dissolved CO_2 is the major reactant with cement, and with a higher gaseous CO_2 saturation, it impacts the aqueous phase flux and amount into the cement, although pH of the brine decreases because of higher CO_2 partial pressure. Moderate amount of gaseous CO_2 could accelerate calcite precipitation and porosity reduction at the cement-fracture interface which further seals the fracture, because more CO_2 could dissolve in the brine and decrease the pH; but when gaseous CO_2 is

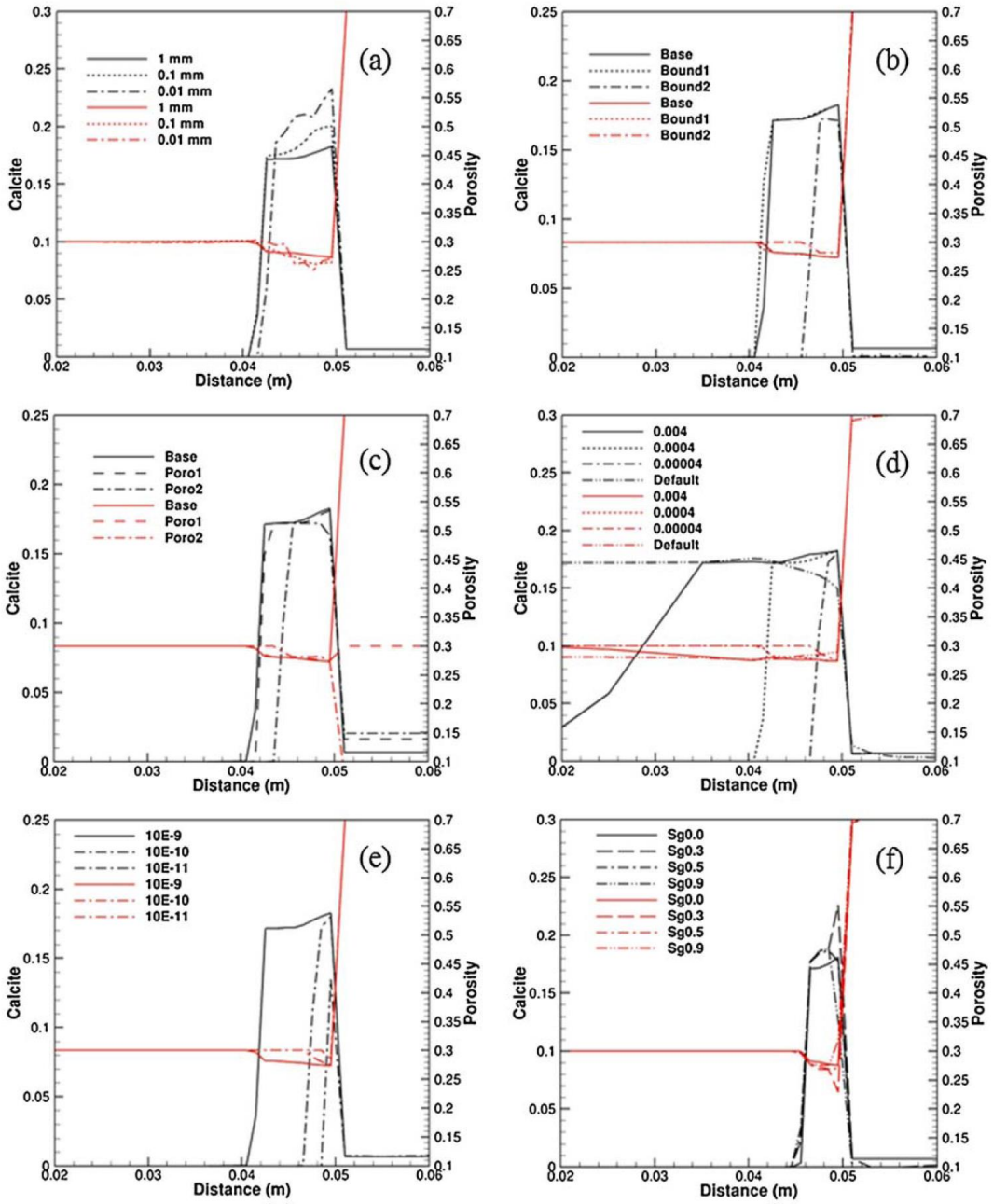

Fig. 5. Calcite (black line) and porosity (red line) profile across the carbonation zone at 30 years with different key variables: (a) mineral surface area; (b) boundary condition; (c) shale porosity; (d) cement tortuosity; (e) cement diffusion coefficient for aqueous species; (f) CO_2 saturation at the source. (For interpretation of the references to color in this figure legend, the reader is referred to the web version of this article.)

dominant in the pore space, its impact is insignificant because of lack of brine.

Under real reservoir conditions, the pressure of the reservoir usually increases when injecting CO_2/water especially near the well leading to pressure driven advections with the leaking plume. The flux into the caprock fractures caused by pressure gradient might be more significant than diffusion, and CO_2-cement interactions might also be impacted. Reservoir pressure was also tested as a potential impact factor with our 1-D model by increasing the pressure of the source grid (A1121, point A in Fig. 1) to 181–190 bar with CO_2 saturation of 0.3–0.9. Results of CO_2 intrusion depth and mineral precipitations at the cement-fracture interface did not show noticeable difference with the cases only

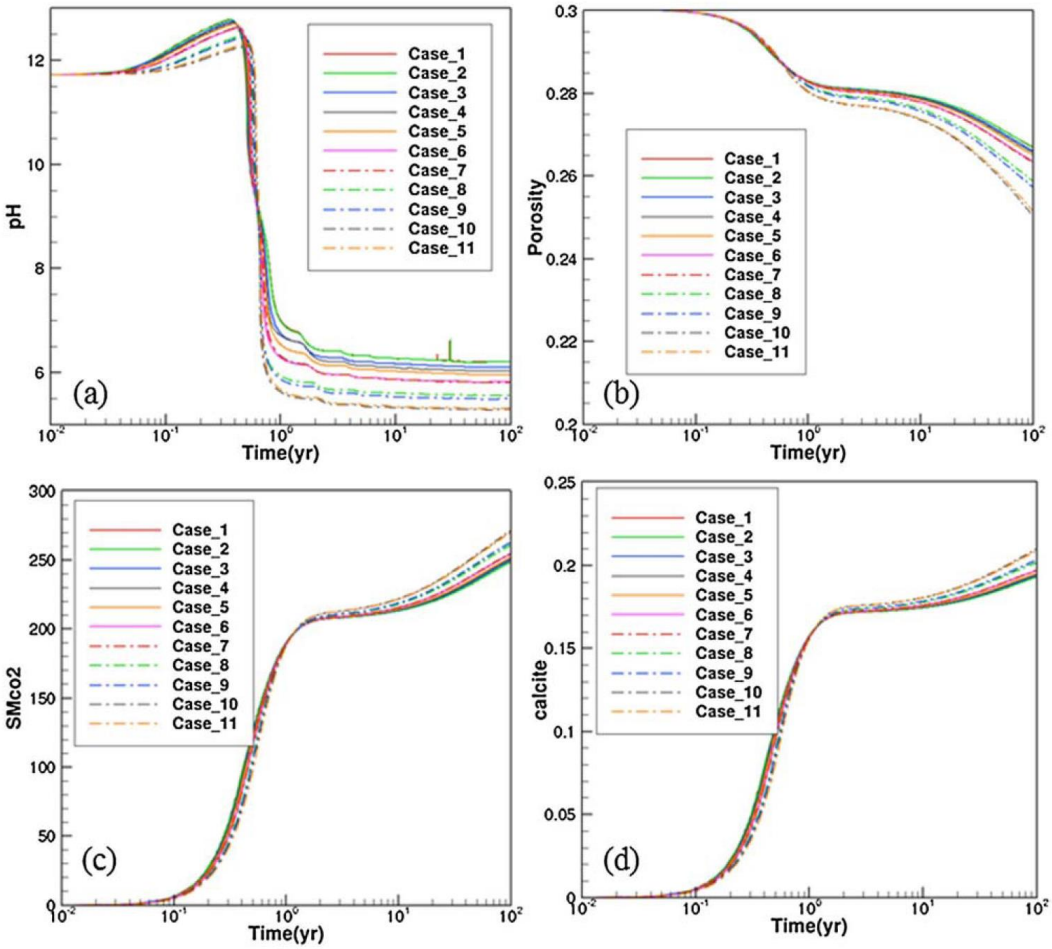

Fig. 6. pH and selected mineralogy changes at cement-fracture interface: (a) pH; (b) Porosity; (c) Total CO_2 sequestered in mineral phases (kg/m^3); (d) Calcite volume fraction.

considering diffusion (figures not shown). The reason for this scenario is that CO_2 does not break the capillary pressure barrier at the cement-fracture interface and hardly enters the cement to dissolve into the cement brine. This also indicates that cement is able to act as a shield to avoid the CO_2 attack. However, if fractures existed in the cement or if it lost its integrity with degradations, gaseous CO_2 would easily penetrate the wellbore cement and further degrade the cement very quickly.

To analyze the impacts of reservoir brine chemistry, a total of 11 scenarios were simulated. Selected mineralogy and pH changes via time at the cement-fractured caprock interface due to cement-CO_2 saturated brine interactions are shown in Fig. 6. With the salinity range between 1 and 14.5% of the leaking brine, the difference of chemical reactions and mineral precipitations are not significant. pH of the cement drops from ~11 to ~6 with the consumption of portlandite and precipitation of calcite after one decade, and show negligible changes afterwards. Meanwhile, porosity and permeability of the cement decreases. CO_2 trapped by minerals ($SMCO_2$) in the cement of these 11 cases does not show significant difference with ~220 kg/m^3 after 30 years and ~270 kg/m^3 after 100 years at the cement-fracture interface. Calcite is the major mineral precipitating during the simulation time (up to 20% of volume fraction), and the same trend of calcite precipitation is observed with CO_2 trapped by minerals, which indicates that calcite is the major mineral that traps CO_2 in the cement. CO_2 solubility decreases with the increasing salinity (Na^+ and Cl^- concentrations increase), but no evidence shows the reduction of dissolved CO_2 impacts the cement carbonation. With the highest salinity simulated in our study, halite (NaCl) does not precipitate. Generally, the leaked reservoir brine salinity (mainly NaCl) does not significantly impact the cement-CO_2 interactions by reducing CO_2 solubility, changing reaction pathways, and increasing the chance of salt precipitation.

3.3. Two-dimensional simulation

Because the leaked brine chemistry does not significantly impact the cement-CO_2 interactions according to the results of the former section, the TDS median value of reservoir brine chemistry (Chem6) was selected for the 2-D simulation. Mineral surface area does not significantly impact cement carbonation zone depth, although more calcite precipitation takes place at the cement-fracture interface with smaller mineral sizes (Fig. 5(a)). In the 2-D simulations, 1 mm mineral particle size was used for the simulations. Cement tortuosity 0.01 and diffusion coefficient 10^{-11} m^2/s were used according to the fitted carbonation zone depth (~5 mm) of the core sample (Fig. 5(f)).

Under operational conditions in the reservoir, the reservoir pressure

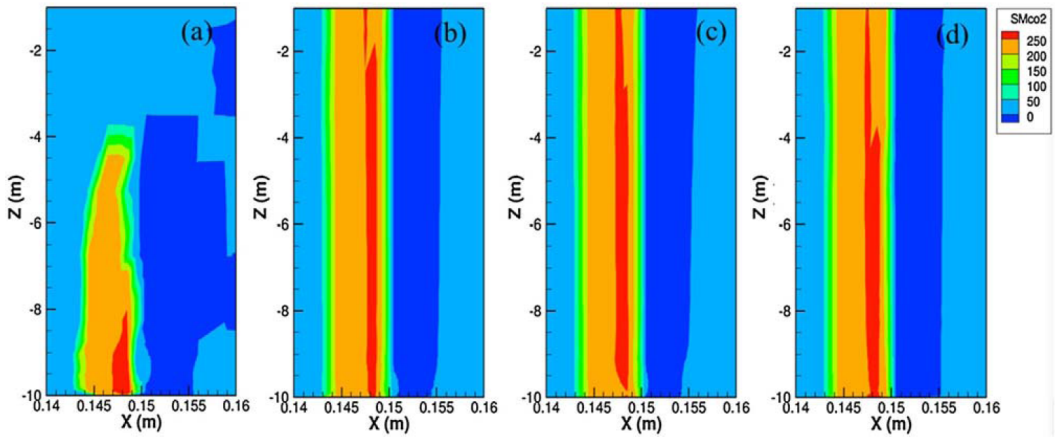

Fig. 7. CO_2 sequestered in mineral phase (kg/m^3) with different reservoir pressure after 30 yr exposure (reservoir gas saturation 0.3): (a) 18 MPa; (b) 18.1 MPa; (c) 18.5 MPa; (d) 19 MPa.

is usually not constant. With water-alternating-gas (WAG) applied, gas (CO_2) saturation (Sg) near the injection well is also changing. After the reservoir is depleted, with further CO_2 spreading, pressure and Sg would decreases near the injection well. Reservoir pressure and Sg could be treated as uncertainty parameters especially with lack of monitoring data. To simplify the models, reservoir pressure and Sg are set as constant parameters in our cases, although they usually change with time.

3.3.1. Impact of pressure

To analyze the impact of reservoir pressure on CO_2 migration and intrusion into the cement, four cases were conducted with constant reservoir Sg (0.3). Fig. 7 shows mineral trapped CO_2 at the cement-caprock-reservoir interface. Because calcite precipitation is the major pattern for trapping CO_2 in the cement according to the results of the 1-D model, this can also indicate the amount of calcite precipitation. Hydrostatic pressure near the injection well (Fig. 7(a)) is quite impossible for real reservoirs with CO_2 injection, but it shows the impacts of CO_2 diffusion and buoyancy on cement degradation. It is obvious that with diffusion and buoyancy but without pressure driven force, the impacted (carbonated) area/height of the cement is far less than the cases with pressure driven flow (Fig. 7(b–d)). Gas phase CO_2 is hardly to migrate to the top of the domain, and it further prevents CO_2 dissolution and diffusion into the cement at the top area. The carbonated zone of cement limits within 6 m above the reservoir under this condition, and the carbonation depth is less at 4–6 m above the reservoir. On the other hand, CO_2 migrates upward easily toward the fracture between cement and caprock with the pressure driven flow (Fig. 7(b–d)), and the carbonation zone of cement is quite uniform along the fracture within the modeling domain. It is because gas phase CO_2 is filled in the fracture area, dissolves in the brine, and diffuses into the cement horizontally. Within 10 m domain above the reservoir, the carbonation zone does not show significant difference among the three cases. However, the vertical impact area might be larger with higher reservoir pressure in a larger scale, which also depends on the length of the fracture to allow CO_2 to migrate.

3.3.2. Impact of reservoir gas saturation

Fig. 8 shows the mineral trapped CO_2 at the cement-caprock-reservoir interface after 30 year exposure with different reservoir Sg at constant 18.1 MPa reservoir pressure. Sg = 0 is considered in this case (Fig. 8(a)), which shows the impact of dissolved CO_2 diffusion only. Under this condition, the carbonation zone of cement is limited, which indicates that the impact of dissolved CO_2 diffusion is not significant, for both degradation depth (~3 mm) and height (~2 m). With higher reservoir Sg (0.3–0.9), gas phase CO_2 fills in the fracture and migrates into the cement with dissolved phase, and the impact area/height is larger (~5 mm all along the 10 m domain). When reservoir Sg = 0.3 and 0.5, the difference of cement carbonation zone is not significant between these two cases. However, when Sg = 0.9, the CO_2 intrusion depth is significantly larger than the other two cases (Fig. 8(d)). The carbonation depth reaches more than 1 cm at the bottom and ~7 mm near the top. The reason could be explained as the pH of the brine further decreases with higher Sg (0.9), and cement-CO_2 interactions are accelerated. Mito et al. (2015) have observed larger alteration depths for the cement exposed to wet supercritical CO_2 than CO_2 saturated brine with their batch experiment. However, the 1-D simulation results do not show significant difference among the three cases (Fig. 5(f)), which is quite different to the 2-D simulation results. The reason could be explained as in the 1-D model, CO_2 dissolution to brine is not as significant as that in the 2-D model due to boundary and initial condition settings (closed boundary and no pressure gradient), and the diffusion of the acid fluid is not as significant as it in the 2-D model. But in the 1-D model, moderate gaseous CO_2 also shows some impacts on the cement carbonation process. This also indicates that the boundary conditions and initial settings should be carefully chosen to get reasonable results.

3.3.3. One-D vs. two-D model

Cement diffusion coefficient, cement tortuosity, reservoir brine chemistry and mineral surface area were also varied with the 2-D model, and it shows similar result with the 1-D model (Figs. 5 and 6). However, those two models show somewhat different results on reservoir gas saturation (Fig. 5(f) vs Fig. 8(d)). Both the 1-D and 2-D models show their own advantages and disadvantages. For example, simulation time is mostly within 2 h for the 1-D model, but it could take up to several days for the 2-D model to reach the same simulation time. On the other hand, the 2-D model could simulate the impacts of the reservoir pressure/gas saturation on the height of the carbonated cement, and heterogeneity could be considered with different formations/layers, which is not possible with the 1-D model. The boundary condition should be carefully picked for the 1-D model to avoid underestimation of CO_2 impacts (Fig. 5(b)). In general, the 1-D model is more time efficient, and the 2-D model is capable for more approaches; the users should choose the model based on their requirements.

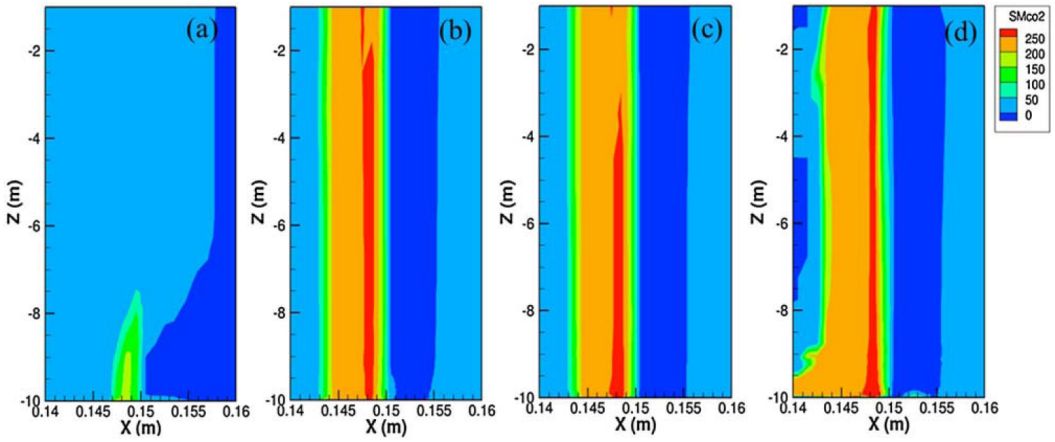

Fig. 8. CO_2 sequestered in mineral phase (kg/m^3) with different gas saturation (Sg) after 30 yr exposure (reservoir pressure 18.1 MPa): (a) 0.0; (b) 0.3; (c) 0.5; (d) 0.9.

4. Application to the Farnsworth Unit

The Farnsworth Unit (FWU) is a CO_2-EOR site, locates in the northern Anadarko basin, Ochiltree County, Texas, and operated by Chaparral Energy, L.L.C. (CELLC). The FWU site is the subject of the Southwest Regional Partnership on Carbon Sequestration (SWP) Phase III, a program sponsored and facilitated by the U.S. Department of Energy (DOE) and its National Energy Technology Laboratory (NETL). CO_2 has been injected since January 2011, and one million tonnes of net CO_2 injection is planed till 2017. Wellbore integrity and leakage through wellbores have been identified as a primary risk factor for this site (Xiao et al., 2016), but samples of well cement and nearby formations are hard to get when the project is ongoing. It is difficult to do the risk assessment without any information of the wellbore cement-caprock-reservoir interface. However, with the analysis of well cement performance with 30 years of CO_2 exposure from the SACROC Unit (Carey et al., 2007), some key factors for wellbore cement could be adopted for the FWU, because both sites applied similar types of cement (Class H Portland cement). In this case study, a 2-D model of CO_2-cement interactions was built at the wellbore cement-caprock-reservoir interface to analyze the impacts on wellbore integrity under CO_2-rich conditions.

4.1. Model setup

The 2-D model (Fig. 2) was used for this case study. Initial temperature was set at 70 °C throughout the domain, and initial pressure was set at 23 MPa at the domain bottom with hydrostatic gradient for other layers. Cement tortuosity was set at 0.01, and diffusion coefficient for aqueous species was set at 10^{-11} m^2/s. The initial reservoir water chemistry was selected from the on-site produced water monitoring data, which was conducted by the New Mexico Institute of Mining and Technology (NMT), part of SWP Phase III. The water chemistry was in equilibrium with different CO_2 partial pressure value that was used in our simulations. Because shallow groundwater was injected into this reservoir, the brine salinity was very low (TDS ~3000 mg/L). The initial caprock water chemistry was chosen from the USGS produced water database (Blondes et al., 2016). The initial cement water chemistry was in equilibrium with the cement composition. Specific water chemistry for the three porous media (reservoir, caprock and cement) is shown in Table 8. X-ray diffraction (XRD) results conducted by NMT were used for the initial caprock mineralogy, and the initial cement composition was calculated from the initial Class H Portland cement composition by simulations. Because the reservoir brine-rock equilibrium was broken by the injected water, the mineralogy of the reservoir was set with non-reactive minerals. The initial mineral abundance for the caprock and cement is shown in Table 9. The other initial settings were taken from the previous SACROC model. The simulation time was 100 years within an operational time scale, which included the operational time exposed to CO_2 (assume 30–50 years) and post injection monitoring period (usually 50 years).

Table 8
Initial fluid compositions used in the FWU case study (unit: mol/kg).

Name	Concentration in shale	Concentration in cement	Concentration in reservoir
pH (unitless)	6.99	11.36	–
Mg^{2+}	1.3×10^{-4}	1.0×10^{-7}	6.3×10^{-5}
K^+	4.5×10^{-7}	1.0×10^{-12}	2.2×10^{-11}
SiO_2 (aq)	5.5×10^{-4}	1.9×10^{-20}	1.0×10^{-11}
NO_3^-	1.0×10^{-10}	1.0×10^{-10}	1.0×10^{-11}
Cl^-	1.9×10^{-1}	1.0×10^{-12}	5.2×10^{-2}
Ca^{2+}	3.0×10^{-3}	1.8×10^{-2}	1.5×10^{-4}
Na^+	2.2×10^{-1}	1.0×10^{-12}	3.9×10^{-2}
Fe^{2+}	1.0×10^{-10}	1.3×10^{-12}	4.4×10^{-14}
HCO_3^-	2.2×10^{-3}	4.2×10^{-12}	2.0
SO_4^{2-}	5.9×10^{-3}	1.0×10^{-5}	2.1×10^{-4}
AlO_2^-	6.1×10^{-8}	1.4×10^{-2}	9.1×10^{-11}

Table 9
List of initial mineral abundance for the FWU case study (% of solid).

Mineral	Volume fraction	Mineral	Volume fraction
Shale		Cement	
Calcite	53.38	CSH	58.21
Dolomite	2.15	Portlandite	28.89
Illite	10.28	Monosulfate	9.96
Kaolinite	1.70	Kaotite	2.90
Quartz	29.3		

4.2. Results

Similar to what is observed from the 2-D model of the SACROC Unit, the cement-CO_2 interactions at the cement-caprock-reservoir interface in the FWU are basically maintained within 5 mm depth after 30 year exposure to CO_2 under various reservoir conditions (Figs. 9 and 10). Calcite is the major product of the cement degradation process with portlandite consumption, which sequesters CO_2 in the mineral phase,

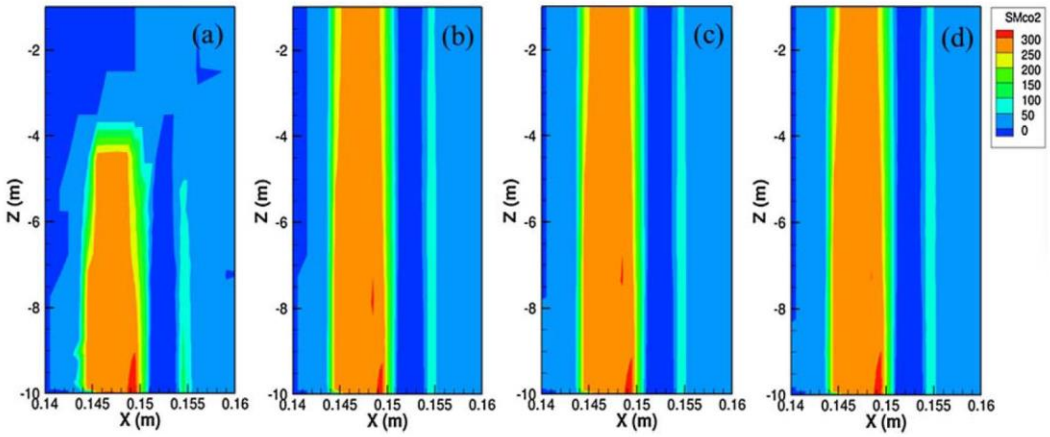

Fig. 9. CO_2 sequestered in mineral phase (kg/m^3) with different reservoir pressure after 30 yr exposure (reservoir gas saturation 0.3): (a) 23 MPa; (b) 23.1 MPa; (c) 23.5 MPa; (d) 24 MPa.

and reduces the porosity at the cement-fracture interface to further hinder CO_2 penetration. Meanwhile, no obvious evidence shows CSH degradation to form amorphous silica or other CSH with lower C-S ratio, which indicates that the cement structure keeps its integrity.

During the 100 year simulation time, when supercritical CO_2 and a pressure gradient exist in the reservoir with a fracture at the cement-caprock interface, CO_2 would migrate upwards and dissolve into the brine to make pH drop. The acid fluid reacts with the cement with diffusion to form calcite, which is the major product of this process (Fig. 11). After 30-year exposure, the carbonation zone of the cement could be about 5 mm thick, and after 100 years it can reach ~8 mm thickness. Porosity at the cement-fracture interface decreases due to the carbonation process (Fig. 12). After 100 year exposure to CO_2, porosity could decrease from 30% to 20%, which provides a protection for the cement from further CO_2 penetration. However, as a limestone formation of the caprock in the FWU, calcite dissolves in the fracture and leads to a larger porosity, because pH in this area is relatively low with CO_2 existence. Within 100 years, porosity at the fracture can reach to 0.85, compared to 0.7 initially. This might cause an increasing area of fracture, which might be harmful for the caprock integrity. Compared to the SACROC Unit (with a clay mineral dominant caprock), it might be a larger concern for CO_2 leakage when the caprock is a limestone formation. Another simulation without the fracture in the domain was also conducted. The results show that CO_2 will not enter the caprock under this condition, and the cement would not degrade except at the contacting interface with the reservoir.

5. Discussion

5.1. Ca and Mg concentrations in the leaking brine

When CO_2-saturated brine attacks the wellbore cement, portlandite releases Ca^{2+} and forms calcite. When Mg^{2+} is available in the brine, it is also possible to form dolomite ($CaMg(CO_3)_2$) or magnesite ($MgCO_3$). With the same salinity of the brine (7% for the SACROC in this study), impacts of different Ca^{2+} and Mg^{2+} concentrations were assessed with a simplified 1-D model with two cement cells connect to an infinite CO_2-rich fracture cell. A total of five sensitivity cases were conducted, and the initial water chemistry is shown in Table 10. The cement-fracture interface was of interest, and the simulation time was 100 years.

Fig. 13 shows pH and some minerology changes during the 100-year simulation time. There is no significant difference of pH with varying Ca^{2+}/Mg^{2+} concentrations, and pH of cement goes down to ~6.0 with the brine intrusion, which is similar to the results shown in Section 3.2. The results also indicate that with higher Ca^{2+}/Mg^{2+} concentration, it

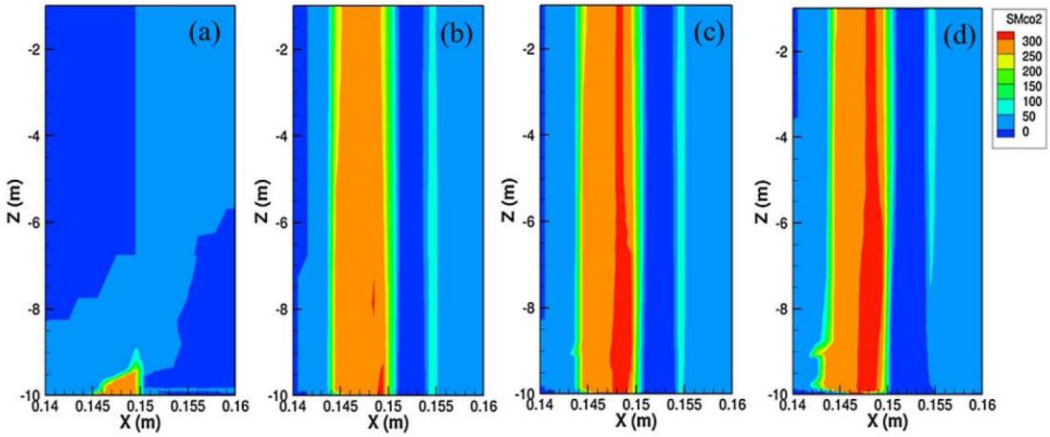

Fig. 10. CO_2 sequestered in mineral phase (kg/m^3) with different gas saturation (Sg) after 30 yr exposure (reservoir pressure 23.1 MPa): (a) 0.0; (b) 0.3; (c) 0.5; (d) 0.9.

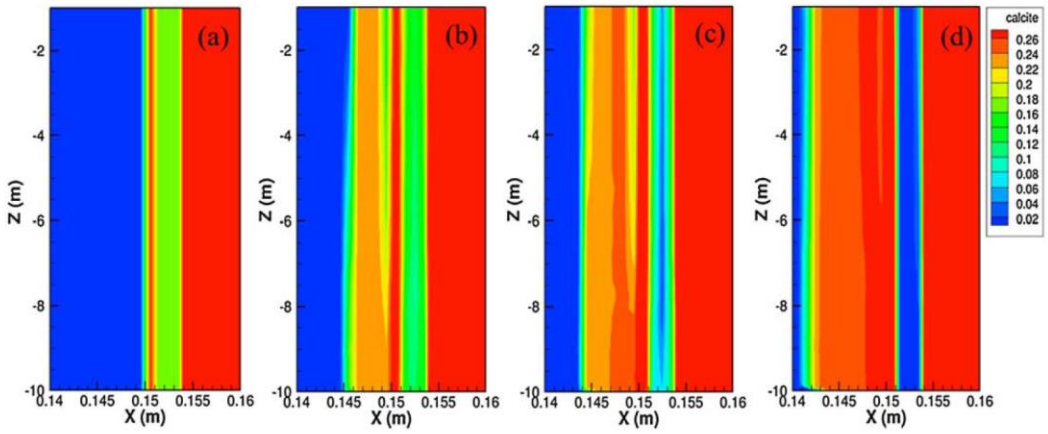

Fig. 11. Calcite volume fraction changes in 100 year simulation time (reservoir Sg 0.3, reservoir pressure 23.1 MPa): (a) 0 year; (b) 10 year; (c) 30 year; (d) 100 year.

is faster for porosity to decrease and CO_2 sequestration in minerals with calcite/dolomite precipitation. Ca^{2+} has a greater impact on CO_2 precipitation in the simulated cases, and the porosity almost drops down to 0 after 100 years with high Ca^{2+} concentration. With high concentration of Ca^{2+} and lack of Mg^{2+}, calcite is the main product when cement interactions with CO_2. With high concentration of Mg^{2+} and lack of Ca^{2+}, calcite precipitates in the beginning with supply of Ca^{2+} from portlandite dissolution and is replaced dolomite later. With the Mg-rich cases, dolomite could occupy as high as 40% of the volume fraction. Magnesite may also precipitate when Mg^{2+} concentration is high, but its abundance is not dominant (less than 5%). Overall, cement carbonation products with CO_2 intrusion are controlled by both of these two ions together accordingly. Ca^{2+} and Mg^{2+} concentrations in the leaking brine do not significantly impact the pH change with cement-CO_2 saturated brine interactions, but they could affect the mineralogy later in the cement.

Fig. 14 shows the relationship among Ca^{2+}, Mg^{2+} and salinity (TDS) of the SACROC and FWU brine with more than 200 monitoring data of produced water from the SACROC reservoir (Blondes et al., 2016) and more than 20 from the FWU obtained from the USGS database (Blondes et al., 2016) and on-site monitoring data conducted by NMT. Ca^{2+} and Mg^{2+} show overall linear correlations with TDS in the SACROC reservoir. With groundwater injection, no such correlations show for the FWU brine, although with higher salinity (TDS), both Ca^{2+} and Mg^{2+} concentrations increase. For both sites, Ca^{2+} concentration is overall significantly higher than Mg^{2+} (Ca:Mg = 4:1 on average). Dolomite and other Mg-minerals show negligible precipitation (~0.01%) with all the simulation cases for these two sites. The reason of this phenomenon could be explained as Ca^{2+} is dominant in the leaking brine and calcite is easier to precipitate. Generally, although brine salinity shows significant difference among the reservoirs, the ratios among Ca^{2+}/Mg^{2+} are relatively stable. For Ca^{2+} rich CO_2 saturated leaking brine reacted with cement, calcite would be the major product for the cement carbonation process.

Table 10
Selected initial water chemistry of the cases (unit: mol/kg).

Case name	Na^+	Cl^-	Ca^{2+}	Mg^{2+}
TDS_only	1.20	1.20	10^{-10}	10^{-10}
Ca_1	1.10	1.20	0.05	10^{-10}
Ca_2	0.97	1.20	0.11	10^{-10}
Mg_1	1.16	1.20	10^{-10}	0.02
Mg_2	1.13	1.20	10^{-10}	0.04

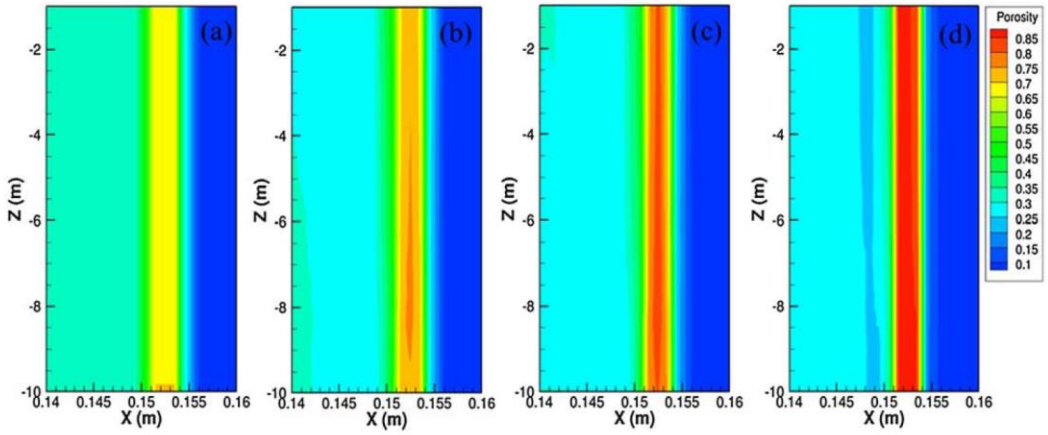

Fig. 12. Porosity changes in 100 year simulation time (reservoir Sg 0.3, reservoir pressure 23.1 MPa): (a) 0 year; (b) 10 year; (c) 30 year; (d) 100 year.

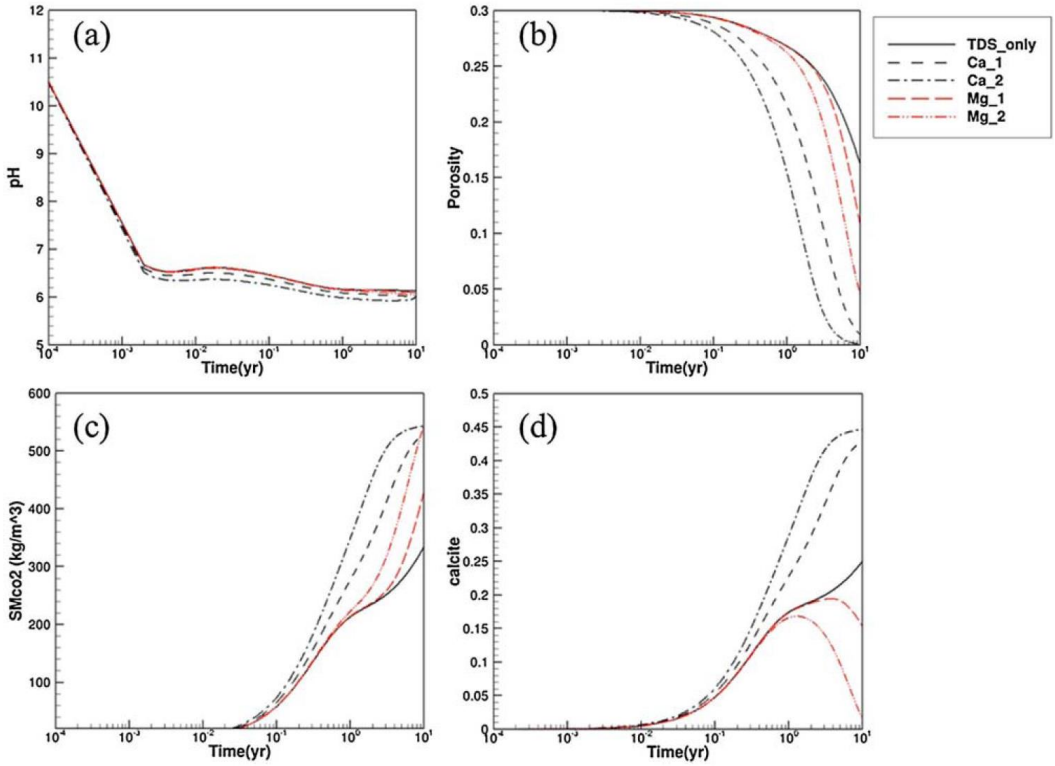

Fig. 13. pH and minerology changes at cement-fracture interface: (a) pH; (b) Porosity; (c) CO_2 sequestered in mineral phase (kg/m^3); (d) Calcite volume fraction.

5.2. Sulfate and chloride attack

Sulfate attack is believed to be one of main factors causing cement to crack and lose its integrity (Li, 2011). Portland cement itself contains limited sulfate as gypsum and it forms monosulfate ($Ca_4Al_2SO_4(OH)_{12}{\cdot}6H_2O$) later with hydration process. Once the wellbore cement is exposed to reservoir brine containing sulfate, it might bring severe degradation associated with Ca^{2+}, Mg^{2+} and Na^{+}, especially when sulfate exceeds 4% by weight of cement (Li, 2011). With sulfate attack, monosulfate and portlandite would degrade to form ettringite ($Ca_6Al_2(SO_4)_3(OH)_{12}{\cdot}26H_2O$) and gypsum, respectively, and it causes cement expansion and even leads to cracks. Carey and Lichtner (2007) simulated sulfate attack to the wellbore cement with a high concentration (saturated) of sulfate in the brine. Ettringite and gypsum were observed as products in their simulation results, but expansion of the cement was not discussed.

Sulfate concentration of the SACROC and FWU brine can be as high as 4000 mg/L but in most cases its concentration is < 3000 mg/L in the SACROC and < 200 mg/L in the FWU (Fig. 15). Sulfate does not show obvious correlations with TDS or pH, which is more "random" for the brine composition. The SACROC cement sample does not indicate any evidence of sulfate attack (Carey et al., 2007), and neither ettringite nor gypsum is observed in the simulations of this study, with sulfate concentration between 0 and 2554 mg/L (Table 6), which suggests

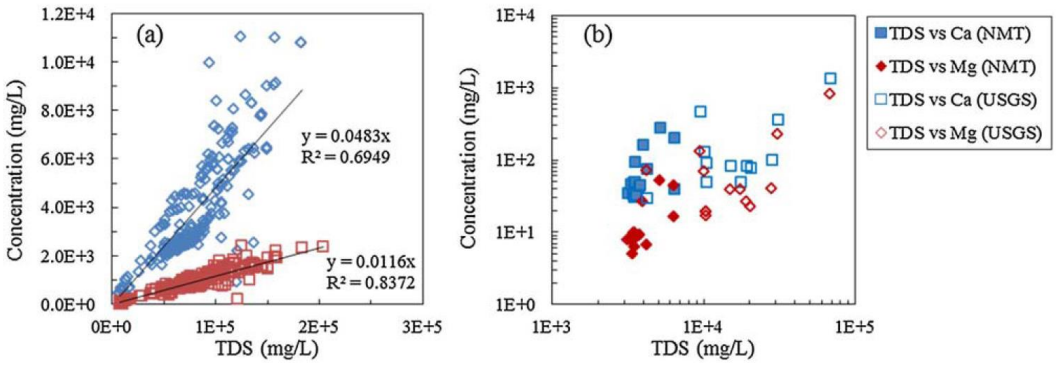

Fig. 14. Ca and Mg concentrations of the SACROC and FWU brine: (a) the SACROC; (b): the FWU.

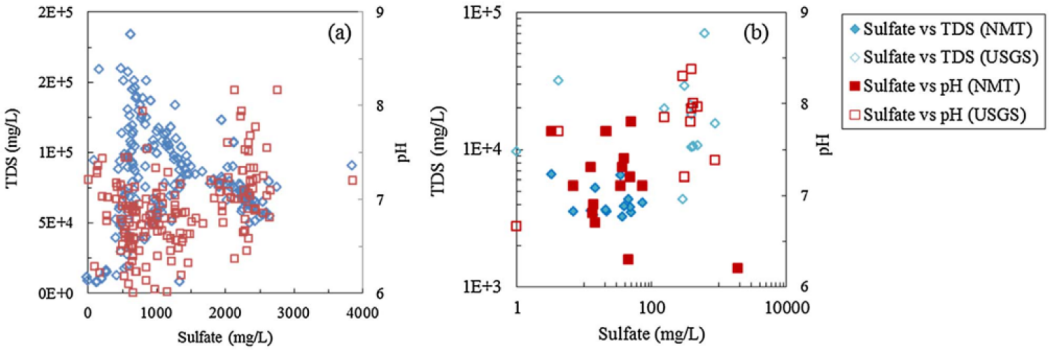

Fig. 15. Sulfate concentrations of the SACROC and FWU brine and their relationship with TDS and pH: (a) the SACROC; (b) the FWU.

that sulfate in the SACROC and FWU brine does not necessarily need to be considered as a concern for cement integrity.

Carey et al. (2007) observed friedel's salt precipitation in their simulations with cement-brine-CO_2 interactions. In our verification cases, friedel's salt did not show precipitation. Suryavanshi and Swamy (1996)'s study showed that the solubility of Friedel's salt would increase with the degree of cement carbonation and pH drop. Under the circumstance of CO_2 attacking, Friedel's salt should dissolve but not precipitate instead. However, further experimental verifications could be done for chloride-cement interactions.

6. Conclusions

This study focused on the impacts of CO_2 leakage through a cement wellbore and surrounding caprock with a gap in between. Sensitivity analyses of key parameters, including cement-CO_2 interactions and reservoir conditions were conducted with the cement core sample from the SACROC Unit, exposed to CO_2 for 30 years. The derived reactive transport model was also applied to a commercial-scale CO_2-EOR field – Farnsworth Unit (FWU) as a case study.

Major findings include:

(1) Cement tortuosity and diffusion coefficient are key parameters for determining the depth of the carbonation zone. With the SACROC cement core sample calibration and the experimental values from other studies, values of cement tortuosity = 0.01 and diffusion coefficient = 10^{-11} m^2/s seem reasonable to fit the carbonation zone depth (~5 mm) of the core sample. For reservoirs that lack wellbore cement samples, to treat these variables as uncertainty parameters might be another option for future studies.

(2) Operational reservoir pressure and reservoir gas saturation (Sg) affect the height of carbonated zone along the existing fracture between the cement and the caprock, because of the buoyancy and pressure driven force for CO_2.

(3) Leaked brine salinity (TDS) from 1 to 14.5% does not significantly impact interactions between cement and CO_2 saturated brine by reducing CO_2 solubility, changing reaction pathways, and increasing the chance of salt precipitation. Calcite ($CaCO_3$) is the major product for cement carbonation. When Mg^{2+} is abundant and Ca^{2+} is lacking, dolomite ($CaMg(CO_3)_2$) will tend to precipitate instead of calcite. However, in real reservoir brines, Ca^{2+} concentrations are usually larger than Mg^{2+} (4.1 times for the SACROC reservoir), thus dolomite is not likely to precipitate.

(4) When CO_2 saturated brine reaches the cement, Portlandite ($Ca(OH)_2$) reacts with CO_2 and forms calcite (> 20% volume fraction), leading to porosity reduction (up to 10% reduction in 100 years), significantly impacting CO_2 leakage rates by infilling pathways. On the other hand, CSH degradation is limited, which indicates that the wellbore maintains its integrity and structure under our simulation conditions.

(5) Simulation results suggest that sulfate concentration < 2500 mg/L in leaking brine would not cause monosulfate degradation.

(6) CO_2 will likely not penetrate an unfractured caprock, and the cement would not degrade significantly in this case.

(7) For the Farnsworth Unit, the wellbore cement will likely maintain its structure and integrity after 100 years. However, if an acid plume were to enter an existing limestone caprock fracture, calcite would likely dissolve because of reduced pH. This process could increase porosity of the fracture and enlarge the volume of the fracture area – a major concern for CO_2 leakage.

Acknowledgements

Funding for this project is provided by the U.S. Department of Energy's (DOE) National Energy Technology Laboratory (NETL) through the Southwest Regional Partnership on Carbon Sequestration (SWP) under Award No. DE-FC26-05NT42591. We would also like to thank Dr. Josep M. Soler from IDAEA-CSIC, Spain, for his generous help with cement reaction equilibrium constants.

References

Allen, A.J., Thomas, J.J., Jennings, H.M., 2007. Composition and density of nanoscale calcium-silicate-hydrate in cement. Nat. Mater. 6, 311–316.

Bachu, S., Bennion, D.B., 2009. Experimental assessment of brine and/or CO_2 leakage through well cements at reservoir conditions. Int. J. Greenh. Gas Control 3, 494–501.

Bachu, S., Watson, T.L., 2009. Review of failures for wells used for CO_2 and acid gas injection in Alberta, Canada. Energy Procedia 1, 3531–3537.

Baur, L., Keller, P., Mavrocordatos, D., Wehrli, B., Johnson, C.A., 2004. Dissolution-precipitation behavior of ettringite, monosulfate, and calcium silicate hydrate. Cem. Concr. Res. 34, 341–348.

Bertos, M.F., Simons, S.J.R., Hills, C.D., Carey, P.J., 2004. A review of accelerated carbonation technology in the treatment of cement-based materials and sequestration of CO_2. J. Hazard. Mater. B 112, 193–205.

Blondes, M.S., Gans, K.D., Rowan, E.L., Thordsen, J.J., Reidy, M.E., Engle, M.A., Kharaka, Y.K., Thomas, B., 2016. U.S. Geological Survey National Produced Waters Geochemical Database v2.2 (PROVISIONAL). (Available at http://energy.usgs.gov/EnvironmentalAspects/EnvironmentalAspectsofEnergyProductionandUse/ProducedWaters.aspx#3822349-data.).

Cao, P., Karpyn, Z.T., Li, L., 2015. Self-healing of cement fractures under dynamic flow of CO_2-rich brine. Water Resour. Res. 51, 4684–4701.

Caré, S., 2003. Influence of aggregates on chloride diffusion coefficient into mortar. Cem. Concr. Res. 33, 1021–1028.

Carey, J.W., Lichtner, P.C., 2007. Calcium silicate hydrate (C-S-H) solid solution model applied to cement degradation using the continuum reactive transport model FLOTRAN. In: In: Mobasher, B., Skalny, J. (Eds.), Transport Properties and Concrete Qeality: Materials Science of Concrete Special Volume. American Ceramic Society, John Willey & Sons, Inc, Hoboken, NJ, USA, pp. 73–106.

Carey, J.W., Wigand, M., Chipera, S.J., WoldeGabriel, G., Pawar, R., Lichtner, P.C., Wehner, S.C., Raines, M.A., Guthrie Jr., G.D., 2007. Analysis and performance of oil well cement with 30 years of CO_2 exposure from the SACROC Unit, West Texas, USA. Int. J. Greenh. Gas Control 1, 75–85.

Carey, J.W., Svec, R., Grigg, R., Zhang, J., Crow, W., 2010. Experimental investigation of

wellbore integrity and CO_2-brine flow along the casing-cement microannulus. Int. J. Greenh. Gas Control 4, 272–282.
Carroll, S., Carey, J.W., Dzombak, D., Huerta, N.J., Li, L., Richard, T., Um, W., Walsh, S.D.C., Zhang, L., 2016. Review: role of chemistry, mechanics, and transport on well integrity in CO_2 storage environments. Int. J. Greenh. Gas Control 49, 149–160.
Dai, Z., Middleton, R., Viswanathan, H., Fessenden-Rahn, J., Bauman, J., Pawar, R., Lee, S., McPherson, B., 2014. An integrated framework for optimizing CO2 sequestration and enhanced oil recovery. Environ. Sci. Technol. Lett. 1 (1), 49–54.
Dai, Z., Viswanathan, H., Middleton, R., Pan, F., Ampomah, W., Yang, C., Jia, W., Xiao, T., Lee, S., McPherson, B., Balch, R., Grigg, R., White, M., 2016. CO_2 accounting and risk analysis for CO_2 sequestration at enhanced oil recovery sites. Environ. Sci. Technol. 50 (14), 7546–7554.
Enick, R.M., Klara, S.M., 1990. CO_2 solubility in water and brine under reservoir conditions. Chem. Eng. Commun. 90, 23–33.
Gherardi, F., Xu, T., Pruess, K., 2007. Numerical modeling of self-limiting and self-enhancing caprock alteration induced by CO_2 storage in a depleted gas reservoir. Chem. Geol. 244, 103–129.
Goto, S., Roy, D.M., 1981. Diffusion of ions through hardened cement pastes. Cem. Concr. Res. 11, 751–757.
Han, W.S., McPherson, B.J., Lichtner, P.C., Wang, F.P., 2010. Evaluation of trapping mechanisms in geologic CO_2 sequestration: case study of SACROC northern platform, a 35-year CO_2 injection site. Am. J. Sci. 310, 282–324.
Houst, Y.F., Wittmann, F.H., 1994. Influence of porosity and water content on the diffusivity of CO_2 and O_2 through hydrated cement paste. Cem. Concr. Res. 24, 1165–1176.
Huerta, N.J., Hesse, M.A., Bryant, S.L., Strazisar, B.R., Lopano, C., 2016. Reactive transport of CO_2-saturated water in a cement fracture: application to wellbore leakage during geologic CO_2 storage. Int. J. Greenh. Gas Control 44, 276–289.
Huet, B.M., Prevost, J.H., Scherer, G.W., 2010. Quantitative reactive transport modeling of Portland cement in CO_2-saturated water. Int. J. Greenh. Gas Control 4, 561–574.
International Panel on Climate Change (IPCC), 2005. IPCC Special Report on Carbon Dioxide Capture and Storage. Cambridge University Press, New York, NY, USA.
Ingebritsen, S., Sanford, W., Neuzil, C., 2006. Groundwater in Geologic Processes, 2nd ed. Cambridge University Press, New York, USA.
Jia, W., McPherson, B.J., Pan, F., Xiao, T., Bromhal, G., 2016. Probabilistic analysis of CO_2 storage mechanisms in a CO_2-EOR field using polynomial chaos expansion. Int. J. Greenh. Gas Control 51, 218–229.
Jia, W., McPherson, B., Dai, Z., Irons, T., Xiao, T., 2017. Evaluation of pressure management strategies and impact of simplifications for a post-EOR CO_2 storage project. Geomech. Geophys. Geo-energy Geo-resour. http://dx.doi.org/10.1007/s40948-017-0056-4.
Kulic, D.A., Kersten, M., 2001. Aqueous solubility diagrams for cementitious waste stabilization system: II, end-member stoichiometries of ideal calcium silicate hydrated solid solutions. J. Am. Ceram. Soc. 84, 3017–3026.
Kutchko, B.G., Strazisar, B.R., Dzombak, D.A., Lowry, G.V., Thaulow, N., 2007. Degradation of well cement by CO_2 under geologic sequestration conditions. Environ. Sci. Technol. 41, 4787–4792.
Kutchko, B.G., Strazisar, B.R., Lowry, G.V., Dzombak, D.A., Thaulow, N., 2008. Rate of CO_2 attack on hydrated class H well cement under geologic sequestration conditions. Environ. Sci. Technol. 42, 6237–6242.
Labus, K., Bujok, P., 2011. CO_2 mineral sequestration mechanisms and capacity of saline aquifers of the Upper Silesian Coal Basin (central Europe) – modeling and experimental verification. Energy 36, 4974–4982.
Li, Q., Lim, Y.M., Flores, K.M., Kranjc, K., Jun, Y.S., 2015. Chemical Reactions of Portland Cement with Aqueous CO_2 and their impacts on cement's mechanical properties under geologic CO_2 sequestration Conditions. Environ. Sci. Technol. 49, 6335–6343.
Li, Z., 2011. Advanced Concrete Technology. John Wiley & Sons Hoboken, New Jersey, USA.
Litynski, J., Rodosta, T., Vikara, D., Srivastava, R., 2013. U.S. DOE's R & D program to develop infrastructure for carbon storage: overview of the regional carbon sequestration partnerships and other R & D field projects. Energy Procedia 37, 6527–6543.
Lothenbach, B., Winnefeld, F., 2006. Thermodynamic modelling of the hydration of Portland cement. Cem. Concr. Res. 36, 209–226.
Møller, N., 1988. The prediction of mineral solubilities in natural waters: a chemical equilibrium model for the Na-Ca-Cl-SO_4-H_2O system, to high temperature and concentration. Geochim. Cosmochim. Acta 52, 821–837.
Mito, S., Xue, Z., Satoh, H., 2015. Experimental assessment of well integrity for CO_2 geological storage: batch experimental results on geochemical interactions between a CO_2-brine mixture and a sandstone-cement-steel sample. Int. J. Greenh. Gas Control 39, 420–431.
NETL, 2012. Carbon Storage Atlas, 4th ed. National energy technology laboratory, Morgantown, WV, USA. Available at http://www.netl.doe.gov/File%20Library/Research/Coal/carbon-storage/atlasiv/Atlas-IV-2012.pdf.
NETL, 2015. Carbon Storage Atlas, 5th ed. National energy technology laboratory, Morgantown, WV, USA. Available at http://www.netl.doe.gov/research/coal/carbon-storage/atlasv.
Promentilla, M.A.B., Sugiyama, T., Hitomi, T., Takeda, N., 2009. Quantification of tortuosity in hardened cement pastes using synchrotron-based X-ray computed microtomography. Cem. Concr. Res. 39, 548–557.
Provis, J.L., Myers, R.J., White, C.E., Rose, V., van Deventer, J.S.J., 2012. X-ray microtomography shows pore structure and tortuosity in alkali-activated binders. Cem. Concr. Res. 42, 855–864.
Pruess, K., Oldenburg, C., Moridis, G., 2012. TOUGH2 User's Guide, Version 2. Lawrence Berkeley National Laboratory, Berkeley, CA, USA.
Pruess, K., 2005. ECO2N: A TOUGH2 Fluid Property Module for Mixtures of Water, NaCl, and CO_2. Report LBNL-57952. Lawrence Berkeley National Laboratory, Berkeley, CA, USA.
Rimmelé, G., Barlet-Gouédard, V., Porcherie, O., Goffé, B., Brunet, F., 2008. Heterogeneous porosity distribution in Portland cement exposed to CO_2-rich fluids. Cem. Concr. Res. 38, 1038–1048.
Scherer, G.W., Celia, M.A., Prévost, J.H., Bachu, S., Bruant, R.G., Duguid, A., Fuller, R., Gasda, S.E., Radonjic, M., Vichit-Vadakan, W., 2005. Leakage of CO2 through abandoned wells: role of corrosion of cement. In: In: Thomas, D.C., Benson, S.M. (Eds.), Carbon Dioxide Capture for Storage in Deep Geologic Formations, vol. 2. Elsevier Ltd, Amsterdam, pp. 827–848.
Sercombe, J., Vidal, R., Gallé, C., Adenot, F., 2007. Experimental study of gas diffusion in cement paste. Cem. Concr. Res. 37, 579–588.
Sobolev, K., Gutiérrez, M.F., 2005. How nanotechnology can change the concrete world: part 1. Am. Ceram. Soc. Bull. 84, 14–17.
Soler, J.M., Vourio, M., Hautojärvi, 2011. Reactive transport modeling of the interaction between water and a cementitious grout in a fractured rock. Application to ONKALO (Finland). Appl. Geochem. 26, 1115–1129.
Soler, J.M., 2007. Thermodynamic Description of the Solubility of C-S-H Gels in Hydrated Portland Cement. Working Report 2007-88. Institut de Ciències de la Terra Jaume Almera (CSIC), Olkilouto, Finland. Available at http://www.iaea.org/inis/collection/NCLCollectionStore/_Public/43/063/43063335.pdf?r=1.
Suryavanshi, A.K., Swamy, R.N., 1996. Stability of friedel's salt in carbonated concrete structural elements. Cem. Concr. Res. 26, 729–741.
Tang, G., Morrow, N.R., 1999. Influence of brine composition and fines migration on crude oil/brine/rock interactions and oil recovery. J. Petrol. Sci. Eng. 24, 99–111.
Tian, H., Xu, T., Wang, F., Patil, V.V., Sun, Y., Yue, G., 2014. A numerical study of mineral alteration and self-sealing efficiency of a caprock for CO_2 geological storage. Acta Geotech. 9, 87–100.
Vest Jr., E.L., 1970. Oil fields of Pennsylvanian-Permian Horseshoe Atoll, West Texas. In: In: Halbouty, M.T. (Ed.), Geology of Giant Petroleum Fields, vol. 14. AAPG Memoir, pp. 185–203.
Viswanathan, H.S., Pawar, R.J., Stauffer, P.H., Kaszuba, J.P., Carey, J.W., Olsen, S.C., Keating, G.N., Kavetski, D., Guthrie, G.D., 2008. Development of a hybrid process and system model for the assessment of wellbore leakage at a geologic CO_2 sequestration site. Environ. Sci. Technol. 42, 7280–7286.
Wertz, F., Gherardi, F., Blanc, F., Bader, A., Fabbri, A., 2013. Cement CO_2-alteration propagation at the well-caprock-reservior interface and influence of diffusion. Int. J. Greenh. Gas Control 12, 9–17.
Wigand, M., Kaszuba, J.P., Carey, J.W., Hollis, W.K., 2009. Geochemical effects of CO_2 sequestration on fractured wellbore cement at the cement/caprock interface. Chem. Geol. 265, 122–133.
Wolery, T.J., 1992. EQ3/6, a Software Package for Geochemical Modeling of Aqueous Systems: Package Overview and Installation Guide, Version 7.0. Report UCRL-MA-110662 PT I. Lawrence Livermore National Laboratory, Livemore, CA, USA.
Xiao, T., McPherson, B., Pan, F., Esser, R., Jia, W., Bordelon, A., Bacon, D., 2016. Potential chemical impacts of CO2 leakage on underground source of drinking water assessed by quantitative risk analysis. Int. J. Greenh. Gas Control 50, 305–316.
Xu, T., Spycher, N., Sonnenthal, E., Zhang, G., Zheng, L., Pruess, K., 2011. TOUGHREACT Version 2.0: a simulator for subsurface reactive transport under non-isothermal multiphase flow conditions. Comput. Geosci. 37, 763–774.
Xu, T., Spycher, N., Sonnenthal, E., Zheng, L., Pruess, K., 2012. TOUGHREACT User's Guide: a Simulation Program for Non-isothermal Multiphase Reactive Transport in Variably Saturated Geologic Media, Version 2.0. Lawrence Berkeley National Laboratory, Berkeley, CA, USA.
Zhou, Q., Liu, H., Molz, F.J., Zhang, Y., Bodvarsson, G., 2007. Field-scale effective matrix diffusion coefficient for fractured rock: results from literature survey. J. Contam. Hydrol. 93, 161–187.

CHAPTER 3

POTENTIAL CHEMICAL IMPACTS OF CO_2 LEAKAGE ON UNDERGROUND SOURCE OF DRINKING WATER ASSESSED BY QUANTITATIVE RISK ANALYSIS

Reprinted from International Journal of Greenhouse Gas Control 50, Ting Xiao, Brian McPherson, Feng Pan, Rich Esser, Wei Jia, Amanda Bordelon, Diana Bacon, Potential chemical impacts of CO_2 leakage on underground source of drinking water assessed by quantitative risk analysis, 305-316, 2016, with permission from Elsevier. http://doi.org/10.1016/j.ijggc.2016.04.009.

In Chapter 2, we analyzed the interaction between CO_2 and wellbore cement, which is considered a major pathway for CO_2 leakage. It is hard for CO_2 to penetrate wellbore cement when there are no pre-existing fractures. However, with an annulus between wellbore and caprock, CO_2 easily leaks from the reservoir due to buoyancy. There also might be micro-fractures in the wellbore cement due to mechanical effects, which provides leakage pathways for CO_2.

Many CO_2 storage reservoirs are overlain by potable groundwater aquifers, and the water quality might be affected by CO_2 leakage. In this chapter, we assess the potential risks to the Ogallala groundwater aquifer overlying the Farnsworth Unit (FWU) due to CO_2 leakage through wellbores with micro-fractures with quantitative response surface methodology (RSM). This chapter focuses on how CO_2 leakage is likely to influence the groundwater quality in the Ogallala aquifer, and what water chemistry components are suitable for early detection criteria.

International Journal of Greenhouse Gas Control 50 (2016) 305–316

Contents lists available at ScienceDirect

International Journal of Greenhouse Gas Control

journal homepage: www.elsevier.com/locate/ijggc

Potential chemical impacts of CO_2 leakage on underground source of drinking water assessed by quantitative risk analysis

Ting Xiao[a,b,*], Brian McPherson[a,b], Feng Pan[a,b], Rich Esser[a,b], Wei Jia[a,b], Amanda Bordelon[a], Diana Bacon[c]

[a] Department of Civil and Environmental Engineering, University of Utah, Salt Lake City, UT 84112, USA
[b] Energy and Geoscience Institute, University of Utah, Salt Lake City, UT 84108, USA
[c] Pacific Northwest National Laboratory, P.O. Box 999, Richland, WA 99352, USA

ARTICLE INFO

Article history:
Received 30 October 2015
Received in revised form 22 March 2016
Accepted 6 April 2016
Available online 4 June 2016

Keywords:
CO_2 leakage
USDWs
Groundwater quality
Risk analysis

ABSTRACT

Many geologic carbon storage site options include not only excellent storage reservoirs bounded by effective seal layers, but also Underground Sources of Drinking Water (USDWs). An effective risk assessment and mitigation plan provides maximum protection for USDWs, to respect not only current policy but also to accommodate likely future USDW-specific regulatory protections. The goal of this study is to quantify possible risks to USDWs, specifically risks associated with chemical impacts on USDWs. Reactive transport models involve tremendous computational expense. Therefore, a secondary purpose of this study is to develop, calibrate and test reduced order models specifically for assessing risks of USDW chemical impacts by CO_2 leakage from a storage reservoir. In order to achieve these goals, a geochemical model was developed to interpret changes in water chemistry following CO_2 intrusion. A response surface methodology (RSM) based on these geochemical simulations was used to quantify associated risks. The case study example for this analysis is the Ogallala aquifer overlying the Farnsworth unit (FWU), an active commercial-scale CO_2-enhanced oil recovery field. Specific objectives of this study include: (1) to understand how CO_2 leakage is likely to influence geochemical processes in aquifer sediments; (2) to quantify potential risks to the Ogallala groundwater aquifer due to CO_2 leakage from the FWU oil reservoir; and (3) to identify water chemistry factors for early detection criteria.

Results indicate that the leakage rate would most likely range between 10^{-14}–10^{-10} kg/(m^2 year) for typical and likely leakage pathway permeability ranges. Within this range of CO_2 leakage rate, groundwater quality is not likely to be significantly impacted. The worst-case scenario yields trace metal concentrations approximately twice as much as the initial value, but these predicted concentrations are still less than one-fifth of regulation-stipulated maximum contamination levels and do not exceed the no-impact thresholds. Finally, the results of this analysis suggest that pH may be an effective geochemical indicator of CO_2 leakage.

1. Introduction

Enhanced Oil Recovery (EOR) with CO_2 (CO_2-EOR) offers the potential economic benefit of increased oil production, which may offset some costs of CO_2 capture and storage (IPCC, 2005). Most CO_2-EOR sites are overlain by groundwater aquifers (DOE/NETL, 2010; USGS Map of the Principal Aquifers of the United States: http://water.usgs.gov/ogw/aquifer/map.html). Although the possibility of CO_2 leakage from a sequestration site is very low (Bachu and Watson, 2009; Gaus, 2010), regulatory policy generally includes protections against CO_2 leakage to potable aquifers through wellbores or faults, including water quality impacts by acidification and trace metal mobilization (Gaus, 2010; IPCC, 2005). Multiple environmental variables such as aquifer geology, mineralogy, and groundwater chemistry also play an important role in controlling groundwater quality (Bacon et al., 2014, 2016; Dai et al., 2014a,c; Frye et al., 2012; Wilkin and Digiulio, 2010). These geological variables suggest site-specific, quantitative risk assessment is essential for safe and effective application of carbon sequestration (Wilkin and Digiulio, 2010) and early leak detection criteria (Little and Jackson, 2010). To date, most research on assessment of chemical impact risks (from CO_2 leakage) rely on lab-scale and

* Corresponding author at: Department of Civil and Environmental Engineering, University of Utah, Salt Lake City, UT 84112, USA.
E-mail address: txiao@egi.utah.edu (T. Xiao).

http://dx.doi.org/10.1016/j.ijggc.2016.04.009
1750-5836/

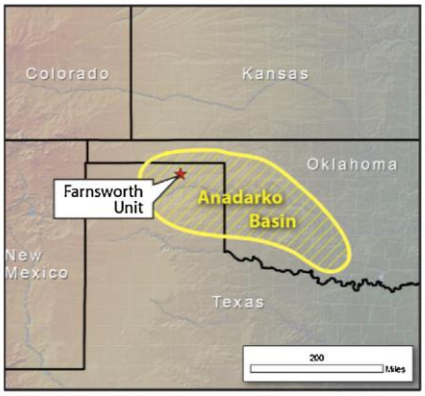

Fig. 1. The Farnsworth unit.

small, short-term site-scale experiments to obtain early detection of aquifer quality changes in non-storage formations (Frye et al., 2012; Little and Jackson, 2010; Lu et al., 2010; Qafoku et al., 2013; Viswanathan et al., 2012; Wells et al., 2007; Yang et al., 2014; Zheng et al., 2012, 2015). However, uncertainty analysis with numerical simulations becomes a key tool for forecasting long-term groundwater quality changes by CO_2 leakage.

In this study, a response surface methodology (RSM) was conducted to quantify uncertainty and risks. Response surface methods are statistical and mathematical techniques used for developing, improving, and optimizing model building and model exploitation (Box and Draper, 1987; Myers and Montgomery, 1995). Such RSM is becoming more widely used than computationally-expensive and time-intensive processes of "traditional" risk and uncertainty analysis methods (e.g. the basic Monte Carlo method). The National Risk Assessment Partnership (NRAP) is pioneering application of RSM specifically for geologic carbon sequestration (Carroll et al., 2014; Dai et al., 2014b; Pawar et al., 2014). For example, Dai et al. (2014b) developed a generic integrated framework for optimizing CO_2 sequestration with RSM. Results suggest that, in order to maximize both oil production and CO_2 injection, the distance between injection and production wells should approach 300 m. Additionally, the best value of water alternating gas (WAG) ratio should be 5–6.5. Other recent work detailing RSM, as applied in carbon sequestration research, includes Rohmer and Bouc (2010) and Li and Zhang (2014).

An active CO_2-EOR field was selected for this study, the Farnsworth Unit (FWU) in Ochiltree County, Texas (Fig. 1), operated by Chaparral Energy, L.L.C. (CELLC). The FWU site is the subject of the Southwest Regional Partnership on Carbon Sequestration (SWP) Phase III, a program sponsored and facilitated by the U.S. Department of Energy and its National Energy Technology Laboratory. The FWU includes an overlying underground source of drinking water (USDW) aquifer, the Ogallala formation, located in the northern Anadarko basin. For this site, our primary goal is to quantify potential risks to groundwater quality due to CO_2 leakage through wellbores. We selected the FWU for case study because: (1) there are considerable brine/water and mineralogy data available for both the FWU and the Ogallala aquifer; and (2) the Ogallala aquifer is one of the largest USDWs in North America (George et al., 2011), which represents a typical drinking water resource in the USA. The main objectives of this study include: (1) to understand how CO_2 leakage is likely to influence geochemical processes in aquifer sediments; (2) to quantify potential risks to the Ogallala groundwater aquifer associated with changes in groundwater chemistry due to CO_2 leakage from the FWU; and (3) to identify water chemistry components as indicators for early detection criteria.

This study is organized into three parts: (1) cement hydration simulations, to obtain the equilibrium composition of wellbore fluids with wellbore cements; (2) quantification of the possible range of CO_2 leakage rates from the FWU reservoir through wellbore fractures (using typical and likely permeability ranges) to the overlying USDW; and (3) quantification of potential risks to Ogallala groundwater quality due to CO_2 leakage.

2. Methods

To analyze potential impacts of CO_2 on the water quality of a USDW, a series of numerical simulations was conducted. Simulation of cement hydration provides associated wellbore cement components, which are major reactants that consume CO_2 through a leakage pathway such as a fissure. Results were then used to determine the possible extent/rate of CO_2 leakage flux through the wellbore cement. Simulation of CO_2 leakage flux through wellbores suggests possible leakage rates as well as the likely probability distribution exhibited by the data. Finally, the forecasted range of CO_2 leakage fluxes was used for RSM-based quantification of risks associated with CO_2 leakage into the Ogallala formation in this case study.

2.1. Response surface methodology

Stages in the application of RSM employed in this study include: (1) determining major independent parameters and experimental design; (2) conducting numerical experiments according to the selected experimental matrix with verification of the RSM model equation; and (3) obtaining the response surface model and

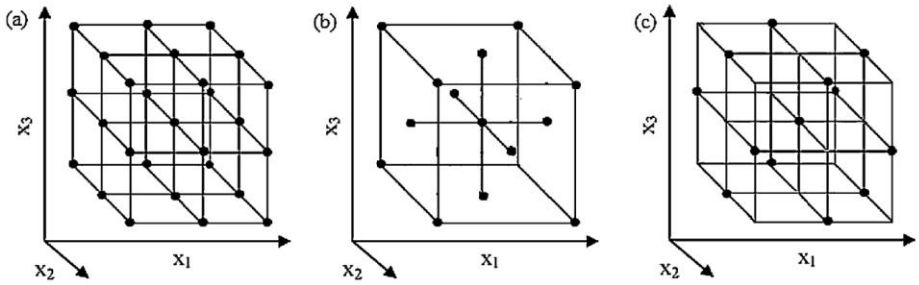

Fig. 2. Symmetrical second-order experimental designs: (a) full three-level factorial design; (b) central composite design; (c) Box-Behnken design (Adopted from Bezerra et al., 2008).

conducting further analysis (e.g. determination of early detection indicators).

Choosing of experimental design has a large influence on the accuracy of the approximation of the response surface. Common designs include the full three-level factorial design, central composite design, and Box-Behnken design (Bezerra et al., 2008). These are widely used for symmetrical second-order experiments (Fig. 2). In this study, the Box-Behnken design was applied because of its mathematical efficiency.

The model equation is defined with a polynomial function,

$$\eta = f(x_1, x_2, \ldots, x_n) + \varepsilon,$$

where η is the response, f is the function of response, $x_1, x_2, \ldots, x_n$ are the independent parameters, n is the number of the independent parameters, and ε is the statistical error.

The units and/or ranges are usually different in the experimental domain, thus potentially having different levels of effects for the response. To overcome uneven impacts and render the units of the parameters irrelevant to responses, the parameters are normalized to the range from −1 to 1. Usually the equation of normalization is written as

$$X = \frac{x - (x_{max} + x_{min})/2}{(x_{max} - x_{min})/2},$$

where X is the normalized parameter, x is the natural variable, and x_{max} and x_{min} are maximum and minimum values of the natural variables.To account for and quantify curvature, usually a second-order equation is used for RSM, written as

$$y = \beta_0 + \Sigma_{i=1}^{n}\beta_i X_i + \Sigma_{i<j}\beta_{ij}X_iX_j + \Sigma_{i=1}^{n}\beta_{ii}X_i^2 + \varepsilon,$$

where β_0, β_i, β_{ij}, and β_{ii} represent the regression coefficients of constant, linear, interaction, and quadratic terms, respectively; X_i and X_j are normalized independent parameters.

The matrix notion of this model is written as

$$\begin{bmatrix} y_1 \\ y_2 \\ \vdots \\ y_k \end{bmatrix} = \begin{bmatrix} 1 & X_{11} & X_{12} & \ldots & X_{1n} \\ 1 & X_{21} & X_{22} & \ldots & X_{2n} \\ \vdots & \vdots & \vdots & \ldots & \vdots \\ 1 & X_{k1} & X_{k2} & \ldots & X_{kn} \end{bmatrix} \begin{bmatrix} \beta_0 \\ \beta_1 \\ \vdots \\ \beta_n \end{bmatrix} + \begin{bmatrix} \varepsilon_1 \\ \varepsilon_2 \\ \vdots \\ \varepsilon_k \end{bmatrix} \text{ or } = X\beta + \varepsilon.$$

The regression coefficient β is solved by using the method of least squares (MLS), which assumes errors are random, independent of each other, and profile with a zero mean and a common unknown variance; β should minimize the sum of the squares of the errors (*SSE*), or

$$\varepsilon = y - \hat{y} = y - X\beta,$$

$$SSE = \Sigma_{i=1}^{n}\varepsilon_i^2 = \varepsilon^T\varepsilon = \left(y - X\beta\right)^T\left(y - X\beta\right),$$

where y is the observed value and $\hat{y}$ is the fitted value. The derivative of *SSE* may be used to yield β, or

$$\frac{\partial}{\partial\beta}(SSE) = -2X^T\left(y - X\beta\right) = 0 \Rightarrow \beta = \left(X^TX\right)^{-1}X^Ty.$$

After the regression coefficients are obtained, model adequacy may be evaluated by several techniques. Usually, coefficient of determination R^2 ($R^2 = 1 - \frac{\sum\left(y_i - \widehat{y_i}\right)^2}{\sum(y_i - \bar{y})^2}$, $\bar{y} = \frac{1}{n}\sum y_i$,) and/or coefficient of variation of the root mean square error ($CVRMSE = \sqrt{\frac{\sum(y_i - \hat{y}_i)^2}{n}}/\bar{y}$) are used to check how well the model fits with the observed data.

Table 1
Initial mineral composition of cement hydration simulation (Scrivener et al., 2004).

Name	Volume fraction: %
Alite	19.8
Ferrite	5.6
Portlandite	17.8
CSH	35.0
Belite	7.5
Aluminate	2.7
Ettringite	7.0

2.2. Simulation of cement hydration

Wells in the FWU are completed with Portland cement. When the cement mixes with water, it starts hydration with chemical reactions, and causes microstructure formations to form a harder structure (Li, 2011; Mehta and Monteiro, 2014). Chemical reactions during hydration involve:

(1) Hydration of aluminates:

$$(CaO)_3 \cdot Al_2O_3\,(aluminate) + 3CaSO_4 \cdot 2H_2O + 26H_2O \rightarrow$$

$$(CaO)_6 \cdot Al_2O_3 \cdot (SO_3)_3 \cdot (H_2O)_{32}\,(ettringite)$$

$$(CaO)_6 \cdot Al_2O_3 \cdot (SO_3)_3 \cdot (H_2O)_{32} + 2(CaO)_3 \cdot Al_2O_3 + 22H_2O \rightarrow$$

$$3(CaO)_4 \cdot Al_2O_3 \cdot SO_3 \cdot (H_2O)_{18}\,(monosulfate),$$

where Al^{3+} in ettringite and monosulfate can also be substituted by Fe^{3+} (Taylor, 1997);

(2) Hydration of the silicates:

$$(CaO)_3 \cdot SiO_2\,(alite) + H_2O \rightarrow CSH\,(calcium\ \ silicate\ \ hydrate)$$

$$+ Ca(OH)_2\,(portlandite)$$

$$(CaO)_2 \cdot SiO_2\,(belite) + H_2O \rightarrow CSH + Ca(OH)_2,$$

where *CSH* does not have a confirmed formula, and the ratio of *Ca/Si* of *CSH* varies.It is the primary binding material of the cement. Saturated *CSH* has the approximate formula $(CaO)_{1.7}SiO_2 \cdot (H_2O)_4$ (Baur et al., 2004);

(3) Hydration of ferrite:

$$(CaO)_4 \cdot Al_2O_3 \cdot Fe_2O_3\,(ferrite) + 3CaSO_4 \cdot 2H_2O + 21H_2O \rightarrow$$

$$(CaO)_6 \cdot Al_2O_3 \cdot (SO_3)_3 \cdot (H_2O)_{32} + Fe_2O_3 \cdot (H_2O)_3.$$

The major cement component that reacts with CO_2 is portlandite ($Ca(OH)_2$):

$$Ca(OH)_2 + CO_2 \rightleftharpoons CaCO_3 + H_2O$$

Most of the reactions take place during a few hours and release a significant amount of heat. After a few days, the chemical reactions and hardening rates decelerate. However, hydration processes may take decades to reach an equilibrium state. To predict the equilibrium wellbore cement composition for the field environment, a batch simulation of cement hydration was conducted with an arbitrary and lengthy time period of 100 years. To avoid vigorous chemical reactions and heat release during the initial several hours, the initial Portland cement composition for this simulation (Table 1) was adopted from Scrivener et al. (2004), and specifically their cement hydration experimental results at the end of the 1st day. Water chemistry was adapted from the average brine chemistry data of the FWU reservoir, which was conducted by the New Mexico Institute of Mining and Technology, part of SWP Phase III.

Table 2
Hydrogeological parameters.

Property	Value
Reservoir (Morrow)	
Thickness	30 m
Permeability	4.52×10^{-14} m^2
Porosity	0.1453
Rock density	2650 kg/m^3
Salinity	6%
Cement	
Permeability	5.0×10^{-20} m^2 [a]
Porosity	0.08 [b]
Rock density	2400 kg/m^3
USDW aquifer	
Thickness	100 m
Permeability	5.0×10^{-13} m^2
Porosity	0.30
Rock density	2600 kg/m^3
Salinity	0.35%
Fracture	
Permeability	1.0×10^{-14} m^2 [a]
Porosity	0.40 [b]
Rock density	2400 kg/m^3

[a] Bachu and Bennion (2009).
[b] Rimmelé et al. (2008).

Table 3
Independent parameters for CO_2 leaking rate simulation.

Parameter name	Low (−1)	Mid (0)	High (+1)	Distribution
CO_2 saturation	0.1	0.5	0.9	Uniform
Reservoir pressure: bar	300	325	350	Uniform
Wellbore fracture proportion	0.01	0.055	0.10	Uniform

2.3. Simulation of CO_2 leakage flux through wellbores

To assess the most likely value of CO_2 leakage rate through wellbore fractures, a vertical 1-D simulation was conducted over a time period of 100 years. The resulting mineralogy of the cement hydration batch model was then utilized for subsequent simulations. Based on the sizes of wells in the FWU, the diameter of the simulated well was set as 17 cm, and the thickness of the wellbore was assigned 2.5 cm. The bottom of the reservoir was assigned at 3000 m depth, and the thickness was assigned 30 m. The overlying aquifer was assigned a thickness of 100 m, and the upper surface boundary was assigned atmospheric pressure. Hydrostatic pressure was set as the initial pressure of the domain, and the initial temperature was set as 20 °C at the top of the domain with a 25 °C/km gradient. Hydrogeological and geochemical parameters of the reservoir were assigned using monitoring/characterization data as much as was possible. Cement permeability was set based on results of previous studies by Bachu and Bennion (2009) and Rimmelé et al. (2008). The Ogallala USDW formation is a typical sand aquifer, and its hydrogeological parameters (i.e. porosity and permeability) were assigned based on its sand properties (Cronin, 1969). The initial chemical parameters were assigned according to monitoring data from the Ogallala formation. A dual permeability domain was utilized for fracture and matrix flow, implemented using the multiple interacting continua (MINC) in the TOUGH2 code (Pruess et al., 2012) for simulation of micro fractures within the cement casing. The major hydrogeological parameters are summarized in Table 2. Saturation of CO_2 and reservoir pressure were chosen as independent parameters, given that the FWU is an active oil production field. It is widely believed that wells used for CO_2 injection would pose less risk because of frequent attention and care (Bachu and Watson, 2009), but micro fractures/cracks can occur when the wells are in use (Bachu and Bennion, 2009). Consequently, wellbore fractures proportion was chosen as another uncertainty parameter. A selected range of these independent uncertainty parameters are summarized in Table 3. The uncertainties of leakage flux were quantified by RSM on the basis of these three parameters.

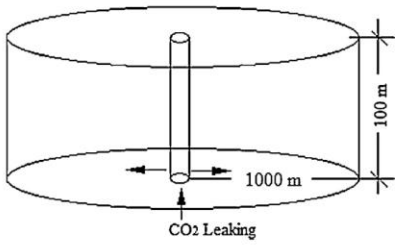

Fig. 3. Simplified conceptual model.

Table 4
Independent parameters for simulations of CO_2 leaking into USDW aquifer.

Parameter name	Low (−1)	Mid (0)	High (+1)	Distribution
Permeability: m^2	10^{-14}	10^{-13}	10^{-12}	Lognormal
Leaking rate: kg/(s m^2)	10^{-21}	10^{-19}	10^{-17}	Lognormal
CEC: meq/100 g	1	6.5	12	Uniform
Absorbent SSA: m^2/g	1	50.5	100	Uniform

2.4. Quantification of risks associated with CO_2 leakage into the Ogallala formation

2.4.1. Model domain and assumptions

A 2-D radial model was assembled and simulated to analyze the potential risks to groundwater quality due to CO_2 leakage (Fig. 3). Regional groundwater flow may dilute potential contaminants, but this was neglected for simplicity in this study, because regional flow velocities in this basin that are maximum ~10 m/year (Nativ and Smith, 1987) is not significant for our simulations to achieve such dilution. In the initial simulation step to quantify CO_2 leakage rate, all simulations assumed that CO_2 dissolves in water instantly when it was injected with gaseous CO_2 injected into the system at a constant rate. Water chemistry results in the Ogallala aquifer were examined for a simulated time duration of 200 years. Based on more than 100 fresh-water well drilling records on/near the FWU (TWDB database), the thickness of the aquifer was assigned 100 m, and the bottom depth was set as 150 m. The distance between monitoring wells of the FWU is around 1000 m; consequently, the dimension of the model was set as 1000 m × 100 m with a total of 230 grid cells. A regression model was created with RSM to assess the impacts to the Ogallala USDW aquifer. Permeability, CO_2 leakage rate, cation exchange capacity (CEC) and absorbent specific surface area (SSA) were chosen as independent parameters (Table 4). The range of CO_2 leakage rate was determined by the results of the previous section, the permeability range was assigned according to typical sand measurements (Beard and Weyl, 1973). Additionally, the ranges of the remaining two parameters are discussed in Section 2.4.3.

2.4.2. Model parameters and boundary conditions

A constant temperature of 25 °C and hydrostatic pressure were assigned as initial conditions. A homogeneous porosity value of 0.3 was used, and heterogeneity neglected (Beard and Weyl, 1973). The initial water chemistry was based on the average composition of more than 100 water analyses of FWU groundwater samples (Table 5), which was conducted by the New Mexico Institute of Mining and Technology, part of SWP Phase III. For the water indexes not available with the water samples, their values were adopted

Table 5
Initial water chemistry of the Ogallala aquifer.

Name	Concentration (mg/L)	Balanced Concentration (mol/kg)
H^+	pH 7.73	$10^{-7.52}$
Mg^{2+}	29.8	1.14×10^{-3}
K^+	5.55	1.42×10^{-4}
SiO_2 (aq)	18.6 (as Si)	6.65×10^{-4}
NO_3^-	15.2	2.45×10^{-4}
Cl^-	60.7	1.71×10^{-3}
$H_2AsO_4^-$	2.40×10^{-3} (as As)	3.41×10^{-9}
Cd^{2+}	3.44×10^{-5}	2.18×10^{-10}
Pb^{2+}	8.70×10^{-4}	2.78×10^{-9}
F^-	1.73	9.12×10^{-5}
Ag^+	3.61×10^{-5}	8.78×10^{-11}
Zn^{2+}	4.50×10^{-1}	5.03×10^{-6}
TDS	570	548 mg/L
Ca^{2+}	51.8	1.04×10^{-3}
Na^+	47.9	2.07×10^{-3}
Fe^{2+}	2.00×10^{-3} [a]	1.49×10^{-8}
HCO_3^-	263[a]	3.70×10^{-3}
SO_4^{2-}	58.9	5.22×10^{-4}
AlO_2^-	1.00×10^{-3} (as Al^{3+})	2.05×10^{-10}
Ba^{2+}	7.20×10^{-2}	5.12×10^{-7}
$Cr(OH)_2^+$	2.00×10^{-3} (as Cr)	3.28×10^{-8}
Cu^{2+}	1.40×10^{-2}	9.19×10^{-8}
$HSeO_3^-$	3.00×10^{-3} (as Se)	1.10×10^{-8}
Mn^{2+}	7.70×10^{-3}	1.17×10^{-7}
ORP	437 mV	–
O_2 (aq)	–	1.48×10^{-40}

[a] Hopkins (1993).

from Hopkins (1993). Total dissolved solids (TDS) was calculated by the sum of concentrations of all ions included and resulting in the simulations.

Selected maximum contaminant levels (MCLs) of drinking water contaminants by Texas and the U.S. E.P.A. (Environmental Protection Agency) are listed in Table 6. All element concentrations except Se do not exceed the Texas MCL; Se does not exceed the EPA standard. TDS exceeds EPA MCL values but not the Texas MCL; NO_3^-, As and Mn are more than 1/10 of the standard value. Former studies suggest that pH is an important indicator for CO_2 intrusion in groundwater. Therefore, this study considered TDS, nitrate, As, Se, Mn and pH as potential water contaminants. The initial dissolved oxygen was calculated using the oxidation reduction potential (ORP) value. A water-mineral equilibrium condition was obtained by performing the simulation without any injection for 100 years (Table 5). The initial mineralogy was set up based on geological data of the High plains aquifer (Qafoku et al., 2013), shown in Table 7. The radius of mineral grain was set to 1 mm, according to

Table 6
Selected MCLs for inorganic contaminants of Texas and EPA.

Name	Texas (mg/L)	EPA (mg/L)
NO_3^-	10 (as N)	10 (as N)
As	0.01	0.01
Se	0.002	0.05
Cd	0.005	0.005
Cr	0.1	0.1
pH	>7.0 (unitless)	6.5–8.5 (unitless)
Mn	0.05	0.05
TDS	1000	500
Al	0.05–0.2	0.05–0.2
SO_4^{2-}	300	250

the results of our size distribution tests for the Ogallala sand samples. Specific surface area (SSA) of each mineral was calculated by SSA = A × v/(V × MW), where A is sphere area, v is molar volume, V is sphere volume, and MW is molecular weight (Labus and Bujok, 2011). Molar volume and molecular weight were obtained from EQ3/6 database (Wolery, 1992).

2.4.3. Chemical reactions

Previous analyses suggest that cation exchange capacity (CEC) and sorption processes with dissolution of carbonates might be the main factors driving the geochemical response to CO_2 injection (Zheng et al., 2012). Aqueous complexation, cation exchange, adsorption/desorption and mineral dissolution/precipitation were considered for chemical reactions. The thermodynamic parameters for aqueous and mineral reactions were taken from the EQ3/6 database (Wolery, 1992). The parameters for the kinetic rate law of minerals were taken from Palandri and Kharaka (2004). For minerals not include in these sources, the kinetic parameters were assumed to be the same as similar minerals in the same category (Table 7).

For adsorption/desorption reactions, the Gouy-Chapman double diffuse layer model was used (Smith, 1999). Hydrous ferric oxide (HFO) was assumed to be the sorbent, because it is a widely existing mineral as a sorbent in shallow natural systems, with the approximate formula $Fe(OH)_3$ used in this model. Constants and sorbent properties were taken from Dzombak and Morel (1990), with the strong site density 9.0×10^{-8} mol sites/m^2, and the weak site density 3.0×10^{-6} mol sites/m^2. Adsorption/desorption reactions are controlled by the total amount of sorption sites (product of amount of sorbent and sorbent SSA). The model sensitivity to the total amount of sorbent sites could be evaluated by varying one of these parameters (Zheng et al., 2012). Sorbent fraction of the

Table 7
List of initial mineral abundance and possible secondary mineral phases.

Mineral	Volume fraction (% of solid)	Reactive SSA (cm^2/g)	Kinetic rate law							
			Neutral		Acid			Base		
			k25 (mol/(m^2 s))	Ea (kJ/mol)	k25	Ea	n (H^+)	k25	Ea	n (H^+)
Primary										
Quartz	60.9	11.328	1.259×10^{-14}	87.5						
Calcite	5.0	11.071	1.600×10^{-6}	23.5	0.501	14.4	1.0			
Kaolinite	8.5	11.565	6.918×10^{-14}	22.2	4.898×10^{-12}	65.9	0.777	8.912×10^{-18}	17.9	−0.472
K-feldspar	23.0	11.735	3.890×10^{-13}	38.0	8.710×10^{-11}	51.7	0.5			
Muscovite	2.5	10.598	3.020×10^{-13}	22.0	7.762×10^{-12}	22.0	0.5			
$Fe(OH)_3$ (HFO)	0.1	9.646	1.000×10^{-11}	61.2						
Secondary										
Illite	0.0	10.858	1.660×10^{-13}	35.0	1.047×10^{-11}	23.6	0.34	3.020×10^{-17}	58.9	−0.40
Smectite-Na	0.0	10.854	1.660×10^{-13}	35.0	1.047×10^{-11}	23.6	0.34	3.020×10^{-17}	58.9	−0.40
Smectite-Ca	0.0	10.880	1.660×10^{-13}	35.0	1.047×10^{-11}	23.6	0.34	3.020×10^{-17}	58.9	−0.40
Dolomite	0.0	10.471	2.951×10^{-8}	52.2	6.456×10^{-4}	36.1	0.5			
Greenrust	0.0	13.483	1.500×10^{-9}	73.0						
Goethite	0.0	7.030	1.148×10^{-8}	86.5						

Table 8
Surface complexation reactions and surface complexation constants on HFO.

Surface complexation reaction	log K
HFO_sOH + H^+ = HFO_sOH_2^+	7.29
HFO_wOH + H^+ = HFO_wOH_2^+	7.29
HFO_sOH = HFO_sO^- + H^+	−8.93
HFO_wOH = HFO_wO^- + H^+	−8.93
HFO_sOH + SO_4^{2-} + H^+ = HFO_sSO_4^- + H_2O	7.78
HFO_wOH + SO_4^{2-} + H^+ = HFO_wSO_4^- + H_2O	7.78
HFO_sOH + SO_4^{2-} = HFO_sOHSO_4^{2-}	0.79
HFO_wOH + SO_4^{2-} = HFO_wOHSO_4^{2-}	0.79
HFO_sOH + Ag^+ = HFO_sOAg + H^+	−1.72
HFO_wOH + Ag^+ = HFO_wOAg + H^+	−5.3
HFO_sOH + Cd^{2+} = HFO_sOCd^+ + H^+	0.47
HFO_wOH + Cd^{2+} = HFO_wOCd^+ + H^+	−2.91
HFO_sOH + $HSeO_3^-$ = HFO_sSeO_3^- + H_2O	4.29
HFO_wOH + $HSeO_3^-$ = HFO_wSeO_3^- + H_2O	4.29
HFO_sOH + $H_2AsO_4^-$ + H^+ = HFO_s H_2AsO_4 + H_2O	10.17
HFO_wOH + $H_2AsO_4^-$ + H^+ = HFO_w H_2AsO_4 + H_2O	10.17
HFO_sOH + Fe^{2+} = HFO_sOFe^+ + H^+	−0.95
HFO_wOH + Fe^{2+} = HFO_wOFe^+ + H^+	−2.98
HFO_wOH + Fe^{2+} + H_2O = HFO_wOFe(OH) + 2H^+	−11.55
HFO_sOH + Cu^{2+} = HFO_sOCu^+ + H^+	2.43
HFO_wOH + Cu^{2+} = HFO_wOCu^+ + H^+	0.14
HFO_sOH + $Cr(OH)_2^+$ = HFO_sO$Cr(OH)^+$ + H_2O	11.63
HFO_sOH + CrO_4^{2-} + H^+ = HFO_sCrO_4^- + H_2O	10.85
HFO_wOH + CrO_4^{2-} + H^+ = HFO_wCrO_4^- + H_2O	10.85
HFO_sOH + CrO_4^{2-} = HFO_sO$HCrO_4^{2-}$	3.9
HFO_wOH + CrO_4^{2-} = HFO_wO$HCrO_4^{2-}$	3.9
HFO_sOH + Mn^{2+} = HFO_sOMn^+ + H^+	−0.4
HFO_wOH + Mn^{2+} = HFO_wOMn^+ + H^+	−3.5
HFO_sOH + Pb^{2+} = HFO_sOPb^+ + H^+	4.65
HFO_wOH + Pb^{2+} = HFO_wOPb^+ + H^+	0.3
HFO_sOH + Zn^{2+} = HFO_sOZn^+ + H^+	0.99
HFO_wOH + Zn^{2+} = HFO_wOZn^+ + H^+	−1.99
HFO_sOH + Ca^{2+} = HFO_wOHCa^{2+}	4.97
HFO_wOH + Ca^{2+} = HFO_wOCa^+ + H^+	−5.85
HFO_wOH + Mg^{2+} = HFO_wOMg^+ + H^+	−4.60

total mineral volume was assigned at 0.1%, and sorbent SSA was treated as an independent uncertainty parameter. Pure sorbent SSA is 600 m^2/g; yet the actual (Ogallala) value is far less. Based on tests of Fe concentrated clay surface areas (Fontes and Weed, 1996) and BET surface area tests for our Ogallala sand samples, 1–100 m^2/g sorbent SSA was used in our study. Adsorption/desorption reactions considered in this study are shown in Table 8.

The CEC of a sediment could often be considered constant (Appelo and Postma, 1993). However, no measured data of the Ogallala formation overlying FWU is available, so CEC was treated as an uncertainty independent parameter. Based on CEC values for various minerals, 1–12 meq/100 g was assigned for this study, which could cover typical values for sands (Ming and Dixon, 1987). The exchange reactions and their selectivity coefficients are shown in Table 9 (Appelo and Postma, 1993).

2.5. Simulation tool

All simulations were performed with TOUGHREACT V2 (Xu et al., 2012) and an equation of state for multiphase CO_2 and brine, ECO2N (Pruess, 2005). TOUGHREACT V2 is enhanced with surface complexation and cation exchange to compute the adsorption and ion exchange processes on mineral surfaces. Although ECO2N does not include a liquid CO_2 phase, the temperature and pressure conditions for the Ogallala suggest only supercritical and dissolved CO_2 phases can exist, indicating that ECO2N is appropriate for this study.

3. Results and discussion

3.1. Cement hydration

The solid phase changes during cement hydration are shown in Fig. 4. With the consumption of alite, belite, ferrite and aluminate, CSH, portlandite and ettringite precipitate as main products, and porosity decrease because of precipitation. These results are consistent with known cement hydration mechanisms (Li, 2011). The composition of cement become stable after 0.1 year, but there are still slight changes for decades of simulated time. Although CSH does not have a confirmed formula, in these simulations the average Ca/Si ratio is about 1.7, corresponding to former studies (Allen et al., 2007). Portlandite ($Ca(OH)_2$) as the major reactant with CO_2 in the wellbore makes up to 40% of the volume of the hydrated cement.

3.2. CO_2 leakage flux through wellbore

The simulated CO_2 leakage rate to the overlying groundwater formation (the Ogallala) during the 100 year time period was of particular interest. The correlation between the original (full reservoir model) simulated CO_2 leakage rates and RSM forecasted rates are above 0.95, which suggests that the RSM forecasts are sufficient. Additional results show that CO_2 leakage rate increase during the first year, but then it maintains a stable value for the remainder of the 100 years. Simulations indicate that no gaseous phase CO_2 leaks, instead only dissolved (aqueous) CO_2 enter the simulated Ogallala. Similar results were also found by Ellison et al. (2012). With the relatively low permeability of wellbore cement, diffusion is assumed to be the main CO_2 leakage mechanism. For CO_2 leakage through wellbore cement obtained in this study, more than 95% is trapped by cement. Only 0.4–4.3% of CO_2 leaks into the USDW formation, at least for the prescribed fracture proportion, reservoir pressure and CO_2 saturation conditions. The cumulative distribution function (CDF) of log CO_2 leakage rate after 100 years fits a normal distribution curve with P value <0.005 by the Anderson-Darling test (Fig. 5). More than 90% probability suggests that the leakage rate for the assigned hydrologic properties range between

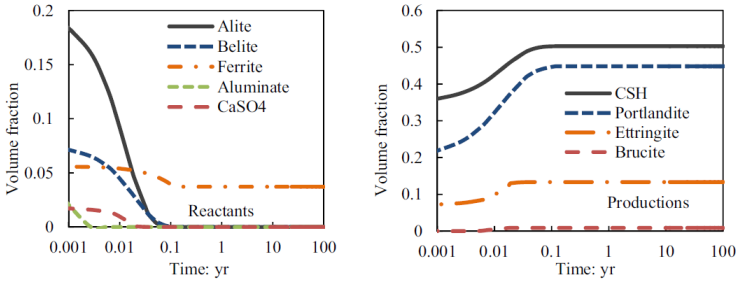

Fig. 4. Composition changes during cement hydration.

Table 9
Cation exchange reactions and selectivity coefficients.

Equation: $Na^+ + 1/i\ M\text{-}X_i \longleftrightarrow Na - X + 1/i\ M^{i+}$ with $K_{Na/M} = [Na - X]\,[M^{i+}]^{1/i}/([M - X_i]^{1/I}\,[Na^+])$

Ion	$K_{Na/M}$	Ion	$K_{Na/M}$	Ion	$K_{Na/M}$
H^+	1	Mg^{2+}	0.5	Ca^{2+}	0.4
K^+	0.2	Fe^{2+}	0.6	Mn^{2+}	0.55
Cu^{2+}	0.5	Zn^{2+}	0.4	Pb^{2+}	0.3
Ba^{2+}	0.35	Cd^{2+}	0.4	Cr^{3+}	0.08

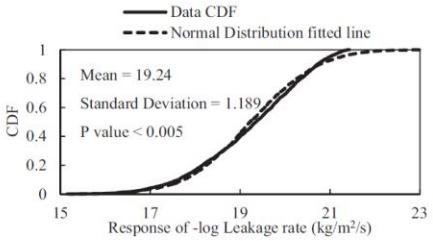

Fig. 5. CDF of CO_2 leakage rate after 100 year.

10^{-21}–10^{-17} kg/(m^2 s), or about 10^{-14}–10^{-10} kg/(m^2 year). This leakage rate is far less than other estimations by former studies (Carroll et al., 2009, 2014; Ellison et al., 2012). However, other studies assumed a much higher wellbore permeability (e.g. 10^{-14}–10^{-10} m^2 used by Carroll et al., 2014) and leaky wells have been assumed to fully penetrate the caprock and connect the storage reservoir and the shallow aquifer (Carroll et al., 2014). Under such conditions, convection would be dominant and result in a much higher leakage flux. If reactive transport within wellbore cement is not considered, CO_2 leakage is also likely to be overestimated—at least in the beginning stages of CO_2 intrusion before cement (portlandite) is consumed. Other studies also confirmed that wellbore cement plays an important role for preventing CO_2 leakage (Carey et al., 2007; Kutchko et al., 2008). Specifically, model simulations with higher permeability (homogeneous 10^{-14} m^2) and without chemical reactions were also executed in this study. Gas phase CO_2 leakage breakthrough occurs much faster than that with chemical reactions, and leakage rate increases significantly up to as high as 10^{-6} kg/(m^2 s), which is similar to the results of other studies. Generally, the model results suggest that these resulting small flux values are due to (1) the scenarios are for non-penetrated micro fractures that naturally occur in the wellbore cement; and (2) the reactions between CO_2 and portlandite ($Ca(OH)_2$) of wellbore cement largely consume CO_2. Note that although porosity decreases due to precipitation of $CaCO_3$, permeability is not considered to be reduced as well; these simulated flux reduction results found in this study are due only to CO_2 consumption by chemical reaction. The reduction in flux rate would be even greater if a permeability-porosity relationship (such as Kozeny-Carman relationships; Carman, 1956) were utilized. We are evaluating such permeability-porosity impacts in more detail in a separate study.

3.3. Risk assessments of CO_2 leakage into the Ogallala formation

3.3.1. Polynomial response surface model and validation of the equations

Generally, the coefficient of determination (R^2) between simulation results and the responses of the regression (RSM) model for all of the water indexes examined exceed 0.9, average values exceed 0.96, and the coefficient of variation of the root mean square error (CVRMSE) is no more than 10%, averaging less than 3% (Table 10). All trace metals (Mn, As, and Se) show similar R^2 and CVRMSE values, thus the table only shows Mn's model adequacy to represent the model adequacy for all trace metals. The high R^2 and low CVRMSE values (Table 10) suggest that the resulting trained ROMs sufficiently fit the original (full reservoir model) simulation outcomes, and the ROMs are adequate for predicting outcomes of interest for full-scaled (non-ROM) simulations within the given range.

To verify the adequacy of the regression models for all the cases in this experimental domain, a total of 50 randomized simulations were conducted. Each independent parameter ranged from −1 to +1, following their distributions. The correlation between simulated outcomes and regression models was calculated for all water indexes of interest. The R^2 and CVRMSE values between these two series of results are shown in Table 11. It shows a nearly linear correlation between simulation and ROM results with an R^2 value that exceeds 0.7 after one year, and exceeds 0.85 afterwards. In the first few years, all water indexes examined do not show significant changes due to CO_2 leakage, which could explain the lower values of R^2 for the first year's results. On the other hand, CVRMSE is no more than 1% for the results after one year, and averaged 5% over a 200 year period. Lower correlations between the response surface model and the verification simulation results are observed for TDS, pH, N, Mn, As and Se, but the regression model can represent the full-scale simulation results with a high confidence level.

3.3.2. Risks of CO_2 leakage into the Ogallala formation (case study) and early detection criteria

For simulations of up to 50 years of CO_2 leakage, no significant changes in TDS, trace metals or pH resulted throughout the entire domain. However, after 100 years, the changes become more obvious. After 200 years, there is more than a 10% possibility that TDS exceeds 780 mg/L (initially 540 mg/L), approaching a 50% increase compared to the initial value (Fig. 6). pH ranges between 7.2–7.7 through the domain (initially 7.5), which is less than 10% different (Fig. 7). Concentrations of other elements (N, Mn, As, Se) show similar trends to TDS (figures not shown).

Both Figs. 6 and 7 indicate the upper layer of the domain generally exhibit stronger impacts because CO_2 buoyancy promotes more contact by CO_2. In this model, CO_2 dissolves in groundwater when it migrates into the USDW formation, increasing the density of that groundwater within the bottom layer of the Ogallala aquifer. However, the CO_2 leakage rates are small enough that the increased density has a negligible impact. Simulated head gradients dictate that dissolved CO_2 as well as some ions flow upward and laterally away from the leaky well. Horizontally, the impacts of CO_2 plume extent reaches more than 1000 m away from the leakage point following initial significant changes after 50 years. These changes facilitate detection at the monitoring wells.

The CDF of responses of TDS at 10, 50, 100 and 200 years (Fig. 8) suggests that as time increases, the uncertainty increases. In the first 50 years, no significant changes of TDS resulted. Even at 100 years, simulation results suggest only about a 10% probability that TDS would exceed 600 mg/L, which is well within what would be considered normal fluctuation. After 200 years, this probability grows to 40%, and with a 10% probability that TDS exceeds 50% variation of the initial value. However, results also suggest less than

Table 10
Model adequacy between simulation results and ROM responses.

	Time, yr	1	10	50	100	200
TDS	R^2	$0.990^{+0.008}_{-0.028}$	$0.993^{+0.006}_{-0.021}$	$0.994^{+0.006}_{-0.020}$	$0.993^{+0.006}_{-0.019}$	$0.993^{+0.007}_{-0.018}$
	CVRMSE, %	$0.013^{+0.039}_{-0.013}$	$0.129^{+0.385}_{-0.100}$	$0.635^{+1.787}_{-0.498}$	$1.267^{+3.716}_{-1.019}$	$2.553^{+7.659}_{-2.142}$
pH	R^2	$0.964^{+0.029}_{-0.032}$	$0.993^{+0.007}_{-0.021}$	$0.993^{+0.006}_{-0.021}$	$0.993^{+0.006}_{-0.020}$	$0.994^{+0.005}_{-0.018}$
	CVRMSE, %	$0.002^{+0.005}_{-0.002}$	$0.013^{+0.040}_{-0.010}$	$0.067^{+0.187}_{-0.049}$	$0.133^{+0.364}_{-0.100}$	$0.264^{+0.715}_{-0.191}$
N	R^2	$0.981^{+0.019}_{-0.029}$	$0.993^{+0.006}_{-0.021}$	$0.994^{+0.006}_{-0.020}$	$0.994^{+0.006}_{-0.019}$	$0.994^{+0.005}_{-0.016}$
	CVRMSE, %	$0.015^{+0.053}_{-0.015}$	$0.139^{+0.415}_{-0.109}$	$0.692^{+1.975}_{-0.538}$	$1.386^{+4.104}_{-1.130}$	$2.809^{+8.473}_{-2.401}$
Mn	R^2	$0.968^{+0.026}_{-0.031}$	$0.994^{+0.006}_{-0.021}$	$0.993^{+0.006}_{-0.020}$	$0.993^{+0.006}_{-0.019}$	$0.993^{+0.006}_{-0.018}$
	CVRMSE, %	$0.019^{+0.055}_{-0.019}$	$0.132^{+0.391}_{-0.095}$	$0.677^{+1.870}_{-0.489}$	$1.356^{+3.902}_{-0.995}$	$2.727^{+8.025}_{-2.101}$

Table 11
Model adequacy between verification simulation results and ROM responses.

	Time, yr	1	10	50	100	200
TDS	R^2	$0.833^{+0.028}_{-0.027}$	$0.878^{+0.031}_{-0.020}$	$0.881^{+0.035}_{-0.020}$	$0.881^{+0.037}_{-0.020}$	$0.883^{+0.039}_{-0.020}$
	CVRMSE, %	$0.028^{+0.034}_{-0.021}$	$0.274^{+0.356}_{-0.213}$	$1.332^{+1.725}_{-1.016}$	$2.608^{+3.341}_{-2.044}$	$5.004^{+6.152}_{-3.614}$
pH	R^2	$0.766^{+0.169}_{-0.043}$	$0.876^{+0.017}_{-0.019}$	$0.877^{+0.018}_{-0.025}$	$0.879^{+0.005}_{-0.044}$	$0.885^{+0.005}_{-0.098}$
	CVRMSE, %	$0.004^{+0.005}_{-0.004}$	$0.028^{+0.036}_{-0.021}$	$0.140^{+0.178}_{-0.106}$	$0.280^{+0.344}_{-0.221}$	$0.568^{+0.632}_{-0.388}$
N	R^2	$0.815^{+0.069}_{-0.029}$	$0.879^{+0.030}_{-0.020}$	$0.881^{+0.035}_{-0.020}$	$0.883^{+0.038}_{-0.020}$	$0.889^{+0.037}_{-0.018}$
	CVRMSE, %	$0.032^{+0.031}_{-0.024}$	$0.295^{+0.390}_{-0.230}$	$1.457^{+1.891}_{-1.125}$	$2.857^{+3.691}_{-2.243}$	$5.486^{+6.821}_{-3.964}$
Mn	R^2	$0.782^{+0.094}_{-0.031}$	$0.877^{+0.035}_{-0.020}$	$0.879^{+0.034}_{-0.020}$	$0.878^{+0.036}_{-0.020}$	$0.879^{+0.039}_{-0.020}$
	CVRMSE, %	$0.035^{+0.042}_{-0.025}$	$0.283^{+0.362}_{-0.212}$	$1.398^{+1.810}_{-1.072}$	$2.737^{+3.495}_{-2.144}$	$5.232^{+6.363}_{-3.708}$

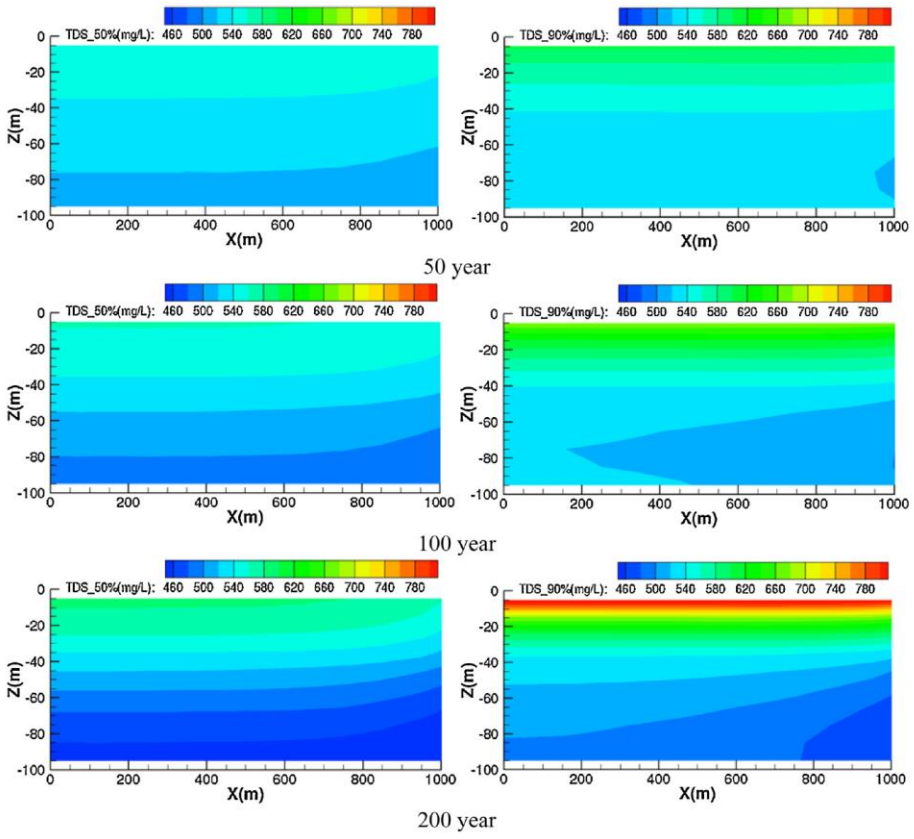

Fig. 6. 50th and 90th percentile probabilities of TDS distribution after 50, 100, and 200 years.

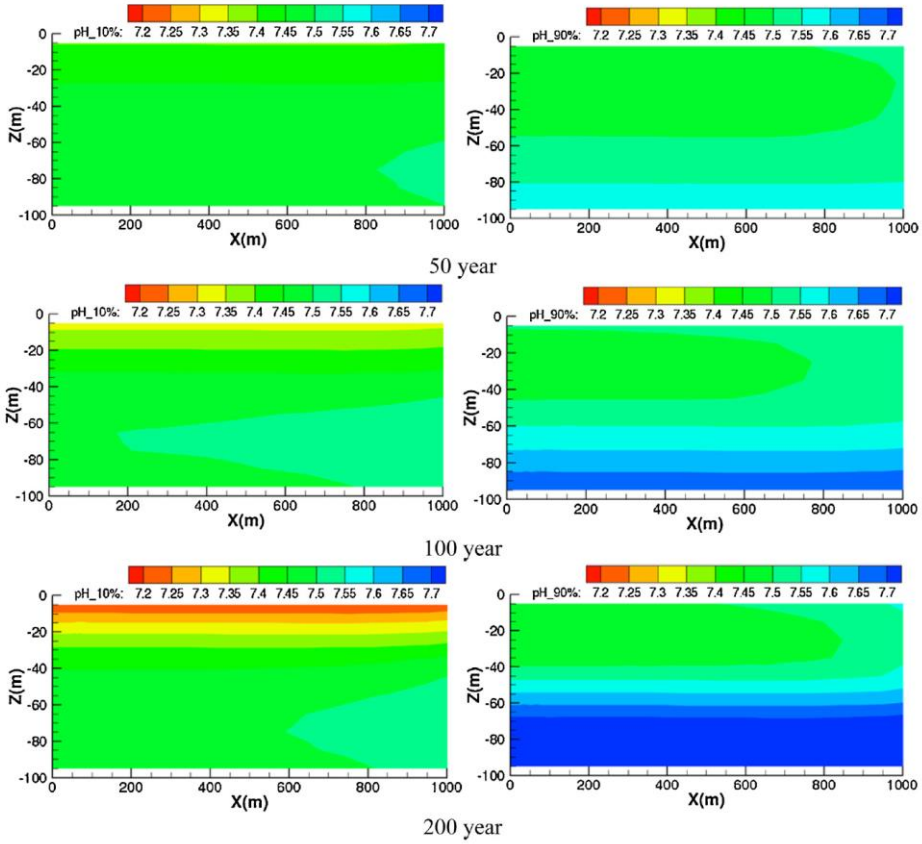

Fig. 7. 10th and 90th percentile probabilities of pH distribution after 50, 100, and 200 years.

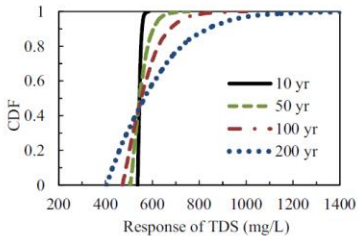

Fig. 8. CDF of TDS responses at 10, 50, 100, and 200 years.

a 4% probability that TDS could exceed 1000 mg/L, which is Texas' MCL threshold.

It is usually believed that the closer test wells are located to the leaking point, the sooner that detections are rendered. However, based on this study, the CDF plots for 100, 500 and 1000 m away from the leakage point only show slight differences within 200 years. The existing monitoring wells are 1000 m away (on average) from the injection/production wells in the FWU, and at this distance a well could detect groundwater quality changes due to CO_2 leakage at later times. This study only considered low CO_2 leakage rates. If CO_2 leakage rates were relatively high, such as those associated with the highly-over-pressured reservoir driving flow into the Ogallala aquifer, earlier detection of the leakage would be likely.

Fig. 9 illustrates concentration changes in water quality indexes examined, with different percentiles at 1000 m away from the leakage point. Within the 95th percentile, the concentrations are not likely to exceed twice the initial values, or exceed the MCL limits. However, Se already exceeds the Texas MCL (0.002 mg/L) value initially, and these simulations forecast a 50% probability that the concentration would increase (worsen) during the 200 year period. On the other hand, Se does not exceed EPA MCL standards for drinking water (<0.05 mg/L), and it is still ~10 times less than the EPA standard.

Usually groundwater chemistry varies over time due to multiple reasons including groundwater flow, experimental errors and other issues, and some differences among tests are typically acceptable. Early detection of CO_2 leakage is more difficult by water chemistry tests if the change is very small, especially if less than 10%. Consequently, suggested principles to choose indicators for early detection include: (1) ease of testing and (2) detection of significant changes due to CO_2 leakage, especially compared to existing monitoring data (Table 12) or they exceed regulatory MCLs. Carroll et al. (2014) introduced "impact thresholds" for a no-impact contaminant level based on site-specific data. This is meaningful for water chemistry change quantification, especially for those water indices that are significantly different from the MCLs. Such no-impact thresholds were also calculated based on more than 100

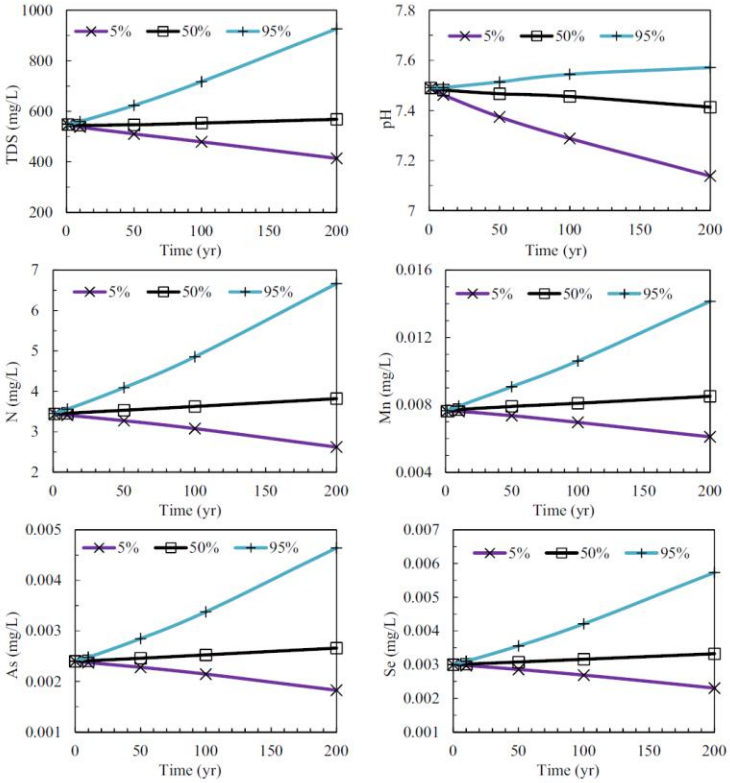

Fig. 9. Selection of water index changes via time at current monitoring wells with 5th, 50th and 95th percentiles.

Table 12
Selection of water index variations at current monitoring wells.

	pH	TDS, mg/L	N, mg/L	Mn, mg/L	As, mg/L	Se, mg/L
Average	7.7	570	3.43	0.008	0.0024	0.003
Median	7.7	415	2.69	0.001	0.0025	0.003
Minimum	7.2	160	0.00	0	0	0.000
Maximum	8.2	1946	7.69	0.147	0.004	0.008
5% threshold	7.5	244	1.20	1.0×10^{-4} [a]	1.0×10^{-4} [a]	1.0×10^{-4} [a]
95% threshold	8.0	1757	7.52	0.03	0.0038	0.008

[a] Detection limit by ICP-MS (http://www.eag.com/documents/icp-oes-ms-detection-limit-guidance-BR023.pdf).

monitoring water samples of the Ogallala groundwater in this study (Table 12), with 5% and 95% thresholds. If a predicted concentration stays between the 5–95% thresholds, it may be considered "no impact" to water quality. The no-impact thresholds for this specific site are overall stricter than the MCLs (except TDS), suggesting that the thresholds could be more sensitive to the water chemistry changes than regulatory MCLs for the sites with high water quality (a scenario described by Carroll et al., 2014).

Manganese, As and Se all exhibit a relatively large number of "no detection" (trace, minor, or none detected) values, so the detection limits are used for their 5% thresholds, respectively. Based on these results, we infer that pH is not likely to exceed EPA and Texas MCLs. However, there is ~50% probability that pH would exceed the 5% threshold in 50 years, suggesting that pH could be considered as indicator for CO_2 leakage. The selected trace metals (Mn, As and Se) exhibit greater than 50% increase of their concentrations in the worst-case scenarios, but chances are low that these would exceed the 95% thresholds or MCLs. Arsenic is the only trace metal even close to being significant, with a ~5% probability that it would exceed the no-impact threshold after 150 years. These data might be considered normal and not suggested as leakage indicators. These trace metals usually require inductively coupled plasma-mass spectrometry (ICP-MS) to be detected, which is hardly portable (current technology), and field methods increase the possibility of larger errors. This is also another reason that the trace metals are not suggested to serve as early detection water quality change indicators. Total dissolved solids is one index that is easily tested in the field, and its concentration could increase more than 50% of its initial value according to these ROM results. However, in-situ tests suggest large error bars (uncertainty) for TDS with a high no-impact threshold; so TDS is not recommended as an early detection indicator. Additionally, this study indicates that nitrate is not recommended as an indicator either. Nitrate is not a reactant with CO_2 and it is not released like trace metals in the simulations, but it

usually shows slight increases when redox changes. For most of the simulated cases, nitrate concentration does not show a significant increase (no more than 50% probability). The reason for its concentration increase in the top layer in worst-case scenarios (with highest nitrate concentration increase) is both the impacts of redox changes due to CO_2 leakage and the up-flow due to slight density changes of the groundwater. In general, the Ogallala groundwater quality is not likely to be significantly impacted due to limited CO_2 leakage (e.g., rates forecasted in this study) through wellbore cement with micro fractures. The value of pH is very sensitive to the intrusion of CO_2 in the early stage (less than 50 years) compared to the no-impact threshold value, suggesting that it may be suitable as a geochemical indicator for CO_2 leakage.

4. Conclusions

This study focuses on assessment of potential risks of CO_2 leakage through wellbores on groundwater quality using an RSM approach, as well as identification of water chemical factors to establish early detection criteria. The case study application is a commercial-scale CO_2-EOR field. Before that, we evaluated the uncertainties of the CO_2 leakage rate with consideration of CO_2-cement chemical reactions.

Major findings include:

(1) This study suggests that a greater than 90% probability of leakage rate values should range between 10^{-14}–10^{-10} kg/(m^2 year). This small leakage rate is explained by the relatively low permeability of wellbore cement, and chemical reactions between CO_2 and portlandite ($Ca(OH)_2$) that consumes CO_2 as well as further decrease the fracture porosity resisting the CO_2 pathways.
(2) RSM-based results are sufficiently robust, as indicated by coefficient of determination (R^2) and coefficient of variation of the root mean square error (CVRMSE) values calculated between simulation results and the RSM-predicted responses. R^2 and CVRMSE between 50 validation simulation results and response surface equations are >0.8 and <10%, respectively. The high R^2 and low CVRMSE values suggest that the results of ROMs are likely sufficiently effective for representing full-reservoir model simulation results.
(3) No-impact thresholds associated with site-specific monitoring data could be a valuable reference for evaluation of CO_2 impacts.
(4) Within the range of CO_2 leakage rate, TDS, nitrate and trace metal concentrations could be twice as much as the initial value with the worst scenarios after 200 years. However, these water indices do not exceed the MCL limit, or exceed no-impact thresholds according to the in situ monitoring data, suggesting that the Ogallala groundwater quality should not be significantly impacted.
(5) Water quality at 100, 500 and 1000 m away from the leakage point indicate only slight differences within 200 years, suggesting that the distance between current monitoring wells and injection/production wells is of limited impact with respect to early detection criteria.
(6) pH is suggested as a likely geochemical indicator for early detection, because it is sensitive to CO_2 leakage and is easy to detect.

This study has limitations that indicate much future work can be done on this topic. Future research may include (1) calibration of the cement hydration simulations with experiments to obtain more accurate data; (2) an improved model for the Ogallala formation could be developed with more field formation data; (3) calibration of geochemical reactions with CO_2 by laboratory experiments could be utilized to obtain site specific reaction parameters, especially for sorbent type, sorption capacity and sorbent surface areas; and (4) additional boundary conditions such as different reservoir pressure could be evaluated, depending on the specific site/location of interest.

Acknowledgements

This study is supported by the U.S. Department of Energy and NETL (National Energy Technology Laboratory), contract DE- FC26-05NT42591.

References

Allen, A.J., Thomas, J.J., Jennings, H.M., 2007. Composition and density of nanoscale calcium-silicate-hydrate in cement. Nat. Mater. 6, 311–316.
Appelo, C.J.A., Postma, D., 1993. Geochemistry Groundwater and Pollution. A. A. Balkema, Rotterdam, Netherlands.
Bachu, S., Bennion, D.B., 2009. Experimental assessment of brine and/or CO_2 leakage through well cements at reservoir conditions. Int. J. Greenh. Gas Control 3, 494–501.
Bachu, S., Watson, T.L., 2009. Review of failures for wells used for CO_2 and acid gas injection in Alberta, Canada. Energy Procedia 1, 3531–3537.
Bacon, D.H., Dai, Z., Zheng, L., 2014. Geochemical impacts of carbon dioxide, brine, trace metal and organic leakage into an unconfined, oxidizing limestone aquifer. Energy Procedia 63, 4684–4707.
Bacon, D.H., Qafoku, N.P., Dai, Z., Keating, E.H., Brown, C.F., 2016. Modeling the impact of carbon dioxide leakage into an unconfined, oxidizing carbonate aquifer. Int. J. Greenh. Gas Control 44, 290–299.
Beard, D.C., Weyl, P.K., 1973. Influence of texture on porosity and permeability of unconsolidated sand. Am. Assoc. Pet. Geol. B 57 (2), 349–369.
Bezerra, M.A., Santelli, R.E., Oliveira, E.P., Villa, L.S., Escaleira, L.A., 2008. Response surface methodology (RSM) as a tool for optimization in analytical chemistry. Talanta 76, 965–977.
Box, G.E., Draper, N.R., 1987. Empirical Model-Building and Response Surfaces. John Wiley and Sons, New York, USA.
Carey, J.W., Wigand, M., Chipera, S.J., WoldeGabriel, G., Pawar, R., Lichtner, P.C., Wehner, S.C., Raines, M.A., Guthrie Jr., G.D., 2007. Analysis and performance of oil well cement with 30 years of CO_2 exposure from the SACROC unit, West Texas, USA. Int. J. Greenh. Gas Control 1, 75–85.
Carman, P.C., 1956. Flow of Gases Through Porous Media. Academic Press Inc., New York, USA.
Carroll, S., Hao, Y., Aines, R., 2009. Geochemical detection of carbon dioxide in dilute aquifers. Geochem. Trans. 10, http://dx.doi.org/10.1186/1467-4866-10-4.
Carroll, S.A., Keating, E., Mansoor, K., Dai, Z., Sun, Y., Trainor-Guitton, W., Brown, C., Bacon, D., 2014. Key factors for determining groundwater impacts due to leakage from geologic carbon sequestration reservoirs. Int. J. Greenh. Gas Control 29, 153–168.
Cronin, J.G., 1969. Ground water in the Ogallala formation in the Southern High Plains of Texas and New Mexico. In: Hydrologic Investigations Atlas HA-330. U.S. Geological Survey, Washington, D.C.
DOE/NETL, 2010. Carbon Dioxide Enhanced Oil Recovery Untapped Domestic Energy Supply and Long Term Carbon Storage Solution. https://www.netl.doe.gov/file%20library/research/oil-gas/small_CO2_EOR_Primer.pdf.
Dai, Z., Keating, E., Bacon, D., Viswanathan, H., Stauffer, P., Jordan, A., Pawar, R., 2014a. Probabilistic evaluation of shallow groundwater resources at a hypothetical carbon sequestration site. Sci. Rep. 4 (4006), http://dx.doi.org/10.1038/srep04006.
Dai, Z., Middleton, R., Viswanathan, H., Fessenden-Rahn, J., Bauman, J., Pawar, R., Lee, S., McPherson, B., 2014b. An integrated framework for optimizing CO_2 sequestration and enhanced oil recovery. Environ. Sci. Technol. Lett. 1, 49–54.
Dai, Z., Stauffer, P.H., Carey, J.W., Middleton, R.S., Lu, Z., Jacobs, J.F., Hnottavange-Telleen, K., Spangler, L.H., 2014c. Pre-site characterization risk analysis for commercial-scale carbon sequestration. Environ. Sci. Technol. 48, 3908–3915.
Dzombak, D.A., Morel, F.M.M., 1990. Surface Complexation Modeling-Hydrous Ferric Oxide. John Wiley & Sons, New York, USA.
Ellison, K., Falta, R., Murdoch, L., Brame, S., 2012. Behavior of brines containing dissolved CO_2 in abandoned wellbores. In: Proceedings, TOUGH, Symposium, Lawrence Berkeley National Laboratory, Berkeley, California, September 17–19, 2012.
Fontes, M.P.F., Weed, S.B., 1996. Phosphate adsorption by clays from Brazilian oxisols: relationships with specific surface area and mineralogy. Geoderma 72, 37–51.
Frye, E., Bao, C., Li, L., Blumsack, S., 2012. Environmental controls of cadmium desorption during CO_2 leakage. Environ. Sci. Technol. 46, 4388–4395.
Gaus, I., 2010. Review: role and impact of CO_2-rock interactions during CO_2 storage in sedimentary rocks. Int. J. Greenh. Gas Control 4, 73–89.
George, P.G., Mace, R.E., Petrossian, R., 2011. Aquifers of Texas. Texas Water Report 380. Texas Water Development Board, Austin, TX, USA.
Hopkins, J., 1993. Water-quality Evaluation of the Ogallala Aquifer, Texas. Texas Water Report 342. Texas Water Development Board, Austin, TX, USA.

International Panel on Climate Change (IPCC), 2005. IPCC Special Report on Carbon Dioxide Capture and Storage. Cambridge University Press, New York, NY, USA.
Kutchko, B.G., Strazisar, B.R., Lowry, G.V., Dzombak, D.A., Thaulow, N., 2008. Rate of CO_2 attack on hydrated class H well cement under geologic sequestration condition. Environ. Sci. Technol. 42, 6237–6242.
Labus, K., Bujok, P., 2011. CO_2 mineral sequestration mechanisms and capacity of saline aquifers of the upper silesian coal basin (central Europe)—modeling and experimental verification. Energy 36, 4974–4982.
Li, S., Zhang, Y., 2014. Model complexity in carbon sequestration: a design of experiment and response surface uncertainty analysis. Int. J. Greenh. Gas Control 22, 123–138.
Li, Z., 2011. Advanced Concrete Technology. John Wiley & Sons, Hoboken, New Jersey, USA.
Little, M.G., Jackson, R.B., 2010. Potential impacts of leakage from deep CO_2 geosequestration on overlying freshwater aquifers. Environ. Sci. Technol. 44, 9225–9232.
Lu, J., Partin, J.W., Hovorka, S.D., Wong, C., 2010. Potential risks to freshwater resources as a result of leakage from CO_2 geological storage: a batch-reaction experiment. Environ. Sci. Technol. 60, 335–348.
Mehta, P.K., Monteiro, P., 2014. Concrete: Microstructure, Properties, and Materials, fourth edition. McGraw-Hill Education, New York, NY, USA.
Ming, D.W., Dixon, J.B., 1987. Quantitative determination of clinoptilolite in soils by a cation-exchange capacity method. Clays Clay Miner. 35, 463–468.
Myers, R.H., Montgomery, D.C., 1995. Response Surface Methodology: Process and Product Optimization Using Designed Experiments. John Wiley & Sons, New York, NY, USA.
Nativ, R., Smith, D.A., 1987. Hydrogeology and geochemistry of the Ogallala aquifer, Southern High Plains. J. Hydrol. 91, 217–253.
Palandri, J.L., Kharaka, Y.K., 2004. A Compilation of Rate Parameters of Water-Mineral Interaction Kinetics for Application to Geochemical Modeling. Report 2004–1068. U.S. Geological Survey, Menlo Park, CA, USA.
Pawar, R., Bromhal, G., Carroll, S., Chu, S., Dilmore, R., Gastelum, J., Oldenburg, C., Stauffer, P., Zhang, Y., Guthrie, G., 2014. Quantification of key long-term risks at CO_2 sequestration sites: latest results from US DOE's national risk assessment partnership (NRAP) project. Energy Procedia 63, 4816–4832.
Pruess, K., Oldenburg, C., Moridis, G., 2012. TOUGH2 User's Guide, Version 2. Report LBNL-43134. Lawrence Berkeley National Laboratory, Berkeley, CA, USA.
Pruess, K., 2005. ECO2N: A TOUGH2 Fluid Property Module for Mixtures of Water, NaCl, and CO_2. Report LBNL-57952. Lawrence Berkeley National Laboratory, Berkeley, CA, USA.
Qafoku, N.P., Lawter, A.R., Brown, C.F., Bowden, M., Wang, G., Harvey, O.R., Sullivan, C., 2013. Geochemical Impacts of Leaking CO_2 from Subsurface Storage Reservoirs to Unconfined and Confined Aquifers. Report PNNL-22420. Pacific Northwest National Laboratory, Richland, WA, USA.
Rimmelé, G., Barlet-Gouédard, V., Porcherie, O., Goffé, B., Brunet, F., 2008. Heterogeneous porosity distribution in Portland cement exposed to CO_2-rich fluids. Cem. Concr. Res. 38, 1038–1048.
Rohmer, J., Bouc, O., 2010. A response surface methodology to address uncertainties in cap rock failure assessment for CO_2 geological storage in deep aquifers. Int. J. Greenh. Gas Control 4, 198–208.
Scrivener, K.L., Füllmann, T., Gallucci, E., Walenta, G., Bermejo, E., 2004. Quantitative study of portland cement hydration by X-ray diffraction/rietveld analysis and independent methods. Cem. Concr. Res. 34, 1541–1547.
Smith, K.S., 1999. Metal sorption on mineral surfaces: an overview with examples relating to mineral deposits. In: Plumlee, G.S., Logson, M.J. (Eds.). The Environmental Geochemistry of Mineral Deposits, Rev. Econ. Geol. 6A–6B, 161–182.
Texas Water Development Board (TWDB) database, http://www.twdb.texas.gov/groundwater/data/drillersdb.asp (accessed 05.16.16).
Viswanathan, H., Dai, Z., Lopano, C., Keating, E., Hakala, J.A., Scheckel, K.G., Zheng, L., Guthrie, G.D., Pawar, R., 2012. Developing a robust geochemical and reactive transport model to evaluate possible sources of arsenic at the CO_2 sequestration natural analog site in Chimayo, New Mexico. Int. J. Greenh. Gas Control 10, 199–214.
Wells, A.W., Diehl, J.R., Bromhal, G., Strazisar, B.R., Wilson, T.H., White, C.M., 2007. The Use of tracers to assess leakage from the sequestration of CO_2 in a depleted oil reservoir, New Mexico, USA. Appl. Geochem. 22, 996–1016.
Wilkin, R.T., Digiulio, D.C., 2010. Geochemical impacts to groundwater from geologic carbon sequestration: controls on pH and inorganic carbon concentrations from reaction path and kinetic modeling. Environ. Sci. Technol. 44, 4821–4827.
Wolery, T.J., 1992. EQ3/6, A Software Package for Geochemical Modeling of Aqueous Systems: Package Overview and Installation Guide, Version 7.0. Report UCRL-MA-110662 PT I. Lawrence Livermore National Laboratory, Livemore, CA, USA.
Xu, T., Spycher, N., Sonnenthal, E., Zheng, L., Pruess, K., 2012. TOUGHREACT User's Guide: A Simulation Program for Non-isothermal Multiphase Reactive Transport in Variably Saturated Geologic Media, Version 2.0. Lawrence Berkeley National Laboratory, Berkeley, CA, USA.
Yang, C., Dai, Z., Romanak, K.D., Hoverka, S.D., Treviño, R.H., 2014. Inverse modeling of water–rock–CO_2 batch experiments: potential impacts on groundwater resources at carbon sequestration sites. Environ. Sci. Technol. 48 (5), 2798–2806.
Zheng, L., Apps, J.A., Spycher, N., Birkholzer, J.T., Kharaka, Y.K., Thordsen, J., Beers, S.R., Herkelrath, W.N., Kakouros, E., Trautz, R.C., 2012. Geochemical modeling of changes in shallow groundwater chemistry observed during the MSU-ZERT CO_2 injection experiment. Int. J. Greenh. Gas Control 7, 202–217.
Zheng, L., Spycher, N., Varadharajan, C., Tinnacher, R.M., Pugh, J.D., Cianchi, M., Birkholzer, J., Nico, P.S., Trautz, R.C., 2015. On the mobilization of metals by CO_2 leakage into shallow aquifers: exploring release mechanisms by modeling field and laboratory experiments. Greenh. Gases Sci. Technol. 5, 403–418.

CHAPTER 4

ARSENIC MOBILIZATION IN SHALLOW AQUIFERS DUE TO CO_2 AND BRINE INTRUSION FROM STORAGE RESERVOIRS

Reprinted from Scientific Reports (open access journal) 7, Ting Xiao, Zhenxue Dai, Hari Viswanathan, Alexandra Hakala, Martha Cather, Wei Jia, Yongchao Zhang, Brian McPherson, Arsenic mobilization in shallow aquifers due to CO_2 and brine intrusion from storage reservoirs, article number 2763, 2017, doi:10.1038/s41598-017-02849-z.

In Chapter 3, we analyzed the chemical impacts of CO_2 leakage on the groundwater quality in the Ogallala aquifer overlying the Farnsworth Unit (FWU), and water chemistry components that are suitable for early detection criteria. Among all the USDW water quality changes due to CO_2 intrusion, toxic trace metals release and mobilization from aquifer sediments are of special interests. An additional risk is the leakage of reservoir brine, which may contain toxic substances, into USDWs.

In this chapter, the mechanisms of toxic trace metal (arsenic in specific) mobilization with an integrated experimental and simulation framework is analyzed. The responses of arsenic (As) release under different water salinities and key kinetic parameters controlling As mobilization processes are identified. The case study includes elevated CO_2 conditions at the Chimayo site in northern New Mexico, a natural analog with CO_2 upwelling. Batch experiments of water-rock-CO_2 interactions are conducted with both fresh groundwater and saline water, to mimic scenarios of CO_2 leakage with and without deeper formation brine. Quantitative interpretation of As mobilization due to leaked CO_2 and brine utilizes an inverse reactive transport modeling approach.

www.nature.com/scientificreports

OPEN

Arsenic mobilization in shallow aquifers due to CO_2 and brine intrusion from storage reservoirs

ceived: 10 March 2017
cepted: 18 April 2017
blished online: 05 June 2017

Ting Xiao[1,2,3], Zhenxue Dai[1,4,5], Hari Viswanathan[1], Alexandra Hakala[6], Martha Cather[7], Wei Jia[2,3], Yongchao Zhang[1,8] & Brian McPherson[2,3]

We developed an integrated framework of combined batch experiments and reactive transport simulations to quantify water-rock-CO_2 interactions and arsenic (As) mobilization responses to CO_2 and/or saline water leakage into USDWs. Experimental and simulation results suggest that when CO_2 is introduced, pH drops immediately that initiates release of As from clay minerals. Calcite dissolution can increase pH slightly and cause As re-adsorption. Thus, the mineralogy of the USDW is ultimately a determining factor of arsenic fate and transport. Salient results suggest that: (1) As desorption/adsorption from/onto clay minerals is the major reaction controlling its mobilization, and clay minerals could mitigate As mobilization with surface complexation reactions; (2) dissolution of available calcite plays a critical role in buffering pH; (3) high salinity in general hinders As release from minerals; and (4) the magnitude and quantitative uncertainty of As mobilization are predicated on the values of reaction rates and surface area of calcite, adsorption surface areas and equilibrium constants of clay minerals, and cation exchange capacity. Results of this study are intended to improve ability to quantify risks associated with potential leakage of reservoir fluids into shallow aquifers, in particular the possible environmental impacts of As mobilization at carbon sequestration sites.

Geologic CO_2 sequestration (GCS) is considered a promising approach for mitigating CO_2 emissions from centralized sources[1–9]. One major concern is the risk of CO_2 and/or brine leakage from deep sequestration reservoirs through highly-permeable zones such as faults and abandoned wells into overlying underground sources of drinking water (USDW)[10]. Carbon dioxide itself is not hazardous to water quality, but increased CO_2 concentrations in shallow groundwater aquifers could reduce pH and enhance geochemical reactions between groundwater and aquifer sediments, resulting in release and mobilization of toxic trace metals[11,12]. An additional risk is the leakage of reservoir brine, which may contain toxic substances, into USDWs[13,14].

To assess the risk of CO_2/brine leakage to overlying USDWs and to detect signatures of aquifer quality changes at early stages, various approaches have been conducted with lab-scale experiments[11,15–17], short-term field-scale tests[18–20], numerical modeling[21–27], and natural analog observations[13,28]. Most of these studies focus on CO_2 leakage and its impacts on groundwater quality, but a limited number of studies have examined the leakage of brine with/without CO_2 into shallow aquifers. Keating *et al.*[29] observed the upward migration of CO_2 and saline water under natural conditions, which affected the salinity and trace metal concentrations in shallow groundwater. To date, modeling approaches combined with laboratory/field observations are necessary for studies of the geochemical impacts of leaked CO_2 in shallow aquifers, to reduce the uncertainties of modeling itself and to interpret the observation data with appropriate reaction patterns. Yang *et al.*[27] developed an inverse multicomponent geochemical modeling approach to interpret responses of water chemistry to the introduction of CO_2 into a set of laboratory batch reactors containing carbonate-poor and carbonate-rich potable aquifer sediments. Bacon *et al.*[21] applied multiphase reactive transport modeling to identify potential trace metal release mechanisms under

[1]Earth and Environmental Sciences Division, Los Alamos National Laboratory, Los Alamos, New Mexico, 87545, USA. [2]Department of Civil and Environmental Engineering, University of Utah, Salt Lake City, UT, 84112, USA. [3]Energy and Geoscience Institute, University of Utah, Salt Lake City, UT, 84108, USA. [4]College of Construction Engineering, Jilin University, Changchun, 130026, China. [5]Key Laboratory of Groundwater Resources and Environment, Ministry of Education, Jilin University, Changchun, 130021, China. [6]U.S. Department of Energy, National Energy and Technology Laboratory, Pittsburgh, PA, 10940, USA. [7]Petroleum Recovery Research Center, New Mexico Institute of Mining and Technology, Socorro, NM, 87801, USA. [8]College of Geosciences, China University of Petroleum, Beijing, 102249, China. Correspondence and requests for materials should be addressed to Z.D. (email: dzx@jlu.edu.cn)

elevated CO_2 conditions in a carbonate aquifer with both batch and column experiments. However, limited studies have been conducted with such combined approaches for geochemical mechanisms under saline conditions to interpret the responses to brine leakage, which is also significant for quantitative risk analysis of GCS projects.

The primary goal of this paper is to elucidate the mechanisms of trace metal mobilization with an integrated experimental and simulation framework. The case study includes elevated CO_2 conditions at the Chimayo site in northern New Mexico, a natural analog with CO_2 upwelling. Arsenic (As) is relatively rich within the sediments and is a potential source of high As concentration in local water, thus As mobilization is of specific interest. Batch experiments of water-rock-CO_2 interactions are conducted with both fresh groundwater and saline water, to mimic scenarios of CO_2 leakage with and without deeper formation brine. Quantitative interpretation of As mobilization due to leaked CO_2 and brine utilizes an inverse reactive transport modeling approach. A specific objective for this study is to identify the responses of As release under different water salinities and to quantify the key parameters controlling As mobilization processes.

Results

Water chemistry changes. When CO_2 is introduced into the water-rock batch systems, pH decreases immediately because of CO_2 dissolution in both background (BG) and saline (S) samples (Fig. 1a,b). After the sharp drop, pH remains stable at ~5.9, even after CO_2 injection is stopped. The simulated pH also shows a sudden drop within 1 h of CO_2 injection, then a slight increase, and finally reaches a steady-state. This phenomenon was also observed by Shao *et al.*[17] and Yang *et al.*[27]. This process is mainly affected by CO_2 diffusion and mineral reactions, and the dissolution of minerals (especially calcite) consumes hydrogen ions and causes the solution pH to increase slightly between 4 and 72 h[17]. For the CO_2-free (control) experiments, both measured and calculated pH remain stable at ~8.3 for BG and ~7.3 for S (Fig. 1a,b), and good matches with high confidence are achieved between calculated and experimental results.

Synthetic groundwater and saline water were used in our experiments, and the fast dissolving minerals (such as calcite) are not abundant in the system. This makes it hard to track major ion concentration changes in the water samples during the experiments, especially for Mg, Na, Si, Cl and SO_4 in the saline-water reactor when CO_2 is introduced. Only Ca shows a more than 50% concentration increase compared to the CO_2-free experiments, indicating that calcium minerals (especially calcite) dissolved during the experiments (Fig. 1c,d).

With CO_2 intrusion into the shallow groundwater aquifer, trace metals of environmental concern might be released. Arsenic is of specific interest in our study due to its high concentration in the shallow groundwater of the Chimayo site[13]. Figure 1e–f shows As concentration changes of the batch experiments and simulated results. The simulated results match well with the experimental measurements, which capture the trends of As concentration changes in all four cases. Without CO_2 introduction, it shows an increase of As concentration and reaches to equilibrium after sediment and water mixed for both BG and S systems. When CO_2 is introduced to the reactors, it shows a sharp increase of As concentration at the initial time, suggesting a large amount of As released from the sediments due to CO_2 intrusion. After a few hours, As concentration starts to decrease slowly, and reaches equilibrium after 26 days. For both reactors with and without CO_2 introduction, the BG reactors show higher increases of As concentrations than that in the S reactors (20.1 µg/L vs. 15.7 µg/L for the sharp increase with CO_2 introduction and 17.9 µg/L vs. 3.8 µg/L of the control reactors), which indicates that salinity impacts the behavior of As mobilization. One possible reason is that high aqueous salinity reduces the dissolution of minerals (e.g. calcite and clay minerals), affects the water-rock equilibrium and system pH, which further hinders As release. Although As concentration exceeds the maximum contamination level (MCL) of the U.S. Environmental Protection Agency (EPA) in the beginning when CO_2 is introduced for both BG and S reactors, it drops below the MCL after 8-day exposure, which might not be considered as a long term concern of the USDWs. This As concentration drop was also observed in other studies[17,30,31]. It is notable that the BG reactor without CO_2 injection shows a large increase of aqueous phase As concentration to exceed the MCL. However, the field samples show low concentrations of As (~1 µg/L) without CO_2 and brine exposure[13]. This reveals the limitation of batch experiments in that they overestimate the water-rock and water-rock-CO_2 reactions within well-mixed water-sediment systems and large reaction areas of mineral surface, which is also pointed out by other researchers[18,27].

Geochemical reaction parameters. The inverse modeling approach is applied for estimating geochemical reaction parameters for each experiment in this study. Estimated mean values of geochemical reaction parameters from the four experiments are shown in Table 1. The coefficient of variation (CV, the ratio of the standard deviation to the mean value) is also shown in the table to suggest the extent of variability of each parameter. Generally, the estimated values are in agreement with those reported by literature[12,25,32,33], which suggests high confidence of the parameter estimation approach. However, the parameters with large CV values indicate high uncertainties among different specific cases. Especially, mineral reaction rates and mineral surface areas of calcite and clay minerals vary with up to two orders of magnitudes among the four cases, indicating that these parameters should be carefully chosen for simulations, and our estimation can provide a reference for determining the range of these parameters. To verify that the estimated mean values could represent the scenarios of all the cases, the model was simulated with these mean values for all the four experiments. The results indicate that these parameters are reasonable for geochemical reaction simulations especially for the analysis of As behaviors with/without CO_2 introduction under a large range of salinity conditions.

A composite sensitivity analysis of the geochemical parameters was conducted to explore the most sensitive parameters to the experimental results by calculating their composite sensitivity coefficients[34,35]. The most sensitive parameters are listed in Fig. 2. Generally, Sensitivity is increased when CO_2 is introduced, indicating that the related reactions are pH dependent. With CO_2 introduction, the model is highly sensitive to the calcite reaction rates (cal_rkf1 and cal_rkf2), hematite dissolution rate (hem_rkf), surface areas of calcite (cal_amin)

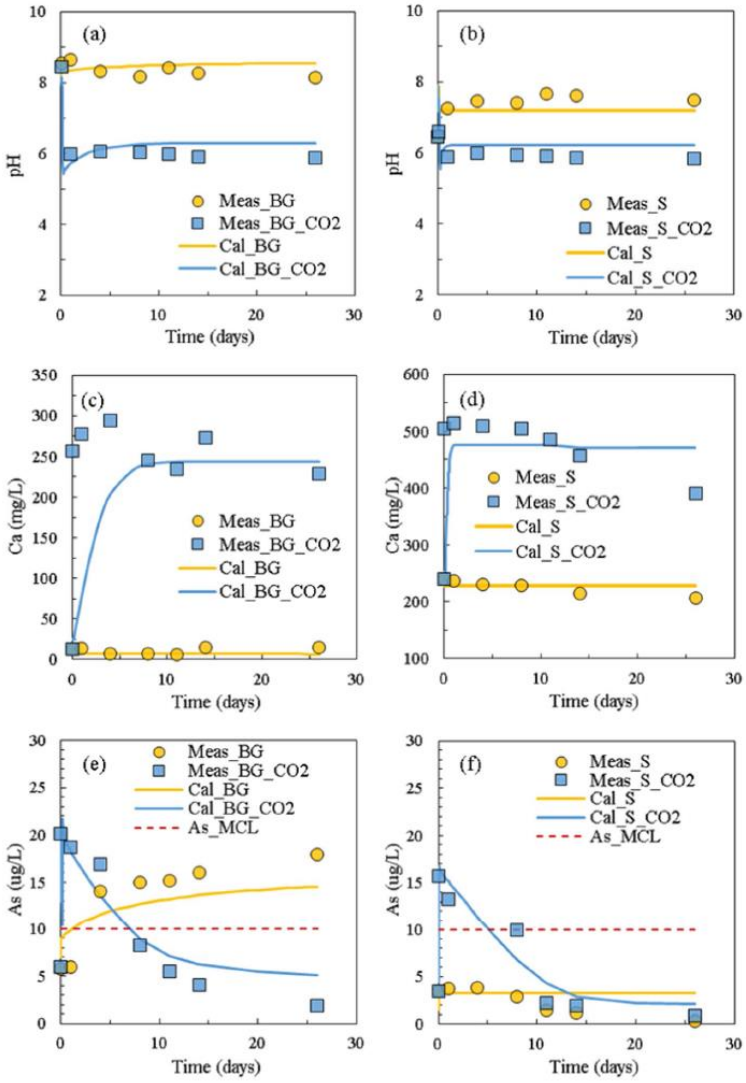

Figure 1. Measured (symbols) and calculated (lines) water chemistry of the batch experiments: (**a**) background (BG, TDS ~200 mg/L) pH; (**b**) saline (S, TDS ~4000 mg/L) pH; (**c**) background Ca; (**d**) saline Ca; (**e**) background As; (**f**) saline As. Maximum contaminant level (MCL) of As is also marked in (**e**) and (**f**).

and hematite (hem_amin), kaolinite adsorption surface area (kao_soh_ssa), and kaolinite adsorption equilibrium constant (logK_kao). The cation exchange selectivity and CEC showed relatively high sensitivities for all the four cases in our study, indicating that cation exchange reactions are significant for aqueous phase ion concentrations including major ions (Ca, Mg, Na, K) and trace metals (As).

Overall, the inverse modeling approaches provide reasonable geochemical reactions for our study, suggesting that it is possible to predict groundwater chemistry responses with CO_2 intrusion in other cases. However, there are still some limitations with such approaches. For example, the range and initial value of key parameters should be carefully chosen to obtain a reasonable outcome; there might be more than one solution leading to a good representation of the observation data; and uncertainties of the model structure and observation data could also impact the estimations[36]. Therefore, experimental studies of mechanisms of geochemical reactions

Category	Name	Symbol	Estimated mean value	CV
Mineral dissolution/ precipitation rate constant (mol/m^2/s)	Calcite dissolution	cal_rkf1	3.52×10^{-6}	0.92
	Calcite precipitation	cal_rkf2	1.42×10^{-6}	0.69
	Kaolinite	kao_rkf	1.06×10^{-12}	1.17
	Illite	ill_rkf	1.18×10^{-12}	0.70
	Smectite	sme_rkf	8.57×10^{-12}	1.23
	Hematite	hem_rkf	1.45×10^{-12}	0.87
	K$^-$feldspar	fel_rkf	1.39×10^{-10}	1.33
	Quartz	qua_rkf	1.94×10^{-14}	0.15
	Albite	alb_rkf	2.70×10^{-12}	0.26
	Anorthite	ano_rkf	1.04×10^{-14}	0.97
Mineral surface area (cm^2/g)	Calcite	cal_amin	53.96	0.98
	Kaolinite	kao_amin	316.84	1.15
	Illite	ill_amin	272.06	1.11
	Smectite	sme_amin	24.90	1.37
	Hematite	hem_amin	274.08	0.43
	K-feldspar	fel_amin	222.42	1.87
	Quartz	qua_amin	23.29	0.24
	Albite	alb_amin	27.48	1.00
	Anorthite	ano_amin	257.60	1.92
Adsorption surface area (cm^2/g)	Hematite-OH	hem_soh_ssa	2.13	0.62
	Kaolinite-OH	kao_soh_ssa	11018.86	0.95
	Illite-OH	ill_soh_ssa	2.82	0.86
	Smectite-OH	sme_soh_ssa	65.83	0.75
Surface complex equilibrium constant (logK)	(Hematite)$_2$−AsO4$^-$	logK_hem	−9.17	0.22
	Illite- HAsO4$^-$	logK_ill	−10.28	0.01
	Smectite-HAsO4$^-$	logK_sme	3.94	0.30
	Kaolinite-AsO$_4^{2-}$	logK_kao	1.15	0.59
Cation exchange capacity (meq/100 g)	CEC	cec	2.92	0.54
Cation exchange selectivity	KNa/H	h_ekx	0.202	0.01
	KNa/Ca	ca_ekx	0.748	0.27
	KNa/Mg	mg_ekx	4.19×10^{-4}	0.45
	KNa/K	k_ekx	2.13×10^{-2}	0.23

Table 1. Estimated geochemical reaction parameters from the batch experiments.

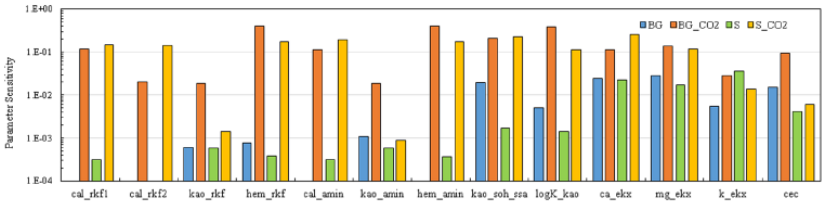

Figure 2. Sensitivity analysis of the geochemical reactive parameters.

are meaningful to provide reasonable reaction pathways and the ranges of key parameters under different conditions. Our study using the combined application of batch experiments with geochemical simulation approaches can provide a good example for future research with multiple reaction parameters for CO_2 and/or brine leakage studies.

Discussion

Arsenic mobilization mechanisms. Arsenic mobilization behavior has been widely discussed by researchers because it is one of the major concerns for groundwater quality in the event of CO_2 leakage. Most of the studies consider the behavior of As to be largely related to adsorption/desorption onto/from the surfaces of clay and Fe-rich minerals[30,37,38], and some researchers believe that As-bond mineral dissolution (i.e. As-carbonate

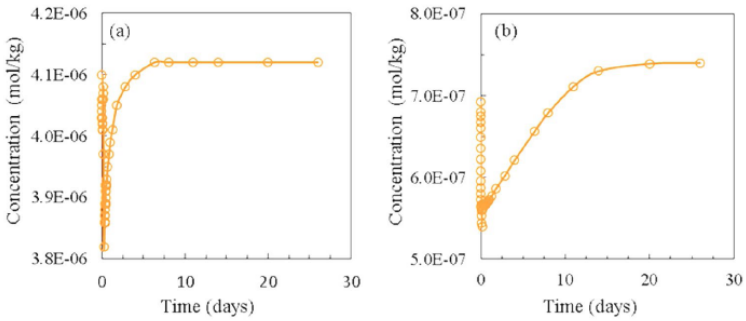

Figure 3. Simulated adsorbed As on kaolinite with CO_2 introduction: (**a**) Background; (**b**) Saline.

minerals and Arsenopyrite) is the primary source of As contamination[12,39,40]. The two mechanisms are sometimes combined to explain As mobilization behavior in experimental and modeling approaches[12,25]. It is hard to quantitatively determine the formula and fractions of such As-bond minerals because of their low concentrations, and estimated formula and volume fractions are usually used in simulations[12]. To verify As mobilization mechanisms and to demonstrate the role of As mineral dissolution and surface adsorption/desorption, a small volume fraction (<0.01%) of As-calcite ($CaCO_3{\cdot}As_2O_5$) was added to the numerical model as an uncertainty parameter to analyze its impact to As behavior. The results show that the sensitivity of As concentrations to such mineral dissolution is far less than that to surface adsorption/desorption process, and As-calcite dissolution shows minimal impact on As concentration in the aqueous phase. The reason is because the mineral dissolution rate is far less than surface complexation processes, and its dissolution is limited during the experiments. According to our simulation results, adsorption/desorption onto/from the surfaces of clays, especially kaolinite, controls As mobilization with water-rock-CO_2 interactions. Arsenic also shows adsorption/desorption to illite, hematite and smectite, but with a few orders of magnitude less than that adsorbed on kaolinite. Figure 3 shows the simulated adsorbed As on kaolinite with CO_2 introduction to both BG and S reactors. With CO_2 introduction, there is an immediate sharp drop of adsorbed As, and it slowly re-adsorbs to local equilibrium in 7–15 days afterwards. The surface complexation reactions of the clay minerals (S represents mineral sites) could be written as[41]:

$$SOH_{(s)} + H^+_{(aq)} \rightleftharpoons SOH^+_{2(s)} \tag{1}$$

$$SOH_{(s)} \rightleftharpoons SO^-_{(s)} + H^+_{(aq)} \tag{2}$$

$$SOH_{(s)} + H_3AsO_{4(aq)} \rightleftharpoons SAsO^{2-}_{4(s)} + 2H^+_{(aq)} + H_2O \tag{3}$$

The mass balance for the total numbers of reactive sites (omit other adsorbed metals) is:

$$[SOH]_T = [SOH] + [SOH^+_2] + [SO^-] + [SAsO^{2-}_4] \tag{4}$$

$[SOH]_T$ is related to the adsorption site density and mineral volume fraction, and the surface functional groups are competitive for the available sites. During the experimental time in our study, clay minerals do not show significant volume change, thus we can assume $[SOH]_T$ to be a constant value for this discussion. With the sudden drop of pH (increase of H^+) at the initial time, it promotes reaction (2), and SOH_2^+ rapidly occupies the surface complexation sites, which results in As release from $SAsO_4^{2-}$ to the aqueous phase (H_3AsO^4). With the buffering effect of calcite dissolution ($CaCO_3 + H^+ \rightleftharpoons Ca^{2+} + HCO_3^-$), the pH of the system starts to increase slowly to a certain extent (Fig. 1a,b), and a series of local equilibriums are reached with $SAsO_4^{2-}/H_3AsO_4$ for gradual As adsorption onto clay minerals (Equation (3)). Without CO_2 introduction, because of the low As concentration in aqueous phase, the adsorbed As releases from the clay mineral adsorption sites to reach to a series of local equilibriums, which results in an increase in As concentration in the water (Fig. 1e,f).

Environmental implications. Trace metal contamination, especially As, is always a major concern when considering the potential risks of CO_2 and saline water leakage from GCS sites. Results of this study suggest that, in general, As may be considered an insignificant long-term concern in a CO_2 rich environment because of clay adsorptions. Likewise, in a saline environment, high concentrations of major ions (Ca, Mg, Na *et al.*) could hinder As release from the clay mineral sites. In such circumstances, if As is present, the reservoir brine might contain low concentrations of As and other trace metals to begin with (i.e. not due to enhanced desorption and mobilization). In many cases, increased salinity of USDW via the leaked saline water may likely be a larger concern than any associated released the trace metals[42]. Observed data from the Chimayo site suggest that the brackish water leaked through faults provides a source of arsenic and other heavy metals[13]. Kirsh *et al.*[39] and Karamalidis *et al.*[40] showed As concentration increased in their experiments under both freshwater and saline environments,

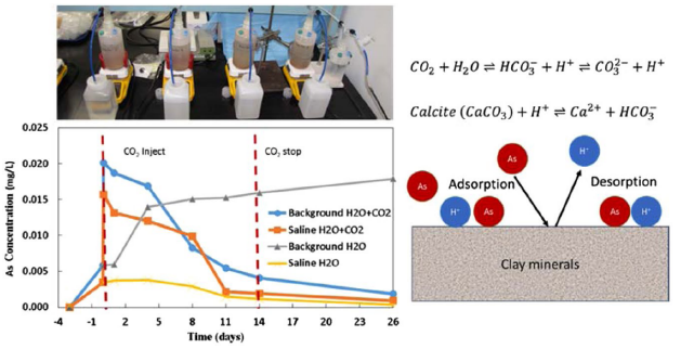

Figure 4. Batch experiments shown arsenic mobilization due to the reactions between the sediments and introduced CO_2.

Element	Background	Saline	Element	Background	Saline
Ca	5.2	222.1	Cl	28.0	2050.0
Fe	1.4×10^{-3}	2.2×10^{-2}	SO4	56.0	333.0
K	0.7	38.6	Si	<DL	<DL
Mg	2.8	220.4	As	<DL	1.5×10^{-4}
Na	73.9	783.9	pH (unitless)	8.5	6.4

Table 2. Concentrations for major ions of the background and saline batch experiments (mg/L).

indicating that As-rich mineral dissolution becomes dominant in such cases. Arsenic mobilization mechanisms should therefore be treated as a site-specific issue, with risk analyses of target GCS sites guided by preliminary assays of As content of both reservoir and USDW strata.

Materials and Methods

An integrated framework of systematically combined batch experiments and reactive transport simulations has been developed for better understanding As mobilization mechanisms with CO_2 leakage into shallow aquifers. The sediment samples for batch experiments are collected from the Chimayo site, a natural CO_2 analog located at the eastern margin of Espanola basin in northern New Mexico[13]. The shallow drinking water aquifer at this site has been investigated by a series of studies[25, 29, 43], and water chemistry was analyzed to evaluate mobilizations of trace metals. Observed data show evidence of upward migration of CO_2 and saline water along the faults, whereas the locations far from the faults are not impacted by CO_2 or brine. This site provides an example for analyzing the impacts of CO_2/brine leaked from a GCS site on overlying USDW quality.

Batch Experiments. Due to high As concentrations in the Chimayo groundwater exposed to CO_2 and saline water, and the relatively high amount of As present in the sediment samples (up to 147 mg/kg), the behavior of As caused by CO_2 and saline water intrusion is of specific interest. Batch experiments were conducted to mimic the influx of CO_2 and saline water into the aquifer in order to evaluate As mobilization due to the reactions between the sediments and CO_2 (Fig. 4). Details of the experiments were described by Viswanathan *et al.*[25]. Two sets of experiments were conducted, with "background" (BG, low salinity, TDS ~200 mg/L) and "saline" (S, high salinity, TDS ~4000 mg/L) synthetic groundwater, to represent the conditions with/without saline water intrusion. The major components of each synthetic groundwater are listed in Table 2. With each set of experiments, one reactor was exposed to CO_2 (maintained 1 atm) and one reactor was kept as a steady-state, CO_2-free control. Before CO_2 injection, the sediment samples were exposed to the synthetic groundwater for ~3 days to reach a steady state. Water samples were then collected over a 26-day experimental period: 14 days for CO_2 injection and 12 days for post injection. Major ion and As concentrations were analyzed subsequently.

Geochemical Modeling Approach. In this study, a reactive transport model considering aqueous species complexation, mineral dissolution/precipitation, adsorption/desorption, and cation exchanges was created, in order to evaluate the mechanisms of As mobilization. All simulations were performed with TOUGHREACT V2 and ECO2N[44, 45].

A total of 54 aqueous complexes that have high impacts on the results were selected for the simulations. The aqueous complexes and their equilibrium constants are listed in Table 3. For all the batch experiments, the reactors were exposed to an oxygen-rich environment (atmosphere). Under this condition, As (V) is considered a dominant form in the aqueous phase, which also corresponds to the conditions of the site (pe > 4). Precipitation/

Species	LogK	Species	LogK	Species	LogK	Species	LogK
OH^-	13.99	$CaCO_3$ (aq)	7.01	SO_2 (aq)	37.57	$HAsO_4^{2-}$	9.01
$CaCl^+$	0.70	KCl (aq)	1.50	HSO_3^-	39.42	AsO_4^{3-}	20.6
$CaCl_2$ (aq)	0.65	$MgCl^+$	0.14	$PbCl^+$	−1.45	$HAsO_2$ (aq)	23.54
$CaSO_4$ (aq)	−2.10	$MgSO_4$ (aq)	−2.38	$PbCl_2$ (aq)	−2.01	H_3AsO_3 (aq)	23.61
NaCl (aq)	0.78	$NaSO_4^-$	−0.81	$PbCl_3^-$	−1.70	$H_2AsO_3^-$	32.78
$FeCl^+$	0.17	KSO_4^-	−0.88	$PbCl_4^{2-}$	−1.50	$UO_2(CO_3)_3^{4-}$	9.15
$FeHCO_3^+$	−2.04	$NaHSiO_3$ (aq)	8.30	$PbOH^+$	7.57	$UO_2(CO_3)_2^{2-}$	4.05
$FeCO_3$ (aq)	4.88	$CaOH^+$	12.85	$Pb(OH)_2$ (aq)	17.07	$UO_2(SO_4)_2^{2-}$	−3.97
$FeCl_4^{2-}$	1.94	NaOH (aq)	14.15	$Pb(OH)_3^-$	28.07	UO_2Cl^+	−0.15
$NaHCO_3$ (aq)	−0.17	$NaCO_3^-$	9.82	$Pb(CO_3)_2^{2-}$	11.24	UO_2SO_4 (aq)	−3.06
$CaHCO_3^+$	−1.04	$H_3SiO_4^-$	9.81	PbO (aq)	16.98	UO_2OH^+	5.22
$MgHCO_3^+$	−1.03	Fe^{3+}	−8.49	$PbHCO_3^+$	−2.89	UO_2CO_3 (aq)	0.39
CO_2 (aq)	−6.34	CH_4 (aq)	144.15	$PbCO_3$ (aq)	3.06		
CO_3^{2-}	10.33	H_2 (aq)	46.11	$H_2AsO_4^-$	2.25		

Table 3. Aqueous complexes and their equilibrium constants at 25 °C (Primary species include: H_2O, H^+, Ca^{2+}, Mg^{2+}, Na^+, K^+, Fe^{2+}, AlO_2^-, SiO_2 (aq), HCO_3^-, SO_4^{2-}, Cl^-, O_2 (aq), Pb^{2+}, H_3AsO_4 (aq), UO_2^{2+}).

dissolution reactions for all minerals detected in the sample (26% quartz, 3.6% K-feldspar, 2.4% albite, 2.4% anorthite, 0.4% calcite, 0.4% hematite, 43.4% illite, 1.5% kaolinite, and 20.2% smectite) were included in the model. Precipitation of possible secondary minerals was allowed to constrain major ion chemistry in the system. The reaction rates and surface areas of the primary minerals were treated as uncertainty parameters. Although it is hard to detect trace As-bearing minerals (such as As-carbonate minerals) by XRD or SEM-EDS analysis, it is possible that As-rich minerals exist in the sediments[12] and impact As concentration in the aqueous phase. In this study, the initial amount of trace As minerals were treated as uncertainty parameters.

Adsorption/desorption of As from clay/Fe-rich mineral surfaces was considered as an important process for As mobilization with CO_2 and saline water intrusion. Hematite, kaolinite, illite and smectite were chosen as principal adsorbents, because they were relatively abundant in the sediment samples and also widely reported by former studies[12,27,46]. Arsenic aqueous species $HAsO_4^{2-}$ and $H_2AsO_4^-$ were chosen as major surface adsorption ions[41]. Adsorption/desorption reactions are controlled by the total amount of reactive sites (product of amount of adsorbent, site density and adsorbent surface area)[20], which has high uncertainty for different samples[41]. The local equilibrium of adsorbed As is affected by salinity and pH[37,38,46]. Therefore, adsorbent surface area and surface complexation equilibrium constant were selected as uncertainty parameters.

Cation exchange reactions were also considered in the model for major cations, which might affect the response of trace metals and pH to CO_2 and saline water intrusion. The Gaines-Thomas convention was used in this study[47]. The site-specific parameters of cation selectivity coefficient and cation exchange capacity (CEC) were not measured for this site, and they were treated as uncertainty parameters.

To obtain the best estimations for the uncertainty model parameters, the nonlinear parameter estimation program PEST[48] was applied. The 26-day experimental data were used to estimate the uncertainty parameters listed above via inversion by minimizing the objective function J[48–50]:

$$J = min\sum_{i=1}^{N} E_i(p);\ \ E_i(p) = \sum_{l=1}^{L_i} w_{li}^2 (u_l^i(p) - \tilde{u}_l^i)^2 \tag{5}$$

where $E_i(p)$ is the sub-objective function from chemical species i, N (=9) is the number of chemical species, w_{li} is the weighting coefficient for the lth measurement of the ith species, which is computed with the inverse of the standard deviation of the experimental data[49], and u_l^i and $\tilde{u}_l^i$ are the simulated and observed concentrations of Ca, Mg, K, Na, Si, Cl, SO_4, As and pH. A composite sensitivity analysis of the uncertainty parameters was also conducted in order to determine the most sensitive parameters[48].

References

1. Bachu, S. Sequestration of CO_2 in geological media: Criteria and approach for site selection in response to climate change. *Energy Convers. Manage.* **41**, 953–970, doi:10.1016/S0196-8904(99)00149-1 (2000).
2. IPCC. *Carbon dioxide capture and storage* 53 (Geneva, Switzerland, 2005).
3. Soltanian, M. R. *et al.* Simulating the Cranfield geological carbon sequestration project with high-resolution static models and an accurate equation of state. *Int. J. Greenhouse Gas Control* **54**, 282–296, doi:10.1016/j.ijggc.2016.10.002 (2016).
4. Soltanian, M. R., Amooie, M. A., Dai, Z., Cole, D. & Moortgat, J. Critical dynamics of gravito-convective mixing in geological carbon sequestration. *Sci. Rep.* **6**, 35921, doi:10.1038/srep35921 (2016).
5. Gershenzon, N. I., Soltanian, M., Ritzi, R. W. & Dominic, D. F. Influence of small scale heterogeneity on CO_2 trapping processes in deep saline aquifers. *Energy Procedia* **59**, 166–173, doi:10.1016/j.egypro.2014.10.363 (2014).
6. Gershenzon, N. I. *et al.* Influence of small-scale fluvial architecture on CO_2 trapping processes in deep brine reservoirs. *Water Resour. Res.* **51**, 8240–8256, doi:10.1002/2015WR017638 (2015).
7. Amponah, W. *et al.* Evaluation of CO_2 storage mechanisms in CO_2 storage mechanisms in CO_2 enhanced oil recovery sites: application to morrow sandstone reservoir. *Energy Fuels* **30**, 8545–8555 (2016).

8. Amponah, W. *et al*. Co-optimization of CO_2-EOR and storage processes in mature oil reservoirs. *Greenh. Gases* **7**, 128–142, doi:10.1002/ghg.1618 (2016).
9. Pan, F. *et al*. Uncertainty analysis of carbon sequestration in an active CO_2-EOR field. *Int. J. Greenhouse Gas Control* **51**, 18–28, doi:10.1016/j.ijggc.2016.04.010 (2016).
10. Harvey, O. R. *et al*. Geochemical implications of gas leakage associated with geologic CO_2 storage – A qualitative review. *Environ. Sci. Technol.* **47**, 23–26, doi:10.1021/es3029457 (2013).
11. Little, M. G. & Jackson, R. B. Potential impacts of leakage from deep CO_2 geosequestration on overlying freshwater aquifers. *Environ. Sci. Technol.* **44**, 9225–9232, doi:10.1021/es102235w (2010).
12. Zheng, L., Apps, J. A., Zhang, Y., Xu, T. & Birkholzer, J. T. On mobilization of lead and arsenic in groundwater in response to CO_2 leakage from deep geological storage. *Chem. Ceol.* **268**, 281–297 (2009).
13. Keating, E., Fessenden, J., Kanjorski, N., Koning, D. & Pawar, R. The impact of CO_2 on shallow groundwater chemistry: Observations at a natural analog site and implications for carbon sequestration. *Environ. Earth Sci.* **60**, 521–536, doi:10.1007/s12665-009-0192-4 (2010).
14. Cihan, A., Birkholzer, J. T. & Zhou, Q. Pressure buildup and brine migration during CO_2 storage in multilayered aquifers. *Groundwater* **51**, 252–267, doi:10.1111/j.1745-6584.2012.00972.x (2013).
15. Frye, E., Bao, C., Li, L. & Blumsack, S. Environmental controls of cadmium desorption during CO_2 leakage. *Environ. Sci. Technol.* **46**, 4388–4395, doi:10.1021/es3005199 (2014).
16. Lawter, A., Qafoku, N. P., Wang, G., Shao, H. & Brown, C. F. Evaluating impacts of CO_2 intrusion into an unconsolidated aquifer: I. Experimental data. *Int. J. Greenhouse Gas Control* **44**, 323–333, doi:10.1016/j.ijggc.2015.07.009 (2016).
17. Shao, H., Qafoku, N. P., Lawter, A. R., Bowden, M. E. & Brown, C. F. Coupled geochemical impacts of leaking CO_2 and contaminants from subsurface storage reservoirs on groundwater quality. *Environ. Sci. Technol.* **49**, 8202–8209, doi:10.1021/acs.est.5b01004 (2015).
18. Trautz, R. C. *et al*. Effect of dissolved CO_2 on a shallow groundwater system: A controlled release field experiment. *Environ. Sci. Technol.* **47**, 298–305, doi:10.1021/es301280t (2013).
19. Yang, C. *et al*. Single-well push-pull test for assessing potential impacts of CO_2 leakage on groundwater quality in a shallow gulf coast aquifer in Cranfield, Mississippi. *Int. J. Greenhouse Gas Control* **18**, 375–387, doi:10.1016/j.ijggc.2012.12.030 (2013).
20. Zheng, L. *et al*. Geochemical modeling of changes in shallow groundwater chemistry observed during the MSU-ZERT CO_2 injection experiment. *Int. J. Greenhouse Gas Control* **7**, 202–217, doi:10.1016/j.ijggc.2011.10.003 (2012).
21. Bacon, D. H., Qafoku, N. P., Dai, Z., Keating, E. H. & Brown, C. F. Modeling the impact of carbon dioxide leakage into an unconfined, oxidizing carbonate aquifer. *Int. J. Greenhouse Gas Control* **44**, 290–299, doi:10.1016/j.ijggc.2015.04.008 (2016).
22. Carroll, S. A. *et al*. Key factors for determining groundwater impacts due to leakage from geologic carbon sequestration reservoirs. *Int. J. Greenhouse Gas Control* **29**, 153–168, doi:10.1016/j.ijggc.2014.07.007 (2014).
23. Celia, M. A., Nordbotten, J. M., Court, B., Dobossy, M. & Bachu, S. Field-scale application of a semi-analytical model for estimation of CO_2 and brine leakage along old wells. *Int. J. Greenhouse Gas Control* **5**, 257–269, doi:10.1016/j.ijggc.2010.10.005 (2011).
24. Dai, Z. *et al*. Probabilistic evaluation of shallow groundwater resources at a hypothetical carbon sequestration site. *Sci. Rep.* **4**, 4006, doi:10.1038/srep04006 (2014).
25. Viswanathan, H. *et al*. Developing a robust geochemical and reactive transport model to evaluate possible sources of arsenic at the CO_2 sequestration natural analog site in Chimayo, New Mexico. *Int. J. Greenhouse Gas Control* **10**, 199–214, doi:10.1016/j.ijggc.2012.06.007 (2012).
26. Xiao, T. *et al*. Potential chemical impacts of CO_2 leakage on underground source of drinking water assessed by quantitative risk analysis. *Int. J. Greenhouse Gas Control* **50**, 305–316, doi:10.1016/j.ijggc.2016.04.009 (2016).
27. Yang, C., Dai, Z., Romanak, K. D., Hovorka, S. D. & Treviño, R. H. Inverse modeling of water-rock-CO_2 batch experiments: Potential impacts on groundwater resources at carbon sequestration sites. *Environ. Sci. Technol.* **48**, 2798–2806, doi:10.1021/es4041368 (2014).
28. Lewicki, J. L., Birkholzer, J. & Tsang, C. Natural and industrial analogues for leakage of CO_2 from storage reservoirs: Identification of features, events, and processes and lessons learned. *Environ. Geol.* **52**, 457–467, doi:10.1007/s00254-006-0479-7 (2007).
29. Keating, E. H. *et al*. CO_2/brine transport into shallow aquifers along fault zones. *Environ. Sci. Technol.* **47**, 290–297, doi:10.1021/es301495x (2013).
30. Lu, J., Partin, J., Hovorka, S. & Wong, C. Potential risks to freshwater resources as a result of leakage from CO_2 geological storage: a batch-reaction experiment. *Environ. Earth Sci.* **60**, 335–348, doi:10.1007/s12665-009-0382-0 (2010).
31. Yang, C., Hovorka, S. D., Treviño, R. H. & Delgado-Alonso, J. Integrated framework for assessing impacts of CO_2 leakage on groundwater quality and monitoring-network efficiency: Case study at a CO_2 enhanced oil recovery site. *Environ. Sci. Technol.* **49**, 8887–8898, doi:10.1021/acs.est.5b01574 (2015).
32. Palandri, J. L. & Kharaka, Y. K. A complication of rate parameters of water-mineral interaction kinetics for application to geochemical modeling (U. S. Geological Survey, Menlo Park, CA, USA, 2004).
33. Goldberg, S. Competitive adsorption of arsenate and arsenite on oxides and clay minerals. *Soil Sci. Arm. J.* **66**, 413–421, doi:10.2136/sssaj2002.4130 (2002).
34. Dai, Z. *et al*. Stepwise inversion of a groundwater flow model with multi-scale observation data. *Hydrogeol. J.* **18**, 607–624, doi:10.1007/s10040-009-0543-y (2010).
35. Dai, Z. *et al*. CO_2 Accounting and Risk Analysis for CO_2 Sequestration at Enhanced Oil Recovery Sites. *Environ. Sci. Technol.* **50**, 7546–7554, doi:10.1021/acs.est.6b01744 (2016).
36. Carrera, J., Alcolea, A., Medina, A., Hidalgo, J. & Slooten, L. J. Inverse problem in hydrogeology. *Hydrogeol. J.* **13**, 206–222, doi:10.1007/s10040-004-0404-7 (2005).
37. Appelo, C. A. J., Van Der Weiden, M. J. J., Tournassat, C. & Charlet, L. Surface complexation of ferrous iron and carbonate on ferrihydrite and the mobilization of arsenic. *Environ. Sci. Technol.* **36**, 3096–3103 (2002).
38. Goldberg, S. & Johnston, C. T. Mechanisms of arsenic adsorption on amorphous oxides evaluated using macroscopic measurements, vibrational spectroscopy, and surface complexation modeling. *J. Colloid Interface Sci.* **234**, 204–216, doi:10.1006/jcis.2000.7295 (2001).
39. Kirsch, K., Navarre-Sitchler, A. K., Wunsch, A. & McCray, J. E. Metal release from sandstones under experimentally and numerically simulated CO_2 leakage conditions. *Environ. Sci. Technol.* **48**, 1436–1442, doi:10.1021/es403077b (2014).
40. Karamalidis, A. K. *et al*. Trace metal source terms in carbon sequestration environments. *Environ. Sci. Technol.* **47**, 322–329, doi:10.1021/es304832m (2013).
41. Goldberg, S., Hyun, S. & Lee, L. S. Chemical modeling of arsenic (III, V) and selenium (IV, VI) adsorption by soils surrounding ash disposal facilities. *Vadose Zone J.* **7**, 1231–1238, doi:10.2136/vzj2008.0013 (2008).
42. Bacon, D. H., Dai, Z. & Zheng, L. Geochemical impacts of carbon dioxide, brine, trace metal and organic leakage into an unconfined, oxidizing limestone aquifer. *Energy Procedia* **63**, 4684–4707, doi:10.1038/srep04006 (2014).
43. Cumming, K. A. Hydrogeochemistry of groundwater in Chimayo, New Mexico. 117, (M. S., Northern Arizona University, Flagstaff, AZ, 1997).
44. Xu, T. *et al*. TOUGHREACT Version 2.0: A simulator for subsurface reactive transport under non-isothermal multiphase flow conditions. *Comput Geosci* **37**, 763–774, doi:10.1016/j.cageo.2010.10.007 (2011).

45. Pruess, K. ECO2N: A TOUGH2 Fluid Property Module for Mixtures of Water, NaCl, and CO_2 http://esd1.lbl.gov/files/research/projects/tough/documentation/TOUGH2_ECO2N_Users_Guide.pdf (2005).
46. Samper, J. *et al*. Inverse modeling of tracer experiments in FEBEX compacted Ca-bentonite. *Phys. Chem. Earth* **31**, 640–648, doi:10.1016/j.pce.2006.04.013 (2006).
47. Appelo, C. J. A. & Postma, D. *Geochemistry groundwater and pollution* (A. A. Balkema, Rotterdam, Netherlands, 1993).
48. Doherty, J. *PEST, model-independent parameter estimation* (Watermark Computing, Corinda, Australia, 2000).
49. Dai, Z. & Samper, J. Inverse problem of multicomponent reactive chemical transport in porous media: Formation and applications. *Water Resour. Res.* **40**, W07407, doi:10.1029/2004WR003248 (2004).
50. Dai, Z. *et al*. Identification of sorption processes and parameters for radionuclide transport in fractured rock. *J. Hydrol.* **414-415**, 220–230, doi:10.1016/j.jhydrol.2011.10.035 (2012).

Acknowledgements

Funding for this project is partially provided by the U.S. Department of Energy's (DOE) National Energy Technology Laboratory (NETL) through the Southwest Regional Partnership on Carbon Sequestration (SWP) under Award No. DE-FC26-05NT42591. The corresponding author (Zhenxue Dai) acknowledges the financial support from Jilin University, China, for a startup funding. We are grateful to the assistance of George Guthrie, Richard Esser, William Ampomah, and Robert Balch for providing guidance and constructive comments on our work.

Author Contributions

T.X. carried out the integrated simulations, performed data analysis and wrote the draft manuscript. Z.D. designed the inverse modeling simulations, performed data analysis, discussed the results and revised the manuscript. A.H. provided the experimental data. H.V., M.C., W.J., Y.Z. and B.M. discussed the results and revised the manuscript.

Additional Information

Competing Interests: The authors declare that they have no competing interests.

Reprints and permissions: information are available online at http://pubs.acs.org/journal/esthag.

Disclaimer: This report was prepared as an account of work sponsored by an agency of the United States Government. Neither the United States Government nor any agency thereof, nor any of their employees, makes any warranty, express or implied, or assumes any legal liability or responsibility for the accuracy, completeness, or usefulness of any information, apparatus, product, or process disclosed, or represents that its use would not infringe privately owned rights. Reference herein to any specific commercial product, process, or service by trade name, trademark, manufacturer, or otherwise does not necessarily constitute or imply its endorsement, recommendation, or favoring by the United States Government or any agency thereof. The views and opinions of authors expressed herein do not necessarily state or reflect those of the United States Government or any agency thereof.

Publisher's note: Springer Nature remains neutral with regard to jurisdictional claims in published maps and institutional affiliations.

CHAPTER 5

CONCLUSION

This work specifically focuses on impacts of CO_2 leakage from geologic CO_2 sequestration (GCS) reservoirs. CO_2-wellbore cement interactions, CO_2 leakage through fractured wellbores, CO_2 intrusion into groundwater aquifers, and its impacts on Underground Sources of Drinking Water (USDW) quality are analyzed. Geochemical reactions due to CO_2 intrusion are of specific interest in this work, which include aqueous species complexation, mineral precipitation/dissolution, adsorption/desorption, and cation exchange. Specific methods of reduce order models (response surface methodology), uncertainty analysis, and inverse modeling are involved in this work. Lab-scale experimental results and field observations are used for key parameters calibration, which improves the reliability of numerical simulations.

Chapter 1 introduces potential risks of CO_2 leakage from storage reservoirs and recent research approaches on this topic. Importance of combining numerical simulations with experimental results and risk assessments is also addressed in this chapter.

In Chapter 2, chemical impacts of CO_2 leakage through wellbore cement and surrounding caprock with a gap (annulus) in between are analyzed. The case study for this analysis is the Farnsworth Unit (FWU), an active CO_2 enhanced oil recovery (EOR) oilfield in the northern Anadarko Basin in Texas. Key parameters for cement-CO_2

interactions are calibrated with the cement core sample from the SACROC Unit exposed to CO_2 for 30 years, and such parameters are used in our reactive transport simulations for forecasting the wellbore structural integrity. The major conclusions drawn include:

(1) Cement tortuosity and diffusion coefficient are key parameters for determining the depth of the carbonation zone. Values of cement tortuosity = 0.01 and diffusion coefficient = 10^{-11} m^2/s are reasonable to fit the carbonation depth of the core sample.

(2) Operational reservoir pressure and reservoir gas saturation (Sg) affect the height of carbonated zone along the existing fracture between the cement and the caprock, because of the buoyancy and pressure driven force for CO_2.

(3) When CO_2 saturated brine reaches the cement, portlandite ($Ca(OH)_2$) reacts with CO_2 and forms calcite (> 20% volume fraction), leading to porosity reduction (up to 10% reduction in 100 years), significantly impacting CO_2 leakage rates by infilling pathways.

(4) CO_2 will likely not penetrate an unfractured caprock, and the cement would not degrade significantly in this case.

(5) For the Farnsworth Unit, the wellbore cement will likely maintain its structure and integrity after 100 years. However, if an acid plume were to enter an existing limestone caprock fracture, calcite would likely dissolve because of reduced pH. This process could increase porosity of the fracture and enlarge the volume of the fracture area – a major concern for CO_2 leakage.

In Chapter 3, a response surface methodology (RSM) is conducted to quantify uncertainty and risks to the water quality of the Ogallala aquifer overlying the Farnsworth Unit (FWU) due to CO_2 leakage through wellbores with micro-fractures. This chapter includes three parts: (1) cement hydration simulations, to obtain the equilibrium

composition of wellbore fluids with wellbore cements; (2) quantification of the possible range of CO_2 leakage rates from the FWU reservoir through wellbore fractures (using typical and likely permeability ranges) to the overlying USDW; and (3) quantification of potential risks to Ogallala groundwater quality due to CO_2 leakage. Major findings include:

(1) This study suggests that a greater than 90% probability of leakage rate values should range between 10^{-14} – 10^{-10} kg/(m^2 ·year). This small leakage rate is explained by the relatively low permeability of wellbore cement, and chemical reactions between CO_2 and portlandite ($Ca(OH)_2$) that consume CO_2 as well as further decrease the fracture porosity resisting the CO_2 pathways.

(2) RSM-based results are sufficiently robust, as indicated by coefficient of determination (R^2) and coefficient of variation of the root mean square error (CVRMSE) values calculated between simulation results and the RSM-predicted responses. R^2 and CVRMSE between 50 validation simulation results and response surface equations are > 0.8 and < 10%, respectively. The high R^2 and low CVRMSE values suggest that the results of ROMs are likely sufficiently effective for representing full-reservoir model simulation results.

(3) No-impact thresholds associated with site-specific monitoring data could be a valuable reference for evaluation of CO_2 impacts.

(4) Within the range of CO_2 leakage rate, TDS, nitrate, and trace metal concentrations could be twice as much as the initial value with the worst scenarios after 200 years. However, these water indices do not exceed the MCL limit, or exceed no-impact thresholds according to the in situ monitoring data, suggesting that the Ogallala

groundwater quality should not be significantly impacted.

(5) Water quality at 100, 500, and 1000 m away from the leakage point indicates only slight differences within 200 years, suggesting that the distance between current monitoring wells and injection/production wells is of limited impact with respect to early detection criteria.

(6) pH is suggested as a likely geochemical indicator for early detection, because it is sensitive to CO_2 leakage and is easy to detect.

In Chapter 4, the mechanisms of arsenic mobilization with an integrated experimental and simulation framework are analyzed. The case study is the Chimayo site in northern New Mexico, a natural analog with CO_2 upwelling, which provides an example of a shallow groundwater aquifer with long-term CO_2 exposure. Quantitative interpretation of As mobilization due to leaked CO_2 and brine utilizes an inverse reactive transport modeling approach. Results of this study are intended to improve ability to quantify risks associated with potential leakage of reservoir fluids into shallow aquifers, in particular the possible environmental impacts of As mobilization at carbon sequestration sites. The main conclusions are:

(1) Arsenic desorption/adsorption from/onto clay minerals is the major reaction controlling its mobilization, and clay minerals could mitigate As mobilization with surface complexation reactions.

(2) Dissolution of available calcite plays a critical role in buffering pH.

(3) High salinity in general hinders As release from minerals.

(4) The magnitude and quantitative uncertainty of As mobilization are predicated on the values of reaction rates and surface area of calcite, adsorption surface areas and

equilibrium constants of clay minerals, and cation exchange capacity.

Future research could be done to improve the approaches of this work. Possible research may include: (1) improved models for the simulated formations with more field monitoring data could be developed; (2) laboratory experiments with site-specific sediments and groundwater samples interacting with CO_2 could be conducted to obtain geochemical reaction parameters for potential impacts on groundwater quality; and (3) integrated frameworks combining experiments, simulation, and field observations are necessary for accurately forecasting CO_2 behavior in the storage sites.